4

Induced Codeposition of Alloys of Tungsten, Molybdenum and Rhenium with Transition Metals

Noam Eliaz[*] and Eliezer Gileadi[**]

[*]*Biomaterials and Corrosion Laboratory, School of Mechanical Engineering,*
[**]*School of Chemistry, Faculty of Exact Sciences,*
Tel-Aviv University, Ramat Aviv, Tel-Aviv 69978, Israel

I. INTRODUCTION

In this section, the process of electrodeposition is reviewed briefly, and its place in the general context of electrode reactions and charge transfer across the metal/solution interface is set (Section 1.1). In Section 1.2, special emphasis is given to deposition of alloys, and particularly to anomalous deposition of alloys (Sections 1.2.3 and 1.2.4). Next, the phenomenon of induced codeposition is defined, and possible mechanisms are discussed briefly (Section 1.2.5). Several electroless (Section 1.2.6) and electrodeposition processes, in which induced codeposition plays a role, are mentioned. A more extensive discussion of electrodeposition of W-, Mo- and Re-based alloys is included in Section 2. Typical

Modern Aspects of Electrochemistry, Number 42, edited by C. Vayenas et al., Springer, New York, 2008.

bath compositions and operating conditions are listed in Appendices A through C, respectively.

Many books have been dedicated over the years to the topic of electrodeposition (see, for example, Refs. 1-6). These books deal with a variety of sub-topics such as surface preparation of the substrate prior to deposition, thermodynamics and kinetics of electrodeposition, the reactions that take place on an atomistic level, the mechanisms of growth, the effect of bath chemistry and operating conditions, the deposition of specific metals and alloys, the structure and properties of deposits, etc.

Electrodeposition has been practiced in industry for more than 150 years. For many years it was considered as an empirical, low-level, technology. Although many useful plating baths have been developed, and additives were identified for specific purposes—macro and micro leveling, brightening, stress relieving, inhibition of hydrogen embrittlement (HE) and so on, most of the advancements in the field were achieved by ingenious trial-and-error methods, rather than by attempting to gain a profound understanding of the scientific aspects of the field. A turning point in this approach can be associated with the announcement by IBM in 1997 of replacing vapor-deposited aluminum by electrodeposited copper wiring in ultra-large-scale integration (ULSI) silicon chips. Following this announcement, electrodeposition gained much interest in the microelectronic industry as a potentially attractive manufacturing process compared to other technologies. At the same time, the awareness of possible advancements through research and development increased, both in academia and in industry, and it stopped being perceived as mostly an empirical technology.[7]

Electrodeposition offers several important advantages compared to most other plating technologies. These include:

- relatively low cost
- fairly simple and available equipment
- the laws governing scaling up and scaling down of electrochemical processes are well understood[7]
- porous, geometrically complex or non line-of-sight surfaces can be coated
- proper design of the cell and the counter electrode can ensure that metal is deposited only where it is needed[7]

- the throwing power is higher than in physical vapor deposition[7]
- production of high-aspect-ratio structures with good precision[7]
- relatively low processing temperature, allowing the formation of highly crystalline deposits, with possibly lower residual stresses
- the thickness, composition and microstructure of the deposit can be controlled precisely
- dense materials with high purity, low defect density and narrow distribution of grain size can be produced.

Representative applications of electrodeposition include, among others, gold-plated brass jewelry; copper plating for fabrication of interconnects in electronic packaging; hard chromium plating of aircraft landing gears made of alloy steels; zinc-nickel alloy plating on steel components; silver-plated mirrors; tin-lead coatings for soldering on printed-circuit boards; plating of nickel, nickel-iron and copper in fabrication of micro-electro-mechanical systems (MEMS) by LIGA, etc.[6,7]

Current distribution on the cathode is a major variable in electrodeposition. It is determined by several parameters, such as the geometry of both the anode and the cathode, as well as their relative position in the bath, the kinetics of charge transfer and the conditions of mass transport.[7] It determines the thickness of the coating and its uniformity, as well as the local chemical composition in alloy deposition. In the past two or three decades, specific interest in pulse plating and periodic reverse pulse plating (where the current is either interrupted or reversed periodically, respectively)[8] has increased significantly. These techniques may have a significant influence on the composition and structure of electrodeposited alloys[7,9-11] as well as on the surface morphology and the micro-throwing power.

A clarification of nomenclature and sign convention, which may often be confusing, is called for in this context. It can be stated categorically that the cathode is always the electrode at which a reduction process (e.g., hydrogen evolution or metal deposition) takes place. Similarly, the anode is always the electrode at which oxidation (e.g., oxygen evolution or metal dissolution) takes place. But, which is the positive and which is the negative elec-

trode? The answer to that depends on the type of reaction taking place in the cell. If the cell is externally driven (namely, electric power is consumed to force a current through it, leading to chemical change), the cathode is the negative terminal and the anode is the positive terminal in a so-called *electrolytic cell*. This applies to electrodeposition, water electrolysis, electrosynthesis, battery charging, etc. It is reflected in Pourbaix (potential versus pH) diagrams and in potential versus current density curves from potentiodynamic polarization experiments by the fact that, as the potential becomes more positive (or less negative), oxidation reactions become more dominant. If, on the other hand, the reaction in the cell is self-driven (i.e., proceeds spontaneously), the anode is the negative terminal and the cathode is the positive terminal in a so-called *galvanic cell*. This applies to battery discharge and fuel cells, where chemical energy is converted to electric energy. It is reflected in the electromotive force (EMF) series (standard potentials) where, as the standard reduction potential becomes more positive (or less negative), the material is said to be more noble. Open-circuit potential (OCP) measurements yield often, but not exclusively, the reversible potential of the system. The reversible potential represents thermodynamic equilibrium, which is not time dependent. The OCP can be time dependent, as a result of changes of the electrode surface, e.g., the formation of a passive oxide layer. A shift of the OCP with time in the positive direction represents the formation of a more noble (better corrosion resistant) surface, and vice versa.

Consider, for example, the lead-acid battery in a car. In the fully charged state, the negative electrode is metallic lead (Pb^0), while the positive electrode is lead dioxide (PbO_2), in which lead is in the Pb^{4+} state. During discharge, the active material in the negative electrode is oxidized to $PbSO_4$, so by definition it is the anode, and that in the positive electrode is reduced to $PbSO_4$, so by definition it is the cathode. When the battery is charged, the reactions at both electrodes are reversed: in the negative electrode $PbSO_4$ is reduced to Pb^0, so it is the cathode, and in the positive electrode $PbSO_4$ is oxidized back to PbO_2, thus it becomes the anode. The polarity of the electrodes in the cell does not change, but the reactions are reversed, so the anode has become the cathode and vice versa (see Ref. 12 for a detailed discussion of this point).

1. Metal Deposition as a Class of its Own

Electrodeposition may be defined in a broad manner as *the process of depositing a substance upon an electrode by electrolysis*.[8] The essence of electrode kinetics is charge transfer across the interface. A profound understanding of the structure of the electrical double layer, as discussed by Helmholz,[13,14] Gouy-Chapman[15-17] and Stern[18] is needed, of course, in the discussion of the mechanism of charge transfer. There are other important factors, such as catalysis and adsorption, mass-transport limitations and so on, all of which may influence the rate and mechanism of charge transfer to some extent, but it is the very act of charge transfer that matters. It is the vehicle that allows the conversion of chemical to electrical energy, as in a fuel cell or a battery during discharge. It is also the venue by which electrical energy is used to produce desired chemicals, as in the chor-alkali industry, the production of aluminum, electroforming, electroplating and all other electrolytic industrial processes.

Electrode reactions can be classified in two groups:

(a) redox reactions, in which both reactants and products are in solution, and
(b) processes in which at least one of them is part of the electrode itself, or is rigidly attached to it.

(*i*) *Redox Reactions*

A good example of a redox reaction is the reduction of ferricyanide to ferro-cyanide, given by

$$\left[\mathrm{Fe(CN)_6}\right]^{3-}_{\mathrm{soln}} + \mathrm{e}^{-}_{\mathrm{crys}} \rightarrow \left[\mathrm{Fe(CN)_6}\right]^{4-}_{\mathrm{soln}} \qquad (1)$$

This is a typical *outer-sphere charge-transfer reaction*, characterized by the fact that the close environment of the central cation is not changed as a result of charge transfer. Furthermore, it is noted that both reactant and product are on the solution side of the interface, specifically at the Outer Helmholtz Plane (OHP), believed to be at a distance of about 0.5-0.6 nm from the surface of the metal. Charge is transferred across the interface by an electron, and there is no reason to assume that the ionic species have crossed the inter-

face at any point during the charge transfer process. Electron transfer is assumed to occur by tunneling, which is inherently a quantum mechanical process. Nevertheless, there is also a classical aspect of the process shown in Eq. (1), since the electron is treated as a particle that crosses the interface – it is either on the *ferri* or the *ferro* species. No intermediate state corresponding to partial charge transfer is considered.

The example given above is not the only kind of redox reaction where both reactant and product are in solution. Consider the hydrogen evolution reaction, which can be written as

$$2\,H_3O^+_{soln} + 2\,e^-_{crys} \rightarrow H_2 + 2\,H_2O \qquad (2)$$

This is a typical *inner sphere* redox reaction. The proton is heavily solvated (and probably exists in solution as $[H_9O_4]^+_{soln}$, while the interaction of molecular hydrogen with water is minimal. The mechanism of hydrogen evolution has been studied in great detail on different metals and under widely different conditions, and will not be discussed here. It is interesting to point out one major characteristic of this type of reaction, compared to outer-sphere redox reactions. The rate of hydrogen evolution is sensitive to the type of metal electrode used. The exchange current density, i_0, can be as low as 10^{-13} A cm^{-2} on Pb, and as high as 10^{-3} A cm^{-2} on Pt, in 1-M $HClO_4$. Note that a high value of i_0 (that is, higher than, say, 1 μA cm^{-2}) indicates a fast reaction and a non-polarizable electrode. Thus, the electrode clearly acts as a heterogeneous catalyst, since an adsorbed hydrogen atom is formed as an intermediate in this reaction. In comparison, the ferri/ferro redox couple has an exchange current density similar to that of hydrogen evolution on Pt, but it is not sensitive to the type of the electrode used.[†] This is not surprising, considering that both reactant and product are located at a distance of at least 0.5 nm from the electrode surface, far beyond the range of covalent bonding.

Hydrogen evolution is clearly an intermediate case between outer-sphere charge transfer and metal deposition. On the one

[†] Some apparent dependence has occasionally been reported, but this is all but eliminated when proper correction is made for the diffuse double-layer effect.

hand, both the reactant (a solvated proton) and the product (molecular hydrogen) are on the solution side of the interface. On the other hand, an adsorbed hydrogen atom is believed to be formed as an intermediate, indicating that both charge and mass have crossed the interface. This case has been discussed recently by one of the present authors.[19]

(*ii*) *Metal Deposition and Dissolution*

Metal deposition, for the simple case of a monovalent metal ion, is commonly written as:

$$\left[\mathrm{Ag}\left(\mathrm{H_2O}\right)_n\right]^{+}_{\mathrm{soln}} + \mathrm{e}^{-}_{\mathrm{crys}} \rightarrow \mathrm{Ag}^{0}_{\mathrm{crys}} + n \cdot \mathrm{H_2O} \tag{3}$$

The number n of water molecules solvating the ion is not important in this context, as long as it is realized that the energy of solvation is very high—about 5 eV for a monovalent ion, and around 20 eV for a divalent ion (482 and 1,927 kJ mol^{-1}, respectively). It is implicit in Eq. (3) that charge is transferred by an electron crossing the interface, just as in the case of the redox reaction given by Eq. (1). But there is a very great difference between Eq. (1) and Eq. (3). In the former, the ligands around the iron ion are held with a total energy that is much higher than the hydration energy of a silver ion, but they are not removed as a result of electron transfer. Admittedly, there is a solvent rearrangement energy involved (which plays a major role in determining the Gibbs energy of activation, according to the theory of charge transfer developed by Marcus,[20-22] Dogonadze et al.[23-25] and Levich,[26] but this is just a small fraction of the total energy that would be needed to break up the ferri-cyanide complex to its components (i.e., of the solvation energy of the iron ion).

In the reaction represented by Eq. (3), all the solvent molecules must be removed, to allow formation of the product—a neutral silver atom, and its incorporation in the metal lattice. But charge transfer, if it were to occur by electron transfer across the interface, would have to be represented by two steps, as shown in Eqs. (4) and (5):

$$\left[\mathrm{Ag}\left(\mathrm{H_2O}\right)_{\mathrm{n}}\right]^{+}_{\mathrm{soln}} + \mathrm{e}^{-}_{crys} \rightarrow \left[\mathrm{Ag}\left(\mathrm{H_2O}\right)_{\mathrm{n}}\right]^{0}_{\mathrm{soln}} \tag{4}$$

followed by

$$\left[\mathrm{Ag}\left(\mathrm{H_2O}\right)_{\mathrm{n}}\right]^{0}_{\mathrm{soln}} \rightarrow \mathrm{Ag}^{0}_{\mathrm{crys}} + n \cdot \mathrm{H_2O} \tag{5}$$

The electron-transfer step represented by Eq. (4) would be very fast, of the order of 1 fs (10^{-15} s). This is too short for atoms to move. On the other hand, it should take about 10^5 fs for the atom-transfer reaction shown by Eq. (5) to occur, i.e. for the water molecules around the neutral atom to relax to their equilibrium position in bulk water, and for the silver atom to reach the surface and be incorporated in it.

It has been stated by several noted authors in electrochemistry that, in the case of metal deposition, charge is carried across the interface by ions rather than by electrons.[27-30] Unfortunately, the above authors did not implement the consequence of this difference in the analysis of the mechanism of metal deposition and dissolution. In one instance,[29] the author went as far as to state that

> "…although charge is transferred across the interface by the metal ions, the mechanism will be treated as though it were electron transfer, for convenience."

This approach cannot be sustained, since electron and ion transfer represent two physically different phenomena, and there is no justification to assume that they would follow the same rules.

The mechanism of charge transfer during metal deposition and dissolution was treated recently by Gileadi,[19,31-34] and will not be discussed here in detail. It was shown that the Gibbs energy of formation of an isolated neutral silver atom in solution is about 2.55 eV higher than that of formation of the same atom in bulk silver.* Hence, the reversible potential for formation of an isolated atom in solution would be –2.55 V vs. Ag^{+}/Ag, and it could not occur anywhere near the reversible potential for silver deposition.

*In general, the difference between these two quantities is approximately equal to the energy of sublimation of the metal considered, which is typically in the range of 1–4 eV.

Moreover, according to the Marcus theory of charge transfer, electron transfer can only occur when the initial and final states are brought temporarily to the same energy level. This follows from the *time-resolved nature of the kinetics of charge transfer*. If electron transfer causes a change in the overall Gibbs energy of the system, it would violate the law of conservation of energy, since rearrangement of the atoms that could provide or dissipate the difference in Gibbs energy occurs on a much longer time scale. Consequently, it was concluded by Gileadi et al.[19,31-34] that in metal deposition and dissolution reactions, charge is carried across the interface by ions rather than by electrons.

Accepting that charge is carried across the interface by ions has a major impact on the way the mechanism of metal deposition and dissolution reactions should be interpreted. First, it can no longer be assumed that the symmetry factor β (that reflects the fraction of total electrochemical Gibbs energy added to the system, which is used to change the electrochemical Gibbs energy of activation of the charge-transfer reaction) is roughly equal to 0.5. Such a value implies that the transition state is formed midway between the reactants and products. To be sure, the experimental evidence for the use of this value in metal deposition was never satisfactory, and the theory of Marcus[20-22] and of Dogonadze et al.[23-25] and Levich,[26] which can predict values close to 0.5 under certain limiting conditions, was developed for outer-sphere charge transfer processes, not for metal deposition. But these theories were at least developed to apply for electron transfer. Moreover, when the discharge of a divalent ion is concerned, it has been the common practice to assume that electrons can only be transferred across the interface one at a time, and mechanisms were postulated to fit the data to this hypothesis (still assuming that $\beta \cong 0.5$). Accepting that charge is carried across the interface by the divalent ion (in the deposition of nickel, for example) renders the question of whether simultaneous two-electron transfer can or cannot occur redundant during metal deposition.* In such a process, the *effective charge* on the ion decreases gradually as the ion approaches the metal sur-

*However, the question of simultaneous two-electron transfer in outer-sphere charge-transfer processes, such as $Tl^{3+} + 2e^- \rightarrow Tl^+$, vs. consecutive transfer of two electrons, one at a time, is still open, as discussed elsewhere.[35]

face, and there is no singular point at which a full electronic charge would have been transferred.

(a) Morphology of the surface

Another distinct way in which metal deposition differs from redox reactions in solution is that the morphology of the surface may change during deposition. The surface roughness usually increases during deposition, particularly if the current distribution is not uniform, and whenever the current applied is close to the mass-transport limited current density in the same system. This would decrease the true current density, which is calculated per unit of *real surface area* taking into account the changes in the roughness factor, although the total current applied is maintained constant, thus distorting the shape of the Tafel plot.

(*b*) *The nature of the substrate*

In most cases the nature of the substrate upon which a metal is deposited is of little consequence, since it is rapidly covered by a layer of the metal being deposited. The continuous renewal of the surface can be used beneficially in the context of maintaining a clean surface. It was shown by Gileadi[36] that for a dropping mercury electrode with a drop time of 1 s, an impurity level of 10 μM can be tolerated without having a significant effect on the results, since the maximum mass-transport limited flux of the impurity can lead to no more than 1% of surface being covered by the impurity, per second. A similar calculation can be made for metal deposition on a solid substrate. Thus, for a divalent ion, a monolayer corresponds to approximately 0.5 mC cm^{-2}. When plating at a rate of, say, 10 mA cm^{-2}, about 20-atomic layers are formed per second. Although it cannot be assumed that the metal is deposited in an orderly fashion, layer by layer, it would be safe to assume that the whole surface would be renewed at least once a second, and probably more often than that. Allowing an impurity level of 10 μM would limit the coverage by impurity to just a few percents of a monolayer per second. Indeed, one of the major stumbling blocks in the study of redox reactions on solid electrodes is the difficulty in maintaining the surface free of impurities during a series of measurements that may take several minutes. During metal deposi-

tion this difficulty is by and large eliminated, since the surface is being renewed continuously, and deposition occurs always on a virgin surface.

(*c*) *Underpotential deposition (UPD)*

A unique feature observed in metal deposition on a foreign substrate is underpotential deposition. It is found that a metal can be deposited on a foreign substrate at potentials positive with respect to the reversible potential for deposition of the metal in the same solution. Considering, for example, the deposition of silver on platinum, which can be written as

$$\left[\mathrm{Ag}\left(\mathrm{H_2O}\right)_n\right]^+_{\mathrm{soln}} + \mathrm{e}^-_{\mathrm{crys}} + \mathrm{Pt} \rightarrow \mathrm{Ag_{ads}/Pt} + n \cdot \mathrm{H_2O} \qquad (6)$$

it is implied here that the discharged silver atom is adsorbed on the surface of the platinum substrate and is chemically bound to it. The reaction represented by Eq. (6) can occur at potentials positive with respect to the reversible potential for silver (i.e., at an underpotential) only if the Ag-Pt bond is stronger than an Ag-Ag bond. This is not always the case, but when it is, it will naturally be the first step in metal deposition, and may have an important role in the binding between the plated coating and the surface of the substrate.

Underpotential deposition, as defined by Eq. (6), should be inherently terminated when a full monolayer has been formed, since the second layer is no longer deposited on the substrate. This is usually the case, but in certain instances (notably, for UPD of Ag on Pt) as much as two atomic layers can be deposited before the reversible potential is reached and bulk deposition takes over.[37] This observation can be rationalized, considering that the properties of Ag atoms in the first layer on top of a Pt surface could be quite different from those in the bulk of silver. In other words, the surface of Pt below a single atomic layer of Ag could influence the chemical properties of this layer and its energy of bonding to the second layer. The effect is, however, short ranged, and it is not expected to extend further.

Underpotential deposition has been studied extensively,[38-42] mostly for single-crystal substrates. The behavior of different crys-

tal faces has been examined,[43-48] two-dimensional phases were observed, and correlation between the UPD potential shift Δ_{UPD} (defined as the potential difference between the reversible potential and the potential observed at a partial surface coverage $\theta = 0.5$) was related to the difference in the work function of the two metals.[38] While these are issues of great importance for the fundamental understanding of UPD formation, applied issues such as the dependence of adhesion of a coating on the formation of a UPD layer have not been discussed.

(*d*) *A complexing agent*

In a large majority of practical plating baths, a complexing agent is used to improve the quality of the product, in particular to obtain smooth and bright deposits. On the other hand, when deposition at a high rate is needed, as for electroforming, the metal is deposited from a simple solution containing no complexing agent. Until about the middle of the 20th century, the most commonly used complexing agent was cyanide. Many metals such as Au, Ag, Cu, Ni, Co, Cd and Zn were plated from alkaline baths containing KCN. This practice was abandoned for environmental considerations, in spite of the fact that it was most satisfactory from the purely engineering point of view. Cyanide has been replaced by other complexing agents, mostly organic poly-acids, having two or more carboxylic groups, such as citrate, oxalate, etc. The main purpose of formation of the complex is to slow down the kinetics of the electrodeposition reaction. It should be noted that in most industrial electrolytic processes, such as the production of metals, the chlor-alkali industry and in organic electrosynthesis, as well as in batteries and fuel cells, fast kinetics is an advantage – decreasing the overpotential and thereby reducing energy consumption. The opposite is true in metal deposition. Decreasing the exchange current density is equivalent to increasing the Faradaic resistance, i.e. the resistance associated with the charge transfer process. This generally leads to improved uniformity of the deposited layer and enhanced smoothness and brightness of the deposit.

(*e*) *The types of overpotential and the relevant scale*

The processes taking place in an electrochemical cell during metal deposition can be modeled by a combination of three resistors in series, each associated with an overpotential given by the product of the applied current density and the relevant resistance:

- *Ohmic solution resistance,* R_{soln}. It is determined by the specific resistivity of the solution and by the configuration of the cathode and the anode with respect to each other, as well as their respective shapes. The corresponding contribution to the observed overpotential is called the iR_{soln} potential drop or η_{iR}, the resistance overpotential. When this is the largest resistance in the system, the process is said to occur under conditions of *primary current distribution*. The relevant scale to be considered is of the order of a few millimeters up to several centimeters. Primary current distribution usually leads to non-uniform current distribution on the cathode, resulting in non-uniform thickness of the coating.
- *Faradaic resistance,* R_F. This resistance is directly related to the Faradaic reaction taking place. It is also called the charge-transfer resistance, R_{ct}, or the (non-Ohmic) activation resistance R_{ac}, since it is associated with the finite rate of the electrode reaction per se. The corresponding overpotential is usually referred to as the activation, or charge-transfer overpotential, η_{ac} or η_{ct}, respectively. Since charge transfer occurs over a distance of about 0.6 nm, the relevant scale is in the range of a few nanometers. When the Faradaic resistance is the largest resistance in the system, the reaction is said to be *activation controlled* and *secondary current distribution* is maintained. It should be obvious that secondary current distribution leads to uniform thickness of the deposit, on the macroscopic scale. For example, in a barrel plating process for plating screws, primary current distribution will lead to excessive coating on the top of the grooves and no coating at the bottom. In contrast, secondary current distribution will lead to much more uniform coating thickness throughout the groove.

The transition from primary to secondary current distribution can be characterized by a dimensionless parameter called the *Wagner number* (W_a), defined as

$$W_a \equiv \frac{\kappa\left(\partial\eta/\partial i\right)_{c,T}}{l} = R_F / R_{soln} \tag{7}$$

where κ is the specific conductance of the solution (S cm^{-1}) and l is a characteristic length, usually related to the dimensions of the electrodes or their distance apart. Values of $W_a > 10$ correspond to secondary current distribution, while $W_a < 0.1$ indicates primary current distribution.

- *Concentration resistance, R_{conc}.* The third factor determining the nature of the deposit is mass transport. The corresponding resistance is referred to as the *concentration resistance*, R_{conc}, which results from the depletion of the electro-active species at the cathode surface, caused by mass-transport limitation. The mechanism of mass transport of the electro-active species (either charged or uncharged) could be diffusion, convection or migration, or some combination of these mechanisms. For the simple one-dimensional case (corresponding to semi-infinite linear diffusion) at steady state, the rate of mass transport, expressed as the current density, can be written as

$$i = nFD\frac{\left(c_{bulk} - c_{surf}\right)}{\delta} \tag{8}$$

where D is the diffusion coefficient (cm^2 s^{-1}), c_{bulk} and c_{surf} (mol cm^{-3}) represent the concentrations of the reactant in the bulk of the solution and at the surface of the cathode, respectively, and δ (cm) is a characteristic length, called *the Nernst diffusion layer thickness*, which is determined by the conditions of the experiment. For example, in a rotating disc experiment, δ is in the range of 5–50 μm, for rotation rates of 1×10^4 to 1×10^2 rpm, respectively.*

*The exact value depends on the diffusion coefficient of the electro-active species and on the viscosity of the solution, as given by the well-known Levich equation. The above range was calculated for $D = 1\times10^{-5}$ cm^2 s^{-1} and $\nu = 1\times10^{-2}$ cm^2 s^{-1}, which is a reasonable approximation to dilute aqueous solutions at room temperature.

In industrial operations, stirring is typically implemented by moving the electrodes, stirring the solution, or pumping it through the bath (the latter provides an opportunity to filter the solution and remove particulate material that could damage the quality of the metal coating, but that issue is outside the scope of this chapter). The typical values of δ, under industrial plating conditions, may be 50-150 μm, placing it between the values relevant for primary and secondary current distributions. If the experiment is set up so that diffusion is the sole mode of mass transport, then δ is given by

$$\delta = \sqrt{\pi D t} \tag{9}$$

yielding values of δ of 80–180 μm after 10 seconds, for a typical range of values of the diffusion coefficient in dilute aqueous solutions.

The limiting current density, i_L, which represents the highest rate at which the metal can be deposited under given experimental conditions, can be derived from Eq. (8) by setting $c_{surf} = 0$

$$i_L = nFD\left(c_{bulk} / \delta\right) \tag{10}$$

In practice, deposition of metals is conducted at current densities well below the limiting current, in the range of $i \leq 0.3\ i_L$. At higher current densities, the deposits tend to be rough, powdery or friable.

As in the cases discussed above, one can define a resistance characterizing the mass-transport limitation and a corresponding concentration overpotential η_{conc}. The value of this parameter, compared to the Faradaic resistance, determines the brightness and smoothness of the deposit, but has little influence on the uniformity of the thickness, since the characteristic length associated with it (ca. 0.01 cm) is

two or three orders of magnitude smaller than that associated with primary current distribution.

It is hardly necessary to point out that non-uniform current distribution can lead to poor performance in any industrial process.* For alloy deposition this may be even more critical, considering that the composition of the alloy is often a function of current density. Thus, a non-uniform current distribution might lead to non-uniformity of the alloy composition, in addition to variation of the thickness of the coating.

(*f*) *The roughness factor*

The roughness factor is an important parameter in the context of the study of electrode kinetics. It is defined as the ratio of *the real to geometric* surface area. But what is the so-called *real surface area*? That depends on the relative values of the three overpotentials, or more precisely, the values of the three resistances associated with them. Thus, under conditions of primary current distribution (or in the transition region between primary and secondary current distribution, where $0.1 < W_a < 10$), maintaining a uniform thickness may be the most important issue. This is determined by the uniformity of the distance between the anode and the cathode, on a scale of about 0.01 cm (i.e. about 1% of the total distance between the electrodes). Whether the cathode is rough or smooth on the atomic scale of 1 nm will have absolutely no effect on the thickness. At the mass-transport limited current, where the characteristic length is 5–150 μm, the roughness on the atomic scale is also irrelevant. On the other hand, when charge transfer or adsorption are concerned, the roughness on the atomic scale is the most important parameter. Specifically, it is important to note that the roughness factor, as determined by the maximum amount of atomic hydrogen or oxygen adsorbed on the surface, or by measurement of the double-layer capacitance, is quite irrelevant when the mass-transport limited current density is considered.

---

* Except in cases where the non-uniformity is intentionally built into the process, to increase the thickness of the plating where it is needed, and vice versa.

This raises some important possibilities, which have not escaped the attention of the electroplating community. For example, while metal deposition is conducted in fairly concentrated solutions of the metal being plated, and at current densities well below the mass-transport limit, additives acting as inhibitors for metal deposition are often introduced at concentrations that are several orders of magnitude lower, to ensure that their supply to the surface will be mass-transport limited. In this way, the tendency for increased rate of metal deposition on certain features on the surface, such as protrusions, will be moderated by the faster diffusion of the inhibitor to the very same areas. Furthermore, if deposition occurs in the region of mixed control, which is usually the case, it must be remembered that the relevant roughness factor is quite different for the charge-transfer and the mass-transport processes, and this may well be a function of current density, since the Faradaic resistance is inherently potential dependent.

(*g*) *Hydrogen evolution*

In most electroplating baths of practical interest, hydrogen evolution occurs as a side reaction. Under cathodic overpotentials, the following reactions can lead to discharge of protons and adsorption of atomic hydrogen on the cathode:

$$H_3O^+ + e^-_{crys} \rightarrow H_{ads} + H_2O \tag{11}$$

$$H_2O + e^-_{crys} \rightarrow H_{ads} + OH^- \tag{12}$$

While Eq. (11) is relevant for relatively low pH values (pH $\leq$ 3),* Eq. (12) applies at higher values of the pH. The adsorbed hydrogen atoms, formed as intermediates, can recombine and evolve as gas bubbles (molecular hydrogen) in solution, following one of two possible mechanisms:

$$H_{ads} + H_{ads} \rightarrow H_2 \tag{13}$$

*This pH value was chosen because at higher pH, the reduction of the protonium ion may become mass-transport limited and reaction 12 would occur instead.

$$H_{ads} + H_3O^+ + e^-_{crys} \rightarrow H_2 + H_2O \quad (14a)$$

$$H_{ads} + H_2O + e^-_{crys} \rightarrow H_2 + OH^- \quad (14b)$$

Equation (13) is called atom-atom recombination, which is not directly dependent on potential, but is influenced by it through the dependence of the fractional surface coverage by atomic hydrogen on potential. Equations (14a) and (14b) represent electrochemical charge transfer steps at low and high values of pH, respectively. Finally, a (typically small) portion of the *ad*sorbed hydrogen may be *ab*sorbed in the metal:

$$H_{ads} \rightarrow H_{abs} \quad (15)$$

This absorbed hydrogen can then be transported inside the metal electrode via a diffusion mechanism, which is enhanced by the high subsurface concentration of hydrogen that can be predicted by Sieverts' Law* for high fugacity. The extent of hydrogen absorption depends on bath composition, temperature and pH, the applied current density, surface barriers (e.g., oxides), and surface poisoning agents such as compounds of As, P, Sb, Te, Se and S, which are known to reduce the partial surface coverage on the one hand, and to interfere with surface recombination of hydrogen atoms (cf., Eq. 13) on the other hand, thus enhancing the alternative reaction pathway of absorption of hydrogen in the bulk of the metal (cf., Eq. 15).

Once inside the metal electrode, diffusing hydrogen atoms can recombine around defects such as micro-voids, inclusions, interfaces and grain boundaries, forming molecular hydrogen. High-

* Sieverts' Law: $c = K_S\sqrt{P}$, where c is the subsurface concentration (solubility) of the dissolved atom in the solid metal, P is the partial pressure of the diatomic gas (sometimes replaced by the fugacity, f), and K_S is the solubility constant (temperature dependent), which is the chemical equilibrium constant between the molecular species in the gas phase and the atomic species within the metal lattice. This empirical relation was first demonstrated by Sieverts in 1929 for the solubility of hydrogen in iron. Departures from this law occur at high gas pressures and/or high concentrations of dissolved atoms.

pressure bubbles may be formed inside the cathode,[49-52] ultimately leading to crack initiation and/or propagation, even in the absence of significant applied loads.[53,54] Other mechanisms, which do not involve bubble formation, can lead to hydrogen embrittlement of electrodeposited parts.[54-56] These include the decohesion (i.e., reduction in the lattice cohesion forces in regions of high hydrogen concentration)[57,58] or adsorption (i.e. reduction in surface energy due to hydrogen adsorption)[59] mechanisms, the hydride formation mechanism (i.e. formation and cleavage of brittle hydrides),[60-62] and mechanisms of hydrogen interaction with dislocations[63-66] (e.g., establishment of drag forces,[67] local hardening at existing crack tips due to hydrogen,[68] hydrogen-enhanced localized plasticity,[62,69] sweep of hydrogen atoms by dislocations[70] that enables local accumulation of hydrogen – exceeding a critical concentration, etc.). The term *hydrogen embrittlement* refers to reduced ductility, non-ductile fracture mode, and reduced tensile strength caused by exposure to hydrogen. Hydrogen-related stresses may also induce shear stresses at the substrate/coating interface. These high stresses might overcome the adhesion strength and lead to delamination of the coating. Cracks in the deposit also provide channels for penetration of humidity and oxygen that, upon reaching the interface between the coating and the substrate metal, can initiate corrosion and/or delamination of the coating. Hydrogen evolution also leads to local increase in pH, increasing the concentration of hydroxide ions that can be incorporated in the electrodeposit, thus changing its properties.

(*h*) *The current efficiency*

The current efficiency, also called the Faradaic efficiency (FE), is the fraction of the total current used to deposit the metal (or metals, during alloy deposition). The danger of hydrogen-induced cracking (HIC), also referred to as hydrogen-assisted cracking (HAC), increases in electrodeposition systems with lower cathode current efficiencies (such as hard chromium). In highly efficient systems, such as Cu and Ag baths, codeposition of hydrogen occurs only when i_L is exceeded, or when the added complexing agents shift the potential of metal deposition to sufficiently negative values. The higher the hydrogen overpotential on a given metal, the lower the amount of hydrogen absorbed in it.

The effects of internal hydrogen are most significant in high-strength steels (yield strength greater than 1.17 GPa, or 170 kpsi). In general, the higher the strength level of the steel, the greater its susceptibility to hydrogen embrittlement. Although hydrogen diffusion in martensitic and ferritic structures is relatively rapid, it is not always a simple task to remove this hydrogen once it has entered the steel. Baking is required following electrodeposition for all steel parts hardened to at least 40 HRC. This process is performed at a temperature in the range of 177-205°C for at least 3 h, and should be applied not later than 4 h after the completion of the plating process.[71] Unfortunately, this post-treatment is not always sufficient. Although hydrogen diffusivity increases exponentially with increasing temperature, the required time to reduce the hydrogen concentration to a desired level increases with the square of the thickness of the part being coated. For thick sections this may mean hundreds of hours of baking. Even then, there is no guarantee that permanent damage or irreversible hydrogen embrittlement has not already occurred.[56] ASTM has suggested a standard test method for mechanical testing of plated specimens in order to identify hydrogen embrittlement due to plating processes and service environments.[72]

It should be noted that the FE is often found to depend on current density. In this context, a decrease in FE with increasing current density could lead to improved uniformity of plating. While the current density is higher on a protrusion, the current efficiency is lower, hence the rate of deposition of the metal may remain constant or even decrease. On a recessed area the opposite behavior is expected, of course. Thus, the variation of the FE could act as a negative feedback, enhancing the uniformity of the thickness of the coating. An increase in current efficiency with increasing current density would have an opposite effect of creating a positive feedback, leading to rapid roughening of the surface. Low FE also leads to increased consumption of electricity, but this is usually not a major issue in electroplating.

2. Specific Issues in Electrodeposition of Alloys

(*i*) *History*

The first alloys to be electrodeposited were brass (Cu-Zn alloys) and alloys of the noble metals. Faust[48] reviewed the principles of alloy deposition. In order to codeposit two metals, they must be in a bath in which the individual reversible potentials are reasonably close to each other. This is the case when the standard potentials E^0 of the two metal are close, as for deposition of tin-lead alloys where the values of E^0 are –0.126 V and –0.136 V vs. SHE for Pb and Sn, respectively. Changing the concentration of one of the metals in solution can bring the reversible potentials closer to each other. However, since the Nernst equation allows for only (59/*n*) mV per decade change in concentration, where *n* is the number of electrons needed to deposit a metal atom, this has a limited range of applicability. When the two metals forming the alloy have widely different values of E^0, their reversible potentials can be shifted closer to each other by adding a complexing agent that forms complexes with different stability constants, since the reversible potential in the presence of a ligand that forms a suitable complex is given by

$$E_{\text{rev}} = E^0 + \frac{2.3\,RT}{nF}\log K + \frac{2.3\,RT}{nF}\log c_{Me^{z+}} \tag{16}$$

where R is the ideal gas constant (8.314 J $K^{-1}mol^{-1}$), T is the absolute temperature, F is Faraday's constant, $c_{Me^{z+}}$ is the bulk concentration of the metal ion being deposited (neglecting activity coefficients), and K is the stability constant of the complex, which is different for different metals. Equation (16) can be rewritten as

$$E_{\text{rev}} = E^{0'} + \frac{2.3\,RT}{nF}\log c_{Me^{z+}} \tag{17}$$

where

$$E^{0'} \equiv E^{0} + \frac{2.3RT}{nF}\log K \tag{18}$$

is the effective standard potential in the presence of the complexing agent.*

(*ii*) *Special Considerations Related to Alloy Deposition*

Alloy deposition is similar to metal deposition in the sense that the surface is being renewed continuously during formation of the deposited layer. Hence, the nature of the substrate is of little importance, except in special situations, where a single-crystal substrate is employed and epitaxial growth of the deposit takes place. Epitaxy, or oriented overgrowth, is a special case of heterogeneous nucleation, where the deposit grows with a crystal structure that conforms to that of the substrate, at least up to a certain thickness. Depending on the binding energy and the crystallographic misfit between the deposit and the substrate, the growth may take place layer-by-layer according to the Frank-van der Merwe model,[73] by three-dimensional islands formation according to the Volmer-Weber model,[74] or by a combination of both according to the Stranski-Krastanov model.[75]

Considerations of the mechanism of charge transfer discussed for metal deposition apply also to alloys, but there are some differences. First, it must be realized that alloy deposition is a complex process, in which at least two parallel reactions take place simultaneously (i.e., the deposition of the two metals constituting the alloy), and in many cases hydrogen evolution constitutes a third parallel reaction.

When a complexing agent is employed, which is usually the case, attention should be paid to the solution chemistry in the mul-

---

* Activity coefficients can, as a rule, be neglected for moderately dilute solutions (say, up to 1–2 M), since they appear in the Nernst equation in logarithmic form. Thus, for example, if the activity coefficient is only 0.8, instead of an assumed value of 1.0, the resulting error in the value of E_{rev} is only (5.7/n) mV. It should be borne in mind, however, that in highly concentrated electrolytes, such as 30% KOH or 85% H_3PO_4, used in some batteries and fuel cells, such an approximation is no longer valid and may introduce significant errors.

ti-component plating baths and to possible formation of complexes containing both metals, in addition to the usual complexes of each metal with the ligand. For two metals Me_1, Me_2 and a monovalent negatively charged ligand L^-, there could typically be several species in solution, such as

$$Me_1^{z+};\ Me_2^{z+};\ [\,Me_1L_n\,]^{(z-n)};\ [Me_2L_n]^{(z-n)};\ [Me_1Me_2L_m]^{(2z-m)} \tag{19}$$

and each of the above species could be electro-active, allowing deposition of one of the metals or both. Thus, the resulting alloy may be formed by deposition of each metal separately, or from the complex containing both metals. Evidently, there could be several parallel reactions taking place simultaneously. Measurement of the current-potential relationship in such complex systems would not be meaningful. Even if the experimental data can be *forced* to provide a linear Tafel region, from which an apparent Tafel slope is obtained, this will have little relevance to the mechanism of formation of the alloy. Although the above observation is well known and could be considered rather obvious, it has been overlooked in many publications.

The above does not imply that it is impossible to study the mechanism of alloy deposition; it only shows that conclusions cannot be drawn from the usual interpretation of the directly observed current-potential relationship employed in the analysis of electrode kinetics. The partial currents for deposition of each of the alloying elements should be determined as a function of potential and other experimental parameters via determination of the atomic composition of the alloy and the FE. The FE during alloy deposition can be different from that of single-metal deposition of one or both metals involved in the process. Hence, the FE can be expected to depend on the composition of the alloy, and the thickness distribution may differ from that expected according to the current distribution.[42]

The Faradaic efficiency can be calculated using the equation:

$$FE = \frac{w}{It_d} \sum \frac{x_i n_i F}{M_i} \times 100 \tag{20}$$

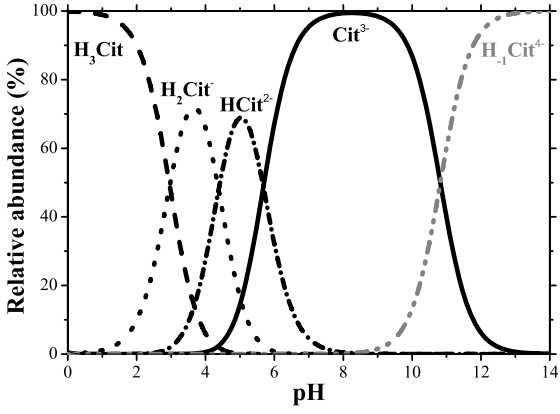

Figure 1. (a) Stepwise deprotonation of citric acid as a function of pH. The notation $H_{-1}Cit^{4-}$ refers to citrate ion in which all three acidic protons, as well as the proton on the alcoholic group, have been removed. (b) Concentration distribution of Ni^{2+}-Cit^{3-} complexes as a function of the overall citrate concentration (0.1 M $NiSO_4$, pH = 8.0).

where w is the measured weight of the deposit (g), I is the total current passed (A), t_d is the deposition time (s), x_i is the weight fraction of the element in the alloy deposit, n_iF is the number of coulombs per mole for the reduction of the element, and M_i is the atomic mass (g mol^{-1}). Detailed consideration of the species that exist at equilibrium in the plating bath, which can be calculated if the relevant stability constants of the complexes are known, would then provide further insight regarding the fundamental factors determining alloy composition, possible anomalies, changes in morphology, and so on.

In Fig. 1 we show two examples. Citric acid, which is a commonly used ligand, has three carboxylic groups and one alcoholic group. It can exist in solution as the neutral molecule or as ions carrying a negative charge of 1-4, depending on pH. The distribution of these species as a function of pH is shown in Fig. 1a. The corresponding pK_i values are given in Table 1. For pH values in the range of 7-10 the predominant species is the triply-charged anion Cit^{3-} ($C_6H_5O_7^{3-}$). The distribution of its complexes with Ni^{2+} is shown in Fig. 1b, as a function of the overall concentration of citrate at pH = 8. The corresponding $\log(\beta_n) \equiv \sum_{i=1}^{n} pK_i$ values, where β_n are the equilibrium constants for the reactions Me + n·L $\rightarrow$ [MeL$_n$] that form the protonated complexes, are provided in Table 1. Two complexes are shown. Free Ni^{2+} and $[NiCit]^-$ are seen to be the predominant species, as long as the concentration ratio is Cit/Ni $\leq$ 1. The concentration of free Ni^{2+} falls almost to zero when the above ratio reaches unity. As the concentration of citrate is increased further, a different complex, $[Ni(Cit)_2]^{4-}$ becomes predominant. When the ratio Cit/Ni $\geq$ 4, all the Ni^{2+} ions are in this highly charged complex, which is very stable, and deposition of Ni from it is strongly impeded. Thus, although citrate is a very useful ligand for plating baths containing nickel, a large stoichiometric excess may be detrimental to their performance.

In this context, it is appropriate to draw attention to an error often committed in electroplating, and particularly in alloy plating. In plating transition metals and their alloys, a citrate bath is often used and the pH is in the range of 6–9. The purpose of using the citrate (or other organic poly-acids) is to form a complex and prevent deposition of hydroxides of the metals. An unspecified

amount of ammonium hydroxide (NH_4OH) is often added to increase the FE and fine-tune the pH to the chosen value. The fact that NH_3 forms well-known complexes with most transition metals, as shown in Fig. 2a for the case of Ni^{2+} (see pK_a and $\log(\beta_n)$ values in Table 1), is ignored, in spite of the fact that it could change significantly the distribution of the metal ions in the different complexes that can be formed in the system. A detailed discussion of this issue is given below, in the section dealing with induced codeposition of Ni-W alloys. Finally, Fig. 3,[6,76,77] summarizes most of the metal pairs that have been codeposited electrochemically, either commercially or in laboratory studies.

Table 1
Equilibrium Constants for Acid Dissociation and Complex Formation. An Increased Index Number Reflects a Higher Deprotonation/Complexation State

Species/Complex	pK_a	$\log(\beta_n)$	Relevant figure	Ref.
$[(H)_n(Cit)]^{-(3-n)}$ n = –1 corresponds to $[H_{-1}Cit]^{4-}$ (c.f. caption to Fig. 1)	$pK_1 = 2.96$ $pK_2 = 4.38$ $pK_3 = 5.68$ $pK_4 = 10.82$	$\log(\beta_1) = 2.96$ $\log(\beta_2) = 7.34$ $\log(\beta_3) = 13.02$ $\log(\beta_4) = 23.84$	1a	193
$Ni(Cit)_n^{-(3n-2)}$	$pK_1 = 5.50$ $pK_2 = 2.30$	$\log(\beta_1) = 5.50$ $\log(\beta_2) = 7.80$	1b	195
$[Ni(NH_3)_n]^{2+}$	$pK_1 = 2.80$ $pK_2 = 2.24$ $pK_3 = 1.73$ $pK_4 = 1.19$ $pK_5 = 0.75$ $pK_6 = 0.03$	$\log(\beta_1) = 2.80$ $\log(\beta_2) = 5.04$ $\log(\beta_3) = 6.77$ $\log(\beta_4) = 7.96$ $\log(\beta_5) = 8.71$ $\log(\beta_6) = 8.74$	2a	194
NH_4^+ / NH_3	$pK_1 = 9.25$	$\log(\beta_1) = 9.25$	2b	193
$[(WO_4)(Cit)(H)_m]^{-(5-m)}$	$pK_1 = 4.64$ $pK_2 = 6.82$ $pK_3 = 10.21$	$\log(\beta_1) = 4.64$ $\log(\beta_2) = 11.46$ $\log(\beta_3) = 21.67$	8	137
$[(MoO_4)(Cit)(H)_m]^{-(5-m)}$	$pK_1 = 4.58$ $pK_2 = 6.83$ $pK_3 = 8.25$	$\log(\beta_1) = 4.58$ $\log(\beta_2) = 11.41$ $\log(\beta_3) = 19.66$	13a	196

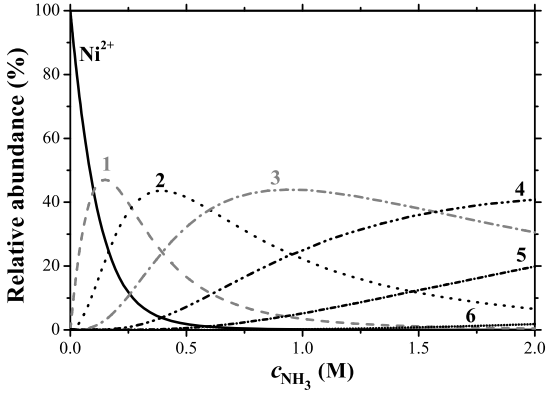

(a)

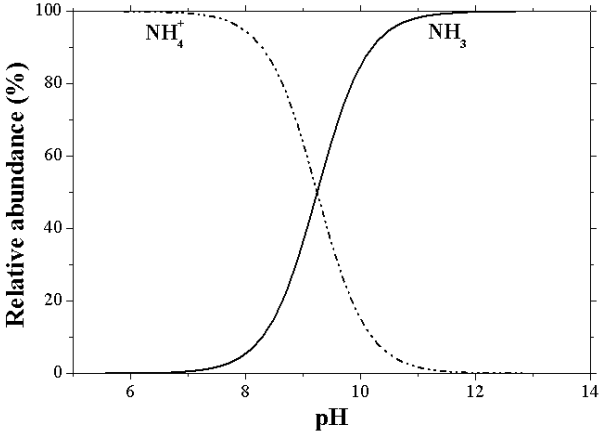

(b)

Figure 2. (a) Concentration distribution of $[Ni(NH_3)_n]^{2+}$ complexes as a function of the overall ammonia concentration (0.1 M $NiSO_4$, pH = 8.0, pK_a = 9.25). The numbers adjacent to the curves represent the values of n in the above formula. (b) The relative abundance of NH_3 and NH_4^+ as a function of pH (pK_a = 9.25).

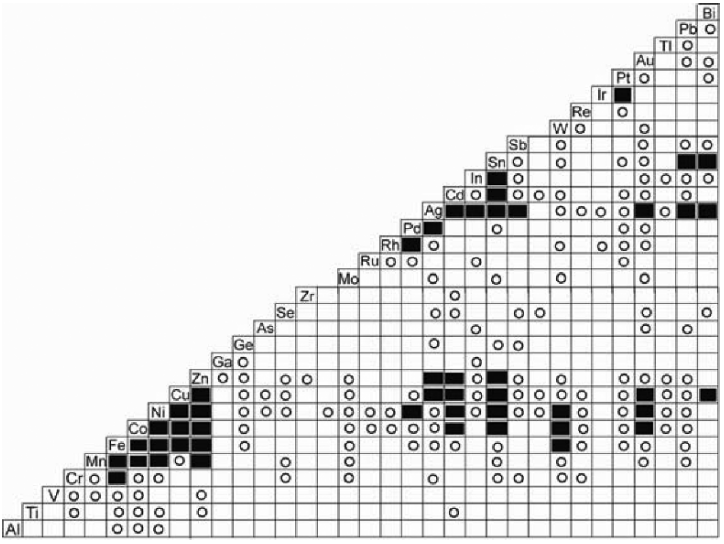

Figure 3. Metal pairs that have been codeposited electrochemically: ○ = Demonstrated in laboratory studies and/or small-scale applications, ■ = Technically interesting, widely employed alloys. Reprinted from Ref. 6, Copyright (2004) with permission from Elsevier.

(*iii*) *Anomalous Alloy Deposition*

The term anomalous codeposition (ACD) was first introduced by Abner Brenner,[78] to describe an electrochemical deposition process in which the less noble metal is deposited preferentially under most plating conditions. This behavior is typically observed in codeposition of iron-group metals (i.e. Fe, Co and Ni) or in codeposition of an iron-group metal with Zn or Cd, with either inhibition or acceleration of the rate of deposition of one of the alloying elements by the other.[7,78-84]

As a first approximation, one might expect that the composition of an electroplated alloy would be related to the current observed for each of the elements, when measured alone in the same solution at the same potential. Assume, for simplicity, that both metals are deposited at high negative overpotentials, within the linear Tafel region (where $\eta/b \geq 1$). Then, one could write the

partial cathodic current densities in terms of the activation overpotentials as

$$i_{c,1} = -i_{0,1}\exp\left(-\frac{\alpha_{c,1}F}{RT}\eta_{c,1}\right) = -i_{0,1}\times 10^{(-\eta_{c,1}/b_1)} \tag{21}$$

$$i_{c,2} = -i_{0,2}\exp\left(-\frac{\alpha_{c,2}F}{RT}\eta_{c,2}\right) = -i_{0,2}\times 10^{(-\eta_{c,2}/b_2)} \tag{22}$$

where b is the Tafel slope (in units of V decade^{-1}), α_c is the cathodic transfer coefficient, and the subscripts 1 and 2 refer to the two elements. It can be noticed that the transfer coefficient is simply the inverse Tafel slope in dimensionless form:

$$\alpha \equiv \frac{2.3RT}{F}\frac{1}{b} \tag{23}$$

Typical values of b_c are in the range 30 to 300 mV decade^{-1}, corresponding to α_c values of 2 and 0.2, respectively, but values close to 0.1 V decade^{-1} are most commonly observed in metal deposition. When the exact value for a specific system is unknown, the approximation $b_a = |b_c| = 0.12$ V decade^{-1} has often been used, although there is no theoretical basis to support this choice, and it would be more accurate to obtain the value of b_a from α_a, employing the simple relationship

$$\alpha_c + \alpha_a = n \tag{24}$$

The exchange current densities and the Tafel slopes for two metals are in general different, although they may happen to be close to each other for a particular case. The overpotential is not the same for the two metals, of course, although deposition takes place at the same potential, measured with respect to a given reference electrode. In other words, at the deposition potential, E_{dep}, one has

$$\eta_1 = E_{dep} - E_{rev,1} \quad \text{and} \quad \eta_2 = E_{dep} - E_{rev,2} \tag{25}$$

Assuming, for simplicity, that the two Tafel slopes are equal, the atom ratio of the two elements in the alloy should be given by

$$\frac{i_{c,1}}{i_{c,2}} = \frac{i_{0,1}}{i_{0,2}} \exp(-\frac{E_{rev,1} - E_{rev,2}}{b_c}) \tag{26}$$

independent of the deposition potential. If this is observed experimentally to be the case, then alloy deposition should be considered *normal* or *ordinary*. As it turns out, such behavior is the exception rather than the rule!

In Fig. 4, the partial current densities for two metals are shown. Having the case of Ni-Fe alloy in mind, typical values were chosen for i_0 and b_c, as specified in the caption of this figure. A line for hydrogen evolution is also shown, from which the Faradaic efficiency could be calculated as

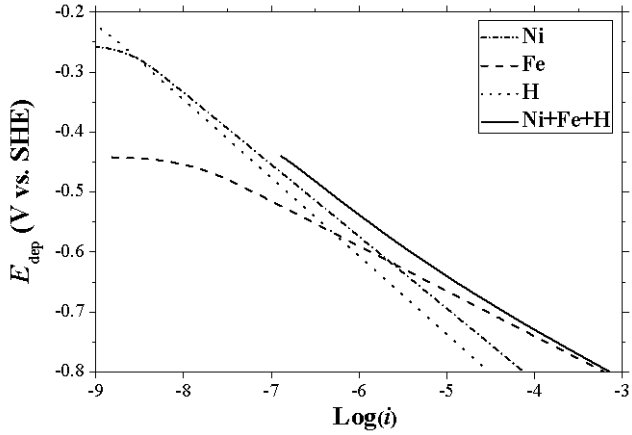

Figure 4. The effect of applied (deposition) potential on the partial cathodic current densities for codeposition of iron and nickel, as well as hydrogen evolution. Parameters used: $i_{0,Ni} = 2\times10^{-9}$ A cm^{-2}, $\alpha_{c,Ni} = 0.49$, $i_{0,Fe} = 1\times10^{-8}$ A cm^{-2}, $\alpha_{c,Fe} = 0.79$, $i_{0,H} = 5\times10^{-10}$ A cm^{-2}, $\alpha_{c,H} = 0.45$.

$$\mathrm{FE} = \frac{i_{\mathrm{Ni}} + i_{\mathrm{Fe}}}{i_{\mathrm{Ni}} + i_{\mathrm{Fe}} + i_{\mathrm{H}}} \tag{27}$$

The only quantity in this equation that can be measured directly is the total current density. The partial current densities for each of the three reactions are obtained by weighing the deposit and analyzing its composition. Each of the current densities is calculated from the Butler-Volmer equation

$$i_{\mathrm{j}} = i_{0,\mathrm{j}} \left[\exp\left(\alpha_a F\eta / RT\right) - \exp\left(-\alpha_c F\eta / RT\right) \right] \tag{28}$$

using the relation given in Eq. (24) to calculate the values of α_{a} corresponding to each assumed value of α_{c}. The total current density that would be measured (also shown in Fig. 4) is the sum of three partial current densities

$$i = i_{\mathrm{Ni}} + i_{\mathrm{Fe}} + i_{\mathrm{H}} \tag{29}$$

The point of presenting Fig. 4 is the following. First, it shows that alloy deposition is complex, including (usually) at least three reactions occurring in parallel. It cannot be over-emphasized that, in the usual interpretation of kinetic parameters such as the Tafel slope, reaction order, effect of pH etc., it is tacitly assumed that only one reaction is taking place. Thus, such analysis is inherently inapplicable to alloy deposition. When three parallel reactions take place simultaneously, each having its own exchange current density, overpotential and Tafel slope, there is no justification to assume that the Tafel plot would be linear. Moreover, its value (or, perhaps, one should say "its apparent value") cannot easily be associated with the mechanism of deposition of one of the alloying elements or the other, or of the alloy as such.

A well-known example of anomalous alloy deposition is the plating of Permalloy™.* Considering that the values of E^0 for

* A trademark of the Western Electric Co. for Ni-Fe alloys containing 20–60 at.% Fe, mostly used as a 80 at.% Ni – 20 at.% Fe alloy, which has high magnetic permeability and high electrical resistance.

nickel and iron are –0.25 V and –0.44 V vs. SHE, respectively, one might expect that nickel would be deposited more readily, and it would be difficult to reach a concentration of 20 at.% iron in the alloy, although the exchange current density of iron is five times larger than that of nickel (1×10^{-5} vs. 2×10^{-6} mA cm^{-2} in 2.0 N solutions of their respective sulfates at room temperature[85]). In fact, the opposite is found experimentally. If the plating bath contains equal concentrations of the two metals, the concentration of nickel in the alloy will be below the desired level. The proper alloy is deposited from a bath containing a much higher concentration of Ni^{2+} than Fe^{2+} ions.[86-88]

It would seem that mixing the two ions creates some interaction between them, which slows down the rate of deposition of the component having a more positive standard potential. It was shown by Landolt et al.[89,90] that adding 0.025 M $FeSO_4$ to a solution of 0.2 M $NiSO_4$ could reduce the partial current density for deposition of nickel by as much as a factor of ten. On the other hand, the same authors found that addition of 0.025 M $NiSO_4$ to a solution of 0.25 M $FeSO_4$ could increase the partial current density for deposition of iron by a factor of two or more. This is evidently a case of anomalous codeposition of two metals.

(*iv*) *Possible Causes of Anomalous Alloy Deposition*

Although this chapter is about induced codeposition, and is not meant to deal specifically with anomalous alloy deposition, a few general comments would seem to be appropriate.

(*a*) *The effect of partial mass-transport limitation*

It should be recalled that the concentration of the electroactive species at the surface of an electrode is always lower than its bulk concentration, following the simple relationship

$$\frac{c_{\text{surf}}}{c_{\text{bulk}}} = 1 - \frac{i}{i_L} \tag{30}$$

Thus, even if the concentrations of two metal ions in the plating bath are equal, their concentrations at the surface, which determine

the rate of deposition, may be quite different, if their partial current densities are different. Plating of interest in industry is usually conducted at the highest current density compatible with production of high-quality coating ($i/i_L \approx 0.3$). However, this might not be a simple guideline to follow because:

- a limiting current may not be observed experimentally, as hydrogen evolution becomes predominant at negative potentials;
- the limiting current that is relevant is that measured for each of the alloying elements separately, and this could be quite different for the two metals. The reason for this is that the desired alloy does not necessarily contain equal amounts of the two metals, hence the partial current densities are different;
- considering that alloy deposition is often anomalous, the composition of the alloy may not scale linearly with the concentrations of the metal ions in solution.

The consequence of all of this is that, during alloy plating, the deposition of the two metals may be under different degrees of mass-transport limitation, while the hydrogen evolution reaction usually occurs under conditions of activation control. Should this be the case, the alloy composition would depend on the total current density applied and on the conditions of mass transport. As it often happens, this may be a mixed blessing. On the one hand, it requires well-controlled and reproducible conditions of mass transport in order to obtain deposited layers of uniform composition. On the other hand, it could be used as a tool for producing alloy coatings of graded or alternating composition in the same solution, which may improve bonding and enhance resistance to thermal shock, by changing the applied current density.

(*b*) *The effect of Faradaic efficiency*

Hydrogen evolution occurring in parallel with metal deposition is a sore point in electroplating. The situation is even worse in the case of alloy deposition. If the plating bath is strongly buffered, which is often the case, the rate of hydrogen evolution is largely activation-controlled over the whole operating range of the bath.

On the other hand, the rate for metal deposition could be partially controlled by mass transport. For deposition of a single metal, the immediate consequence is that the FE could be a function of the mass transport regime (stirring, movement of the cathode in an actual plating bath, and rotation rate in a laboratory experiment). Moreover, since the rate laws for the kinetics of hydrogen evolution and metal deposition are in general different, it follows that the FE would also be a function of both the applied current density (or potential) and the temperature. In the case of alloy deposition, if the FE is significantly lower that 100%, the situation could be more complicated, since the composition of the alloy could be a function of the FE. But the kinetics of hydrogen evolution is itself a function of alloy composition and surface morphology, since the two alloying elements will, in general, have different catalytic activities with respect to this reaction. If the alloy is a solid solution, one may expect that the exchange current density for hydrogen evolution on the surface of the alloy would be a weighted average of its values on the two elements. However, if the alloy consists of segregated phases, or if intermetallic compounds are formed during deposition, there is no telling how the rate of hydrogen evolution (and, hence, the FE) may change. The point to remember is that the overall FE observed will affect the partial currents of deposition of the different alloying elements, which will influence the composition of the alloy, thus possibly having a pronounced effect on the overall FE, and so on.

(*c*) *Formation of adsorbed intermediates*

The formation of a monovalent species in deposition and dissolution of divalent ions of the iron-group transition metals is commonly assumed in the literature. Since the monovalent ions (such as Fe^{+}) are unstable in solution, they are assumed to be adsorbed on the surface, either as the ion itself or as a hydroxide, such as $FeOH_{ads}$. This could stabilize the monovalent form of the element. Moreover, since a monovalent hydroxide is not known to exist in solution, one does not know its solubility product, and the possibility of the existence of this adsorbed species, even in solutions of low pH, cannot be ignored a priori. Unfortunately, the nature of the adsorbed intermediate, or even the evidence for its existence on the surface, is at best circumstantial.

In the work of Landolt et al.[89,90] inhibition of the partial current density of nickel by the addition of iron to the plating bath occurred when the concentration of Ni^{2+} ions was eight times larger than that of Fe^{2+} ions. This would seem to support the notion that inhibition is due to formation of some adsorbed species containing iron, since there is not enough Fe^{2+} in solution to interact with all the Ni^{2+}, reducing its rate of deposition.* It is more difficult to explain the mechanism of enhancement of deposition of iron by nickel. Although the above authors[89,90] did provide a simulation that could explain the behavior observed experimentally, at least partially, further detailed studies of this phenomenon would be needed to verify the mechanism proposed.

(*d*) *The solution chemistry*

Alloy deposition could involve rather complex solution chemistry, as noted above, which has not been investigated at sufficient depth in the analysis of the anomalies observed.

When a suitable complexing agent is used, different complexes could be formed. For example, complexes of the form $[Ni(NH_3)_n]^{2+}$ with n = 1-6 can be formed. In this case, the stability constants for each of the species are known, hence the relative concentrations of all the Ni-NH_3 complexes can be calculated as a function of the concentration of Ni^{2+} and of NH_3 (cf., Fig. 2a). Deposition of nickel can take place from each of these complexes, but the relative rate may depend on the number of ligands in the complex. When citric acid is added and the pH is adjusted to 8, the predominant species in solution is Cit^{3-}. This can form two different complexes with Ni^{2+}, either $[Ni(Cit)]^{-}$ or $[Ni(Cit)_2]^{4-}$ (cf., Fig. 1b). Nickel can readily be deposited from the former, but not from the latter. Moreover, when the molar ratio $Cit^{3-}/Ni^{2+} > 4$, most of the nickel is sequestered in the second complex above, inhibiting almost completely the deposition of nickel.

In alloy deposition, the possibility of formation of mixed-metal complexes containing ionic species of both metals and a

---

* It could well be that even a lower concentration of iron in solution would have a strong inhibiting effect, but this was unfortunately not tested in the above papers.[89,90]

suitable ligand should also be considered. For the induced codeposition of W-Ni alloys, the mixed-metal complex $[(Ni)(HWO_4)(Cit)]^{2-}$ was assumed to be the electro-active species,[91-93] as will be discussed below.

(*v*) *Induced Codeposition*

Certain elements, such as W, Mo, Ge and P cannot be deposited alone from their aqueous solutions. Nevertheless, they may readily be codeposited with iron-group elements. The term *induced codeposition* was coined by Brenner in 1963[78] to describe a situation where

> "a metal that cannot be deposited alone from its aqueous solution is codeposited in the presence of another metal, forming an alloy."

It was applied first to describe the electroless deposition of Ni-P alloys,[94] and later for electroplating of alloys of W and Mo with the iron-group metals.

It is of great interest from the scientific point of view, as well as for the development of plating baths, to understand the mechanism of induced codeposition. This may undoubtedly be considered to be *anomalous* in the sense that the composition of the alloy cannot be predicted from the electrochemical behaviors of the individual alloying elements. It cannot be measured by the criterion given in Eq. (26) above for anomalous codeposition of alloys, since one of the alloying elements cannot be deposited by itself. Nevertheless, some similarities do exist. Podlaha and Landolt[95-97] studied the induced codeposition of Mo-Ni alloys and concluded that the precursor for deposition of the alloy was an adsorbed complex containing both metals. In a later study of anomalous codeposition of iron-group transition metals,[89,90] Landolt et al. found an inverse influence of the two metals in solution on their respective rate of deposition. For example, adding Fe^{2+} to a nickel-plating bath inhibited the rate of deposition of nickel, while adding Ni^{2+} to an iron-plating bath accelerated the rate of deposition of iron. The catalytic effect of Ni^{2+} on the rate of deposition of iron was explained assuming a model similar to that proposed for the effect of Ni^{2+} on deposition of molybdenum.

In recent studies of induced codeposition of Ni-W alloys, Gileadi et al.[91,92] reported that increasing the concentration of Ni^{2+} in the bath led to a distinct increase of the partial current density for deposition of tungsten. However, unlike the case of anomalous codeposition of Fe-Ni alloys, it was also observed that increasing the concentration of WO_4^{2-} in solution led to an increase of the partial current density for deposition of nickel. Thus, induced codeposition of Ni-W alloys seems to be a true synergistic effect, where increasing the concentration of either metal ion in solution leads to an increase of the partial current density of the other. This behavior was explained by postulating the formation of a soluble complex containing both Ni^{2+} and WO_4^{2-}, which is the precursor for the deposition of the alloy.

(*vi*) *Electroless Deposition of Alloys*

Electroless deposition, or autocatalytic plating, may be defined as "deposition of a metal coating by a controlled chemical reduction, catalyzed by the metal or alloy being deposited." Electroless deposition has been known for a long time. One of its early uses was the deposition of a mirror-like layer of silver on the internal surfaces of Dewar flasks for improved thermal isolation, and as the back coating of mirrors. Later, it was used for deposition of different metals and alloys, and even for induced codeposition of alloys.

An electroless-plating bath consists of a soluble salt of the metal or metals being deposited and a suitable reducing agent. As in any plating bath, suitable additives are also used to improve the product, but these will not be discussed here. It is important to remember that electroless deposition is inherently an electrodeposition process, conducted under (nearly) potentiostatic conditions. The source of electrons for the reduction process is, of course, different—in electrodeposition it is the power supply, via the metallic electrode; in electroless deposition it is the reducing agent. In both cases the potential is maintained by and large constant, even if the current is the externally controlled parameter, as long as the solution is not exhausted from its electro-active components. In electroless deposition the potential across the interface is controlled through a corrosion-type mechanism, by the balance between the rate of oxidation of the reducing agent and the rate of

reduction of the metal ions, either of which could be the rate-limiting factor, depending on the composition of the bath. Hence, the rate of metal deposition can be determined, in principle, by micro-polarization measurements, following the common method to determine the corrosion current.

The composition of the bath should be chosen such that the rate of metal deposition will be well below the mass-transport-limited rate. Proper selection of the type and concentration of the reducing agent can achieve this. The main advantage of electroless deposition, compared to electroplating, is that metals can be deposited on non-conducting surfaces. This is widely used as a first step for electrodeposition in many engineering applications, as well as for ornamental purposes. The other advantage is that the primary current distribution, caused by the shape of the part being plated and the distance of various parts from the anode, has no effect in electroless deposition, because there is obviously no anode. In this sense electroless deposition can be considered as being conducted under conditions equivalent to electrodeposition under secondary current distribution. On the other hand, partial mass-transport limitation is not eliminated, hence ternary current distribution, which determines the micro-throwing power and, in some cases, the surface morphology of the deposit, cannot be ignored.

Electroless deposition is usually a slow process, and it is therefore limited to formation of relatively thin layers. Since the development of surface roughness in metal deposition has a built-in positive feedback effect, causing the roughness to increase with increasing thickness of the deposit, this is less of a problem in the case of electroless deposition.

The main disadvantage of electroless deposition is that the plating bath is inherently unstable. Hence, a delicate balance must be struck between the desire to have a stable bath and, yet, allow reasonably high rates of deposition. The surface of the substrate being plated must be activated, to ensure that deposition will only occur where needed. The rate of electroless deposition cannot be controlled as readily as the rate of electroplating, although some control can be achieved by varying the concentration of the reducing agent in the bath and by controlling the rate of mass transport and the temperature.

In view of the inherent similarity between electroless deposition and electroplating, it is not surprising that anomalous codeposition and induced codeposition can be performed by both methods. A most important early case was the development of an electroless plating bath for deposition of amorphous Ni-P alloys by Brenner.[78,94] The reducing agent in this bath was sodium hypophosphite (NaH_2PO_2). The same reducing agent was used recently by Shacham-Diamand et al.[98-102] in electroless deposition of Co-W-P alloys as barrier layers for ULSI devices.

II. CASE STUDIES

1. Tungsten Alloys Containing Ni, Co and Fe

(*i*) *Properties of Tungsten Alloys*

Selected properties of tungsten (W) are listed in Table 2, in comparison to the respective properties of molybdenum (Mo) and rhenium (Re), which will be discussed in the following sections. The attribute ranges were taken from the Cambridge Engineering Selector[103] material database, and reflect different thermal conditions and suppliers of the commercially pure metals. Of all metals in the periodic table, tungsten possesses the highest melting point, the lowest linear thermal expansion coefficient, the highest tensile strength, the fourth Young's modulus of elasticity, and the sixth thermal conductivity. It maintains most of its strength and hardness at fairly high temperatures, and is also highly corrosion resistant, being stable in any single mineral acid at room temperature. At the same time, it is one of the densest metals, lacks ductility, and is oxidized in air only at temperatures above 1,000°C. It is fairly expensive and has limited availability.

Attempts to electrodeposit pure tungsten date approximately 140 years back. Nowadays, however, it is commonly accepted that this metal cannot be deposited alone from its aqueous solutions, but can be codeposited as an alloy, exhibiting a unique combination of properties. For example, Ni-W alloys have good mechanical properties (e.g., high tensile strength and premium

Table 2
Selected Properties of Tungsten, Molybdenum and Rhenium

Property	W	Mo	Re
Atomic number	74	42	75
Atomic mass, M (g mol^{-1})	183.8	95.9	186.2
Oxidation states	2,3,4,5,6	2,3,4,5,6	–1,2,4,6,7
Crystal structure	bcc	bcc	hcp
Atomic radius, r_{metal} (Å)	1.41	1.39	1.37
Density, ρ (g cm^{-3})	19.25–19.35	10.1–10.3	21.00–21.02
Melting temperature, T_m (°C)	3,410–3,420	2,607–2,622	3,157–3,181
Linear thermal expansion coefficient, α (°C^{-1})	4.2-4.6×10^{-6}	4.8-5.5×10^{-6}	6.00-7.25×10^{-6}
Thermal conductivity, κ (W m^{-1}K^{-1})	170-175	129-147	45-48
Specific resistivity, ρ (Ω·m)	5.4-6×10^{-8}	5.2-6×10^{-8}	18.7-20.0×10^{-8}
Tensile strength, σ_u (MPa)	1,670-3,900	380-2,100	1,000-2,500
Yield strength, σ_y (MPa)	1,350-3,500	170-2,000	280-2,350
Young's modulus of elasticity, E (GPa)	340-405	315-343	461-471
Strain at fracture, ε_f (%)	1-25	1-45	1-30
Poisson's ratio, ν	0.27-0.29	0.29-0.295	0.255-0.265
Hardness (MPa)	4,500-8,500	1,500-6,500	2,600-7,500
Fracture toughness, K_{Ic} (MPa $\sqrt{m}$)	120-150	20-40	120-150

hardness, as well as superior abrasion resistance), good resistance to strong oxidizing acids, and high melting temperature.[78,91-93,104,111] It was reported,[109] for example, that the corrosion rate of an amorphous Ni-W deposit in hydrochloric acid at 30°C is only 1/40 that of type 304 stainless steel, commonly used in industry. In general, the passivation current density (i_{pass}) drops remarkably with the addition of tungsten to nickel. While the hardness of the *as-plated* alloy is typically in the range 650-750 VHN, heat treatment at temperatures ranging from 190°C to 600°C for 12 to 24 hours can raise the hardness to 1,200–1,400 VHN due to precipitation hardening.[110,111]

(*ii*) *Applications of Tungsten Alloys*

Tungsten and its alloys, including those with iron-group metals, have been used in filaments of incandescent lamps, electrical contacts, resistors, heating elements, thermocouples, cutting tools, X-ray targets, balance weights, anti-vibration tooling, bearings, radiation shields, nozzles of rocket engines, heat sinks, mold inserts, magnetic heads and relays, crucibles, extrusion dies, high-strength wires and springs.[103] Tungsten is also used as an alloying element in high-speed tool steels and corrosion-resistant alloys.[78] Recently suggested applications include barrier layers or capping layers in copper metallization for ULSI devices or MEMS, electrodes catalyzing hydrogen evolution from alkaline solutions, and substitutes for hard chromium plating with a good combination of wear and corrosion resistance (e.g., in the aerospace industry).[91-93,104-116]

(*iii*) *Electrodeposition of Tungsten Alloys*

The first deposition of a tungsten alloy (W-Fe) may be attributed to Fink and Jones,[117] although these authors mistakenly claimed to have deposited pure tungsten. Soon afterwards it was realized that, although tungsten could not be electrodeposited from an aqueous solution of sodium tungstate (Na_2WO_4) or any other soluble compound containing this element, induced codeposition could take place if the plating bath contained iron-group metals, namely nickel, cobalt or iron. Golt'tz and Kharlamov[118] developed already in 1936 practical plating baths for alloys, by replacing the highly alkaline carbonate solutions with ammoniacal solutions. From these ammoniacal baths, they deposited W-Ni alloys 0.2-mm thick at FE of up to 30%. However, porous and weak deposits resulted from the excessively high current densities with respect to the low metal content of the bath. Next, several investigators found that the addition of organic poly-hydroxy acids (e.g., citric, tartaric, malic, gluconic, hydroxy acetic, or saccharic) into ammoniacal baths improved the FE and the solubility of the metal ions in the bath. Consequently, smooth, hard and thick deposits of the alloys could be formed at lower current densities and at FE approaching 100%.[78]

Here, we shall focus only on moderately alkaline solutions for electrodeposition of tungsten-based alloys. The reason is that acidic solutions have been reported to be of limited practical value, because of the poor deposits that were obtained from them. Nevertheless, for comparison to electrodeposition in moderately alkaline solutions, several characteristics of electrodeposition from acidic baths are summarized. Iron was found to induce codeposition of tungsten more effectively than nickel or cobalt. An increase of pH in the range of 2 to 5 had a negligible effect on the composition of the alloy, but at the same time increased significantly the FE. Variations in the current density and temperature had little effect on the composition of the alloys, except for the Fe-W alloys, for which the tungsten content decreased considerably as the current density was decreased. Increasing the temperature resulted in the production of deposits having a more metallic appearance, and in an increase in the FE.[78]

The binary alloys of tungsten with iron, cobalt and nickel are readily deposited from moderately alkaline baths. Typical bath compositions and operating conditions are listed in Appendix A. A complexing agent is typically added and forms a soluble complex ion with the iron-group metal. The W-Fe alloys are the most readily obtained with high W-contents, but the quality and thickness that could be achieved were the least satisfactory. The W-Ni alloys were reported to produce the lowest tungsten content, which was usually found to be in the range of 5–25 at.% (13–50 wt.%).[78] In order to further improve the tribological properties and thermal stability of the coating, it is sometimes desirable to increase its tungsten content. Unfortunately, this has been found difficult, even when the WO_4^{2-} ion in solution is in large excess compared to the Ni^{2+} ion. One possible way to increase the tungsten concentration in the alloy is to apply periodic reverse pulse plating, which may also increase the throwing power and the deposition rate, as well as improve the properties of the deposit (e.g., reduce residual stresses and porosity, refine the grain size, improve wear and corrosion resistance, etc.)[104] Another route was suggested by Gileadi and co-workers, who removed the NH_3 from the plating bath, while using citrate as a complexing agent, thus increasing the tungsten content of the alloy to nearly 50 at.% .[91,93,104-108] The best plating conditions for obtaining sound and thick deposits at good FE are high concentrations of the iron-group metal in the bath,

elevated bath temperatures and moderate current densities. However, some of these conditions may lower the concentration of tungsten in the resulting alloy.

Brenner reviewed several variables that affect the tungsten content in the deposit.[78] The most important parameter is the ratio of concentrations of tungstate to nickel ions. In general, as this ratio is increased, the tungsten content in the deposit increases, until it approaches a limit of approximately 50–60 wt.% for Fe-W and Co-W alloys, and 30 wt.% for Ni-W alloys. Another variable, the type of complexing agent, had a moderate effect on the tungsten content in the deposit. The composition of the alloy deposits obtained from ammoniacal baths, on the other hand, was not significantly affected by variations of pH between 8.0 and 10.0. This claim of Brenner, however, is contradictory to the recent findings of Gileadi et al.[92,93] Typically, the tungsten content in Co-W and Ni-W alloys increases slightly and the FE decreases with increased current density. For Fe-W alloys, the W-content in the deposit was found to be less affected by current density. The bath temperature has an important effect on the FE and soundness of deposits. In addition, the tungsten content of the deposit usually increases at elevated temperatures.

The effects of several variables on the FE, tungsten concentration in the alloy, the deposit structure, thickness and hardness on stationary working electrodes were studied recently by Eliaz et al., for ammonia-free, citrate-containing Ni-W plating baths.[104,108] The FE was found to increase with the concentration of Ni^{2+} and decrease with increasing current density. The nickel content of the bath also affected tungsten content in the deposit. While the W-content was in the range 30–35 at.% for both the 0.05 M Ni^{2+} and the 0.10 M Ni^{2+} baths (containing 0.4 M tungstate and 0.5 M citrate) at all current densities, it increased significantly to 67 at.% for the 0.01 M Ni^{2+} bath. However, this was associated with very low FE and reflects a poorly adhering, thin deposit, rather than the good Ni-W deposits obtained at higher concentrations of Ni^{2+} in solution and, correspondingly, lower tungsten concentration in the alloy. For comparison, Younes and Gileadi[105] previously reported a maximum FE of 11% and a maximal tungsten content of about 67 at.% in two different baths containing different concentrations of Na_2WO_4. An increase in the concentration of Ni^{2+} was also reported to cause a significant increase in the FE.[92,124] Furthermore,

it was reported that an increase in the concentration of Ni^{2+} results in an increase in the rate of both Ni and W deposition,[125,126] but the tungsten content in the alloy decreases.[93]

The *concentration* of citrate ions also affects the FE and W-content of the deposit. The effect was found to depend on current density and on the concentration of nickel ions in the bath. In general, the FE was found to decrease as the concentration of Cit^{3-} was increased. At a low current density (5 mA cm^{-2}), the tungsten content increased from 10 to 33 at.% as the concentration of Cit^{3-} was increased from 0.25 M to 0.60 M. At a higher current density (15 mA cm^{-2}), however, the trend reversed and the tungsten content increased from 31 to 60 at.% as the concentration of Cit^{3-} was decreased. The effects of the citrate ion concentration on the FE and on the tungsten content in the deposit were studied in solutions of very low concentration of Ni^{2+} ions, and the FE was also found to decrease with increasing Cit^{3-} concentration.

It is well known that the tungsten content of the alloy depends, among others, on the type of the complexing agent used in the bath. Citrate baths were reported to yield higher tungsten content than those containing tartrate or malate. However, an increase in the concentration of Cit^{3-} was sometimes found to result in a decrease in both the FE and the tungsten content.[78,93,125] Huang,[127] on the other hand, reported that addition of diammonium citrate to a sulfamate bath resulted in an increased concentration of tungsten in the alloy, but the residual stresses were also increased. In a bath containing 0.10 M Ni^{2+} and 0.10 M WO_4^{2-}, Younes and Gileadi observed[92] that the tungsten content of the alloy increased when the concentration of Cit^{3-} was increased up to 0.50 M, but then started to decrease. The FE decreased dramatically when the concentration of citrate exceeded 0.20 M, i.e., when the molar concentration of citrate exceeded the sum of concentrations of nickel and tungstate ions. The deposition potential shifted in the negative direction with increasing citrate concentration, first sharply and then moderately. The decrease of FE and the shift of potential indicate that the main reaction taking place in the presence of excess Cit^{3-} is hydrogen evolution, and this side reaction has a dominant effect on the potential. It was concluded that citrate, being a strong complexing agent for Ni^{2+}, tends to sequester this ion in a stable complex of $[Ni(Cit)_2]^{4-}$, decreasing the availability of Ni^{2+} to form a mixed Ni-WO_4-Cit complex, which is

essential for the induced codeposition of tungsten (cf., Section 2.1.4). The relative effect on nickel was found to be stronger up to a concentration of 0.50 M citrate and weaker at higher concentrations, leading to a maximum tungsten content at a Cit^{3-} concentration of about 0.50 M.

The effect of nickel sulfamate, saccharin and sodium chloride as *additives* was studied by Eliaz et al.[104,108] The effect of adding nickel sulfamate to a bath containing 0.10 M Ni^{2+}, 0.40 M WO_2^{2-} and 0.50 M Cit^{3-} was to increase the FE. This observation was more pronounced at high than at low current densities. The increase in the FE was accompanied by a slight decrease in the tungsten content of the alloy. The morphology of the coating, observed by SEM, did not change significantly as a result of nickel sulfamate addition. However, metallographic cross-sections did show a remarkable increase in the thickness of the coating at a high current density. The addition of saccharin (14.6 mM) increased the FE at high current densities and decreased the tungsten content of the alloy at low current densities.

Adding sodium chloride (2–5 mM) stabilized the FE at a nearly constant value, independent of current density. In contrast, the FE dropped significantly at high current densities when chloride was absent. The addition of chloride ions did not change the composition of the alloy significantly. It should be noted, however, that excess chloride might be harmful to brightness and leveling.

Temperature is another important variable in the operation of W-Ni plating baths. The effect of this variable depends on the composition of the bath. When the bath contained tartaric and boric acids, both the tungsten content and the FE increased with increasing temperature in ammonia-containing baths,[128] whereas the effect of temperature on the tungsten content was small in ammonia-free baths.[120] Younes and Gileadi similarly observed that in ammonia-free solutions, almost no effect of temperature on the tungsten content exists, while the FE increases with temperature.[105] Krishnan et al.[113] also reported an increase in FE with increasing temperature, while Yamasaki et al.[123] described temperature effects both on the tungsten content and the ductility of the deposit. Atanassov et al.[112] observed an increase in the tungsten content with increasing temperature, both in unstirred and in stirred baths, and explained this behavior in terms of favorable conditions for tungsten transport toward the cathode surface. This argument can

be questioned, however, since (a) it was not shown that mass-transport limitation played a role in the deposition of tungsten, and (b) it is not clear why the rate of mass transport of tungstate to the surface would be enhanced by increasing temperature more than the rate of transport of Ni^{2+} ions.

Eliaz et al.[104] also studied the effect of temperature within the range of 30°C to 70°C in an ammonia-free bath, containing 0.10 M Ni^{2+}, 0.40 M WO_4^{2-} and 0.50 M Cit^{3-}. As the bath temperature was increased, the FE increased. The tungsten content of the deposit did not change much with temperature, and showed a rather irregular behavior, with perhaps some tendency to decrease with increasing temperature. These results are in good agreement with the previous work of Younes and Gileadi,[105] keeping in mind that the latter was conducted at a current density of 15 mA cm^{-2} only. It was observed, rather unexpectedly, that in the higher temperature range (50–70°C), a Ni_4W phase could be formed by electrodeposition.

Increasing the *current density* in the same bath composition led to a decrease of the FE, whereas the tungsten content either increased or passed through a maximum at 10 mA cm^{-2}. At high current densities, where the FE is low, hydrogen evolution becomes more dominant and causes additional agitation in solution. Moreover, because Ni is deposited easily compared to W, higher FE is expected to result if the concentration of Ni in the alloy is higher. This implies some degree of mass-transport limitation, as will be discussed below (cf., Section 2.1.4). The effect of current density in the W-Ni system was also studied by others. Brenner et al.[119] observed a significant increase in tungsten content with increasing current density in ammonia-citrate bath. Yamasaki et al.[123] reported a similar trend. Atanassov et al.[112] noted a linear increase in tungsten content with increasing current density, when vigorous stirring was applied. On the other hand, a maximum was observed at 50–70 mA cm^{-2} in the absence of stirring. At current densities higher than 20 mA cm^{-2}, the FE was 15–40% higher in the stirred bath, where hydrogen evolution was less pronounced, compared to an unstirred bath. Krishnan et al. [113] also monitored a decrease in the FE with increasing current density. Finally, Huang et al. [129] reported an increase in residual stresses with increasing current density.

X-ray diffraction (XRD) studies have shown that the structure of electrodeposited tungsten alloys is different from that of thermally prepared tungsten alloys.[78] Several structures have been observed in the W-Ni system, depending on the operating conditions and the chemical composition of the resulting deposit.[91,93,104,105,108] Below 20 at.% tungsten, a solid solution of W in Ni, in the form of an fcc phase, is formed (as shown in Fig. 5a). An amorphous Ni-W phase was observed[91,93,105] when the tungsten content fell within the range of 20–40 at.% (Fig. 5a). This metastable phase cannot be predicted from the equilibrium binary phase diagram, according to which dual crystalline phases should form within this concentration range. Younes et al. also observed the formation of an orthorhombic NiW phase when the concentration of tungsten in the deposit exceeded 40 at.%,[91,105] as shown in Fig. 5a. It was argued that formation of equal amounts of Ni and W in the alloy may be regarded as evidence, albeit circumstantial, for the existence of a mixed nickel-tungstate-citrate complex. Later,[93] Younes et al. also reported the first plating of a body-centered tetragonal NiW_2 phase. It was found that the NiW and NiW_2 phases can be formed when the sum of the molar concentrations of nickel and tungstate ions exceeds slightly the molar concentration of the citrate ion, and the ratio of concentrations of WO_4^{2-} to Ni^{2+} ions is much larger than unity. It should be noted, however, that the concentration of citrate should not be much lower than the sum of concentrations of tungstate and nickel ions, otherwise precipitation will occur. At higher citrate concentrations, the amorphous Ni-W phase forms at room temperature and different current densities. On the other hand, under conditions of low current density (5 mA cm^{-2}) and higher temperature (50°C and above), the body-centered tetragonal Ni_4W phase can be formed electrochemically in a reproducible manner,[108] as shown in Fig. 5b.

Several studies were published in recent years on electrodeposition of W-Co alloys. Donten and Stojek[130] used pulse electrodeposition to increase the tungsten content in amorphous Co-W alloys. These alloys contained, in addition, small amounts of boron or phosphorous. They showed that, if a symmetrical current pulse was used, the tungsten content in the alloys reached a maximum value of 41.4 at.%, which is higher than in the case of direct current deposition. However, when using any asymmetrical

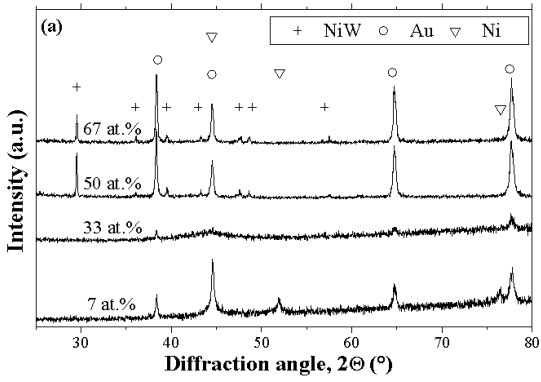

(a)

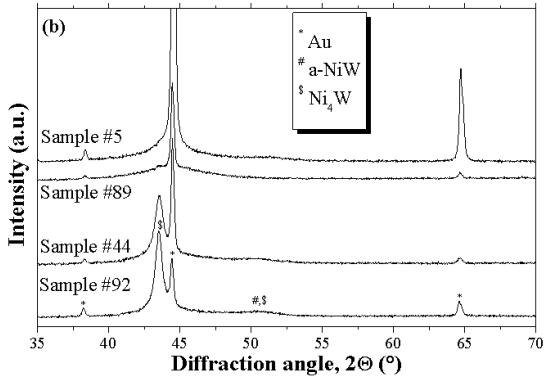

(b)

Figure 5. X-ray diffraction spectra, demonstrating the effect of bath temperature and operating conditions on the structure of Ni-W electrodeposits. (a) A solid solution of W in Ni at 7 at.% W with fcc structure, an amorphous Ni-W phase at 33 at.% W, and an orthorhombic Ni-W phase at 50 and 67 at.% W. Reprinted from Ref. 93, Copyright (2003) with permission from Elsevier. (b) The top two spectra demonstrate the deposition of amorphous Ni-W phase on gold. The lower two spectra show the (211) strongest reflection of the bct Ni_4W phase. Reprinted from Ref. 108, Copyright (2005) with permission from Elsevier.

current wave form, the tungsten content in the alloy decreased. The authors offered no explanation for this difference. Wikiel and Osteryoung[131] used anodic stripping voltammetry for monitoring in-situ the concentration of cobalt ions during electrodeposition of Co-W alloys on platinum micro-disk electrodes. A mechanism of electrodeposition of a Co-W alloy using cyclic voltammetry was suggested by Aravinda et al.[132] These authors assumed that the deposition of W-Co alloys occurs from a cobalt-tungstate complex, while the deposition of Co^{2+} occurs via a stepwise reaction involving Co^{+} ion as an intermediate. Although the present authors would agree tentatively that the precursor for deposition of a Co-W alloy is indeed a mixed-metal complex (based on the similarity of this system to the Ni-W system), it is not clear how this conclusion could have been reached based on measurements of cyclic voltammetry alone, considering that the current observed represents the sum of at least three different reactions occurring in parallel (cf., Section 1.2.2).

Several theories were proposed to explain the mechanism of induced codeposition of tungsten, but none could be confirmed experimentally. Here, we summarize a few of these theories. Firstly, it was assumed that tungsten-containing ions cannot be discharged on a pure tungsten surface due to the *self-polarizing* nature of tungsten, and that the presence of the iron-group metal alters the characteristics of the surface, e.g., increases the overpotential for the hydrogen evolution reaction.[78] However, this mechanism was later discredited, when it was observed that tungsten could not be deposited even on mercury, although the rate of hydrogen evolution on this metal is known to be very low.[133] Secondly, it was suggested that initially an oxide of tungsten is formed on the cathode. This oxide is subsequently reduced by atomic hydrogen, a reaction that is catalyzed by the presence of the iron-group metal.[134] Thirdly, it was suggested that the deposition potential of tungsten is too negative to be attained in aqueous solutions, but becomes more positive as a result of formation of a solid solution of tungsten with an iron-group metal.[123,128,135,136] One of the drawbacks of this mechanism is that measurements of the heat of solution of the two metals showed that it was too small to explain the shift in potential.[78] Finally, it has been postulated that a complex ion, containing both tungsten and an iron-group metal,

forms in solution and that the discharge of this ion enables the simultaneous deposition of both metals.[78]

(*iv*) *New Interpretation of the Mechanism of Ni-W Codeposition*

With respect to the last type of mechanism, Gileadi and coworkers recently studied the induced codeposition of W-Ni from moderately alkaline baths containing citrate as a complexing agent, with or without ammonia.[91-93,105-107] The range of bath compositions and operating conditions is shown in Appendix A. The working hypotheses in these studies were that:

1. A tungstate-citrate complex reacts with a nickel-citrate complex, to form a mixed-metal complex, of the type $[(Ni)(HWO_4)(Cit)]^{2-}$.
2. This mixed-metal complex is the precursor for the deposition of the W-Ni alloy.
3. Nickel can also be deposited from its complexes with either citrate (e.g., $[NiCit]^-$) or NH_3 complexes of the form $[Ni(NH_3)_n]^{2+}$, where $n = 1–6$.

Although there has been no direct evidence for the formation of the above mixed-metal complex, there are ample experimental observations supporting the assumption that it is indeed formed and serves as the precursor for deposition of the Ni-W alloys. These indications include:

1. The mutual synergistic effect of nickel and tungsten on each other. Thus, the partial current density for deposition of W is increased as the concentration of $NiSO_4$ is increased. Similarly, increasing the concentration of Na_2WO_4 in solution results in an increase in the partial current density for deposition of Ni.
2. The W-content in the alloy increases markedly upon removal of ammonia or ammonium salts from the bath.
3. The W-content in the alloy decreases markedly as the pH exceeds 8.
4. An unexpected mass-transport limitation of the partial current density for deposition of W is observed.

In Fig. 6b the partial current density for deposition of tungsten is shown to increase by a factor of about 10 with increasing concentration of nickel in a solution containing 0.1 M Na_2WO_4 and 0.6 M citrate. In the same range of concentrations of Ni^{2+} ions, the concentration of W in the alloy decreases (by a factor of about 7.5). This is by no means surprising, and is consistent with the fact

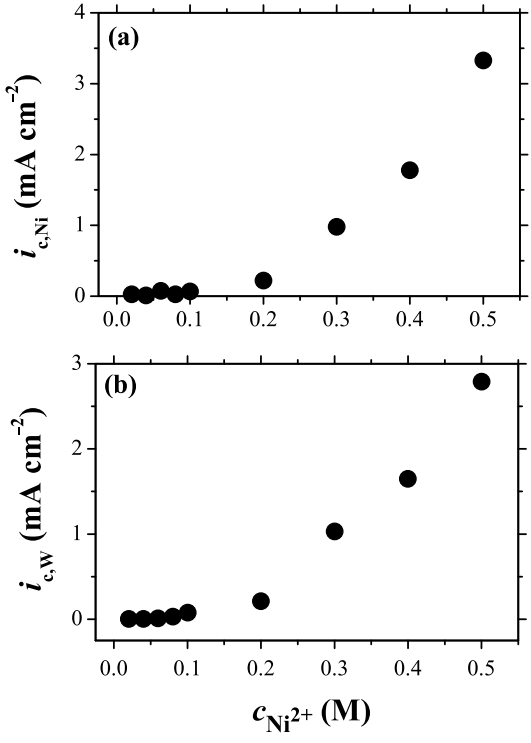

Figure 6. The effect of Ni^{2+} ion concentration on the partial current densities of nickel (a) and tungsten (b). All baths contained 0.1 M WO_4^{2-} and 0.6 M Cit^{3-}. Reprinted from Ref. 93, Copyright (2003) with permission from Elsevier.

that nickel can be deposited from several complexes in solution, in addition to its being deposited as an alloy with tungsten. Thus, the total increase in the partial current density for deposition of nickel upon increasing its concentration in solution (Fig. 6a) far exceeds the increase in the rate of deposition of tungsten. For the same reason, the FE is found to increase dramatically with increasing rate of deposition of nickel.[92,106]

A similar synergistic effect of addition of WO_4^{2-} on the rate of deposition of Ni is shown in Fig. 7 for solutions containing 0.1 M

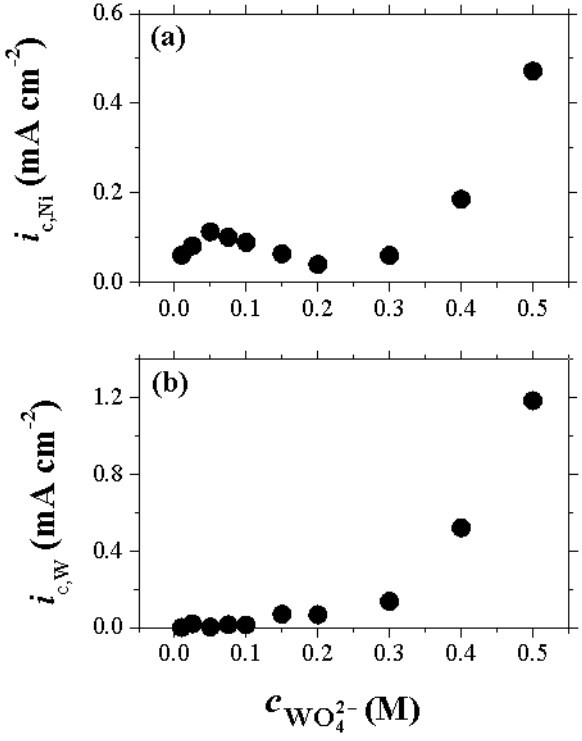

Figure 7. The effect of WO_4^{2-} ion concentration on the partial current densities of nickel (a) and tungsten (b). All baths contained 0.1 M Ni^{2+} and 0.6 M Cit^{3-}, pH = 8.0. Reprinted from Ref. 93, Copyright (2003) with permission from Elsevier.

$NiSO_4$ and 0.6 M citrate. As the concentration of WO_4^{2-} is increased above 0.3 M, the partial current density for W deposition increases sharply, while the partial current density for Ni deposition also increases. This is probably not due to any direct effect of WO_4^{2-} on the rate of deposition of Ni, but to the fact that an increasing proportion of Cit^{3-} ions is complexed by WO_4^{2-}. Hence, for WO_4^{2-} concentrations of 0.3, 0.4 and 0.5 M, the ratio of *free* Cit^{3-} (i.e., citrate not complexed with tungstate) to Ni^{2+} changes from 3 to 2 to 1, respectively, making it gradually easier to deposit Ni, as its predominant species in solution changes from the highly charged $[Ni(Cit)_2]^{4-}$ to the simpler $[NiCit]^-$, and it is well known that the complex containing two citrate ions sequesters the Ni^{2+} ions. In addition, increasing the concentration of WO_4^{2-} in solution, at a constant concentration of all other components of the bath, can increase the rate of formation of the mixed-metal complex, from which both tungsten and nickel are deposited.[93]

The effect of ammonia is discussed below, in conjunction with the effect of pH. As described in Section 1.2.2 and in Fig. 1a, citric acid can exist in different forms, depending on pH. The pK_a values corresponding to the three acidic groups and the alcohol group are 2.96, 4.38, 5.68, and 10.82, respectively (see Table 1). The complexes of tungstate with anions of citrate are of the form

$$[(WO_4)_k(Cit)_l(H)_m]^{-(2k+3l-m)} \tag{31}$$

depending on the pH of the solution and the relative concentrations of citrate and tungstate.[137] Several protonated forms, which can be represented by the equation $[(WO_4)(Cit)(H)_m]^{-(5-m)}$ exist, where m can assume values of 1–3. The corresponding $\log(\beta_n)$ values are given in Table 1. Figure 8 shows the calculated concentration distributions for tungstate-citrate complexes as a function of pH. According to this figure, in the range of pH = 6.8–10.2, the predominant species is the complex containing only one proton (m = 1), which can be notated as $[1,1,1]^{4-}$ for brevity. Since Cit^{3-} is not protonated at this pH, it may be assumed that the hydrogen atom originates from the partially protonated HWO_4^- ion.[92] It is assumed that the complex $[(WO_4)(Cit)(H)]^{4-}$ is the precursor for the formation of the mixed-metal complex with Ni^{2+}, $[(Ni)(HWO_4)(Cit)]^{2-}$. When the pH is further increased, the $[1,1,1]^{4-}$ complex is deprotonated. The resulting complex would have been $[(WO_4)(Cit)]^{5-}$,

but this is destabilized by its high negative charge of –5, so that WO_4^{2-} is formed. As a result, the concentrations of the mixed-metal complex in solution and the W-content of the deposit are decreased. At pH lower than 7.0, the concentration of the $[1,1,1]^{4-}$ complex is decreased, and at pH 6.0 most of the tungstate is bound in the $[1,1,2]^{3-}$ complex. At pH lower than 4.0, the dominant complex in solution is the $[1,1,3]^{2-}$ complex,[91,92] but this range of pH is not relevant in the context of the studies discussed above.

The reduction of the mixed-metal complex in mildly alkaline solutions requires the transfer of eight electrons, and seven hydroxyl ions are formed, as shown in Eq. (32). Consequently, the evaluation of a detailed mechanism, including the sequence of transfer of protons and electrons, the possible adsorbed intermediates and the rate-determining step or steps, seem like an impossible task. This is true in particular in view of the fact (discussed in Section 1.2.2 above), that there are several reactions

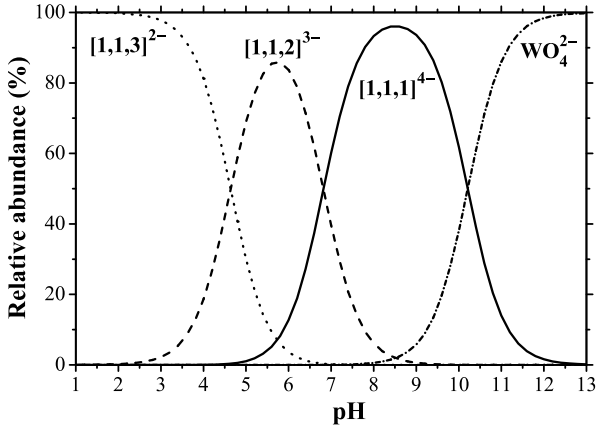

Figure 8. The relative abundance of the protonated tungstate-citrate complexes, $[(WO_4)(Cit)(H)_m]^{(-5-m)}$ as a function of pH (0.5 M Cit^{3-}, 0.1 M WO_4^{2-}). The abbreviated forms $[1,1,1]^{4-}$, $[1,1,2]^{3-}$, and $[1,1,3]^{2-}$ refer to values of m = 1, 2 and 3, respectively, in the above complex.

occurring in parallel, and measurement of current density only provides the sum of rates of all such steps.

All one can do is to write the overall reaction as:[105,106]

$$[(\mathrm{Ni})(\mathrm{HWO_4})(\mathrm{Cit})]^{2-} + 8\mathrm{e}^- + 3\mathrm{H_2O} \rightarrow \mathrm{NiW} + 7(\mathrm{OH})^- + \mathrm{Cit}^{3-} \quad (32)$$

The mixed-metal complex shown in Eq. (32) can be formed in the reaction

$$[(\mathrm{Ni})(\mathrm{Cit})]^- + [(\mathrm{HWO_4})(\mathrm{Cit})]^{4-} \rightarrow [(\mathrm{Ni})(\mathrm{HWO_4})(\mathrm{Cit})]^{2-} + \mathrm{Cit}^{3-} \quad (33)$$

Plotting the partial current densities for deposition of W as a function of the product of the concentrations of the two anions on the left-hand side of Eq. (33), a linear dependence was found for a wide range of solution compositions, supporting the proposed interpretation for the induced codeposition of W.[105,106] Unfortunately, the complex on the right-hand side of Eq. (33) has not been detected directly, either in solution or as an adsorbed species, even though its existence is strongly supported by all the experimental data discussed above. The rate of the reaction shown in Eq. (33) is expected to be quite low, in view of the fact that it involves an interaction between two negative ions, one of them highly charged, and requires the removal of a citrate ligand from one of the two complexes. This should lead to a low concentration of the mixed-metal complex at steady state, which could be the reason that this complex has not yet been detected. This is also consistent with the fact that the partial current density for deposition of tungsten is partially mass-transport limited, even though it is very low compared to the limiting current density calculated for the concentration of WO_4^{2-} in solution, as discussed below. The likelihood of a similar reaction involving the complex of nickel with two citrate ions, $[Ni(Cit)_2]^{4-}$, is low because of the electrostatic repulsion between the reacting anions, each having a charge of –4. [92]

In solutions where the ratio of concentrations of tungstate to nickel ions is very high, Eq. (33) could be followed by a reaction of the type

$$\left[(\mathrm{Ni})(\mathrm{HWO_4})(\mathrm{Cit})\right]^{2-} + \left[(\mathrm{HWO_4})(\mathrm{Cit})\right]^{4-} \rightarrow \left[(\mathrm{Ni})((\mathrm{HWO_4})_2(\mathrm{Cit})\right]^{3-} + \mathrm{Cit}^{3-} \quad (34)$$

The mixed-metal complex shown on the right-hand side of this equation could lead to an alloy having the composition of NiW_2. This was indeed observed in solutions containing 0.5 M Cit^{3-}, 0.4 M WO_4^{2-} and 0.01 M Ni^{2+}.[93]

In ammoniacal-citrate baths, Ni^{2+} can also form complexes with NH_3, the latter serving as a ligand, of the form $[Ni(NH_3)_n]^{2+}$, as shown in Fig. 2a, where n = 1–6, depending on the relative concentrations of the Ni^{2+} ion and ammonia. The $\log(\beta_n)$ values for these complexes are given in Table 1. The formation of these complexes can lead to a decrease in the concentrations of other complexes of Ni^{2+}, including the mixed-metal complex that is assumed here to be involved in the codeposition of W. Consequently, the rate of W deposition would be lowered. The fact that in ammoniacal-citrate baths the concentration of tungsten in the alloy could not exceed about 25 at.% W is easily understood if we remember that there are parallel paths through which Ni can be deposited alone, from its complexes either with citrate or with ammonia.[92,105]

The concentration of free NH_3 depends on pH in view of the equilibrium, given by the following equation:

$$\mathrm{NH_4^+ + H_2O \rightleftarrows NH_3 + H_3O^+} \quad (35)$$

The acid dissociation constant, pK_a, corresponding to Eq. (35) is 9.25. As the pH is increased, Eq. (35) is shifted to the right, thus increasing the concentration of NH_3 in solution, as shown in Fig. 2b, allowing the formation of nickel-ammonia complexes:

$$\mathrm{Ni^{2+} + \mathit{n}\cdot NH_3 \rightarrow \left[Ni(NH_3)_n\right]^{2+}} \quad (36)$$

This could explain the effect of pH on the composition of the alloy in solutions containing ammonium salts. However, a similar decrease in the tungsten content in the alloy was also observed when the pH was increased from 8.0 to 9.0 in citrate baths free of am-

monia. This was explained by considering Fig. 8, according to which, above pH = 8.5 the complex $[(WO_4)(Cit)(H)_m]^{-(5-m)}$ starts loosing its last proton, thus forming the unstable $[(WO_4)(Cit)]^{5-}$ complex, which decomposes to form three tungstate ions. Since the mixed-metal complex cannot be formed by the reaction of nickel citrate with bare tungstate, a sharp decline of its concentration with increasing pH leads to a similarly sharp decline in the concentration of tungsten in the alloy, as discussed before.

The mechanism of induced codeposition of W must account for the effect of pH on other complexes or reactions too. Addition of ammonia to citrate baths lowers the tungsten content in the alloy significantly. This implies that the deposition of Ni from complexes with NH_3 is faster than from its complexes with citrate. This statement is also supported by the fact that both partial current densities for deposition of Ni and W are decreased with large excess of citrate.[106] Similarly, increasing the temperature should drive part of the NH_3 out of solution, allowing the formation of more of the mixed-metal complex, thus increasing the concentration of W in the alloy. Hence, the effects of both temperature and pH reported in the literature for ammonia-containing baths may be related to changes in the concentration of NH_3 in solution rather than to the effect of temperature or pH on the electrodeposition reaction per se.[105] In addition, because an effect of deaeration was observed only at high pH values, where NH_3 exists in solution, it is most likely that oxygen concentration in solution and the associated oxygen reduction reaction do not play an important part in the induced codeposition of W. Figure 9 shows the decrease in the W-content of the alloy upon the addition of ammonia.[92] On the other hand, the FE is seen to increase. Hence, adding ammonia could improve the properties of the plating bath if a high concentration of W in the alloy is not needed. It should be pointed out that the addition of ammonia should decrease the concentration of W in the alloy for any mechanism of induced codeposition, as long as there is a synergistic effect of Ni^{2+} in solution upon the deposition of W from aqueous solutions containing WO_4^{2-}, which is a well-established experimental fact.

Further support for the role of the mixed-metal complex in induced codeposition of W is the measured effect of mass transport. Gileadi et al. used rotating cylinder electrode (RCE) experiments to study this effect in two ways – by varying the rotation rate at a

constant current density, or by changing the current density at a constant rotation rate. The limiting current density at a rotating cylinder electrode, operating in the region of turbulent flow, is given by:

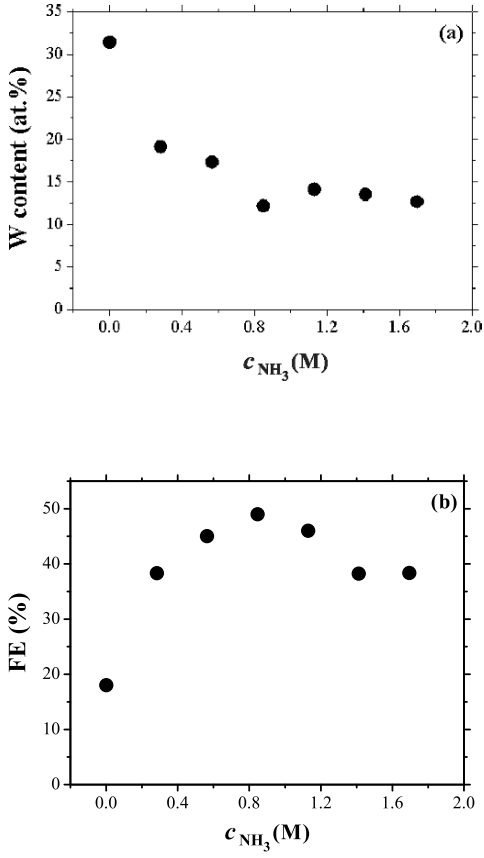

Figure 9. The effect of ammonia concentration in the plating bath on the W-content in the alloy (a), on the FE (b), and on the partial current densities for deposition of nickel (c) and tungsten (d). Plating conditions: 0.1 M $NiSO_4$, 0.5 M Na_2WO_4, 0.6 M Na_3Cit, pH = 8.0, i = 15 mA cm^{-2}, ω = 2,000 rpm. Reproduced with permission from Ref. 92. Copyright (2003) The Electrochemical Society.

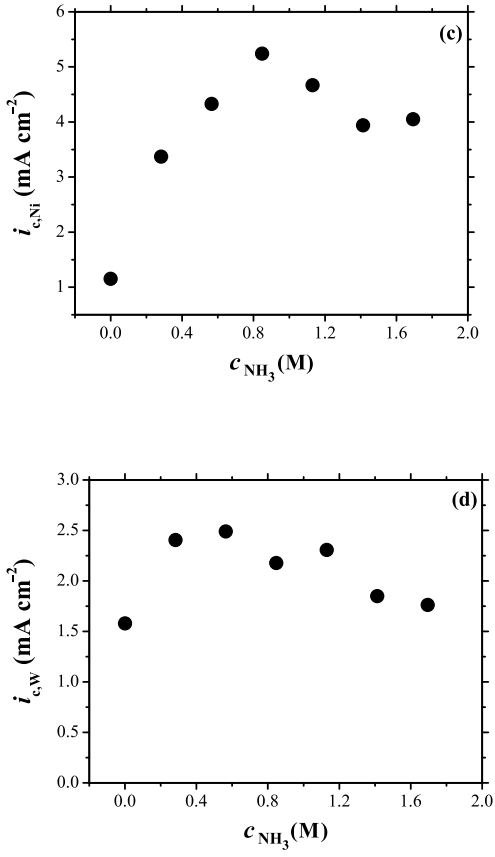

Figure 9. Continuation.

$$i_L = 0.079\, n\, \mathrm{F} r^{0.4}\, D^{0.644}\, \nu^{-0.344}\, c_\infty\, \omega^{0.7} = B\omega^{0.7} \tag{37}$$

where r is the radius of the rotating cylinder (cm), ν is the kinematic viscosity (cm^2 s^{-1}), ω is the angular velocity (rad s^{-1}), and c_∞ is the bulk concentration of the electro-active species (mol cm^{-3}).

The use of baths with different ratios between the nickel and tungstate ions allowed concluding that the ion that is the minority component controls the rate of deposition of W. The current density calculated for deposition of tungsten was much lower than that expected, if WO_4^{2-} had been the electro-active species, indicating that either the formation of the mixed-metal complex or its activation-controlled rate of discharge is the slow process.[106]

The effect of rotation rate was studied in the range of 2,000 to 5,000 rpm, which represents a 90% (= $2.5^{0.7}$) increase in the rate of mass transport to a RCE. The effect of rotation rate on the deposition process is shown in Fig. 10. As the concentration of WO_4^{2-} is increased tenfold, from 0.04 to 0.40 M, the current density increases by a factor of only two. The limiting current density, calculated on the basis of the concentration of WO_4^{2-} in solution, is much higher than the partial current densities for deposition of this metal, so one would not expect a 40% increase of the rate of deposition of W with the increase of the rate of mass transport, as found experimentally. The explanation of these unexpected observations lies in the formation of the mixed-metal complex, as shown in Eq. (33). The concentration of this complex is low, and its rate of formation is also expected to be low. From the dependence of the partial current density for W deposition shown in Fig. 10a, the activation-controlled and the mass transport-limited current densities can be estimated, using the Levich equation, as applied to RCE experiments, namely

$$\frac{1}{i} = \frac{1}{i_{ac}} + \frac{1}{B\omega^{0.7}} \tag{38}$$

The concentration of the mixed-metal complex can now be obtained from the value of B. Neglecting the difference in diffusion coefficients (taking $D = 6.9\times10^{-6}$ cm^2 s^{-1}), this turns out to be 2.3 mM in a solution containing 0.04 M WO_4^{2-}. When the concentration of WO_4^{2-} is increased tenfold and that of Ni^{2+} is decreased by

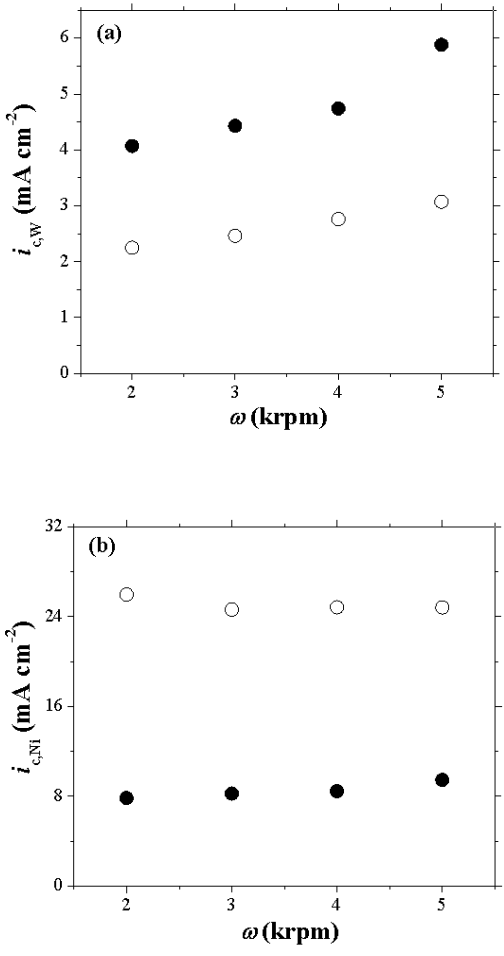

Figure 10. The effect of rotation rate on the partial current density for deposition of tungsten (a) and nickel (b), the W-content in the alloy (c), and the steady-state deposition potential (d). Plating conditions: excess of NH_4OH, 0.4 M Na_3Cit, pH = 8.0, i = 30 mA cm^{-2}. (•): 0.4 M Na_2WO_4, 0.04 M $NiSO_4$; (o): 0.04 M Na_2WO_4, 0.4 M $NiSO_4$. Reproduced with permission from Ref. 92. Copyright (2003) The Electrochemical Society.

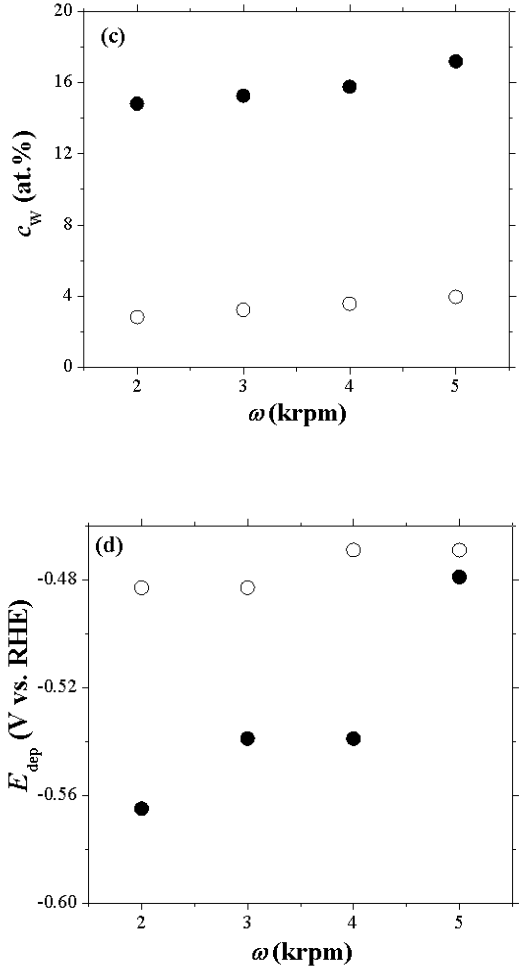

Figure 10. Continuation.

the same factor, both the activation-controlled current density and the limiting current density increase by a factor of 1.8 (from 5 to 9 and from 4.1 to 7.4 mA cm^{-2}, respectively, at 2,000 rpm). It may be concluded that the concentration of the precursor for the deposition of W increased by the same factor, to a value of 4.1 mM.

The partial current density for Ni deposition was found to be essentially independent of the rotation rate. An apparent anomaly is observed, however, even in this case, since increasing the concentration of Ni^{2+} in solution by a factor of 10 causes an increase of its partial current density only by a factor of 2–3, as seen in Fig. 10b. It should be recalled, however, that the Ni^{2+} ion can exist in solution in many different forms. There are six possible complexes with NH_3 and two complexes with Cit^{3-}, in addition to the mixed-metal complex with tungstate and citrate. The overpotential for deposition depends on the nature of each complex, and the relative abundance of the various complexes depends on the concentration of Ni^{2+}. Hence, the resulting partial current density for Ni deposition cannot be expected to depend linearly on concentration in such a complex system.[92,106]

In summary, even though the partial current density for deposition of tungsten $i_{c,W}$ is very small compared to the calculated limiting current density, $i_{L,W}$, a significant dependence of $i_{c,W}$ on the rate of mass transport is observed. This is taken as a strong indication that the electro-active species is indeed a mixed-metal complex of the type shown in Eq. (32), which exists in solution at a low concentration. On the other hand, $i_{c,Ni}$ is independent of rotation rate, indicating that this metal is also deposited by an independent parallel route from its complexes with either NH_3 or Cit^{3-}, which exists in solution at high concentrations.[93]

2. Molybdenum Alloys Containing Ni, Co and Fe

(*i*) *Properties of Molybdenum Alloys*

Molybdenum (Mo) is a silvery-white, hard, fairly ductile, refractory metal suitable for alloys that are required to exhibit a combination of high strength and rigidity at temperatures as high as 1,650°C. Selected properties of molybdenum are listed in Table 2, in comparison with the respective properties of tungsten and

rhenium. Molybdenum is found in molybdenite (MoS_2) and wulfenite ($PbMoO_4$) ores. It is also recovered as a by-product of Cu and W mining. Molybdenum has the fifth highest melting point of all elements. Its electrical conductivity (30% IACS) is the highest of all refractory metals, about one third that of Cu, but higher than those of Ni, Pt and Hg. It has high-thermal conductivity—approximately 50% higher than that of Fe, steels or Ni-based alloys, and consequently finds wide usage as heat sinks. Its low thermal expansion coefficient plots almost linearly with temperature over a wide range, thus facilitating its use in bimetal thermocouples. Its mechanical properties include high tensile strength, high Young's modulus of elasticity, high hardness and toughness (it is softer and more ductile than W). Its high specific elastic modulus makes it attractive for applications that require both high stiffness and low weight. The high thermal conductivity, low coefficient of thermal expansion and low specific heat of Mo provide resistance to thermal shock and fatigue; these properties are also important in electronic applications. Molybdenum also exhibits good machinability and low vapor pressure at elevated temperatures. It is stable in a wide variety of chemical environments, including halogens, but oxidizes in air more readily than W at temperature higher than 760°C. Under these conditions, the oxide layer (MoO_3) sublimes, and the base metal is attacked. Therefore, Mo performs best in inert or vacuum environments. The corrosion resistance of Mo is very similar to that of W. It resists non-oxidizing mineral acids and reducing atmospheres containing hydrogen sulfide. It also offers excellent resistance to some liquid metals, including Li, Bi, Na and K, in the absence of oxygen.

(*ii*) *Applications of Molybdenum Alloys*

More Mo is consumed annually than any other refractory metal. The major use for Mo is as an alloying element in alloy steels, tool steels, stainless steels, Ni-based and Co-based superalloys. In these materials, it increases the hardenability, toughness, high-temperature strength, and corrosion resistance. Molybdenum is important in the missile industry, where it is used for high-temperature structural parts, such as nozzles, leading edges of control surfaces, support vanes, struts, reentry cones, radiation shields and heat sinks. In the electrical and electronic industries, Mo is

used as cathode supports for radar devices, magnetron end hats, heat sinks for matching Si for semiconductor chip mounts, and sputtered layers for gates and interconnects on integrated circuit chips. Molybdenum has also been used in forging dies, rotating X-ray anodes in clinical diagnostics, furnace tubes, high-temperature solid lubricants (e.g., molybdenum sulfide), chemical processing equipment, flame retardants, light bulb filaments, inorganic paint pigments, chemical catalysts (e.g., in refining of petroleum), and scrubbers in flue gas desulfurization in coal-fired power stations. Finally, Mo alloyed with Re (e.g., Mo-41Re and Mo-47.5Re) is used in electronics, space programs and nuclear industries, while Mo-25Re alloys are used for rocket engine components and liquid-metal heat exchangers.

(*iii*) *Electrodeposition of Molybdenum Alloys*

A phenomenon of induced codeposition, similar to that discussed above for W, is observed when Mo is codeposited with iron-group metals. Similarly to tungsten, molybdenum cannot be deposited alone from aqueous solutions. Electrodeposition of Mo alloys exhibits similar dependencies on experimental variables as that of W. It should be noted that, although the two systems are very similar, some differences are found in the literature, as described bellow.

An early comprehensive review on electrodeposition of Mo alloys with iron-group metals was presented by Brenner.[78] The development of different baths, as well as the effect of operating conditions on the Mo content of the alloy is described in detail in that work. Electrodeposited alloys of Mo were claimed to be of limited practical value, because of their poor physical characteristics compared to the corresponding alloys of W.

The acid baths for electrodeposition of Mo alloys have been divided into two types: those that are wholly inorganic, and those that contain organic poly-acids as chelating agents. The addition of organic complexing agents, typically poly-hydroxy acids, considerably improved the quality and increased the Mo content of the electrodeposited alloys. This was attributed to complexing of the molybdate ion, the effectiveness being related to prevention of the formation and inclusion of partially reduced Mo compounds. The alkaline baths, which are considered to be preferential, were

divided into several types, namely: ammoniacal baths, pyrophosphate, carbonate and caustic baths containing organic complexing agents. Representative bath compositions and operating conditions are listed in Appendix B. While Mo-Ni alloys were found to be the soundest among those of Mo-iron-group-metal alloys, their Mo content was the lowest.[78]

Ammoniacal baths have been found most suitable for codeposition of Mo alloys. The presence of free ammonia in the baths was claimed to be essential; similar to W codeposition – ammonia-containing baths had a higher FE. In contrast to W plating baths, there appeared to be no advantage of operating the Mo plating baths at elevated temperatures. Similar to W codeposition, the concentration of Mo in the deposit was higher than its metal ion concentration in the bath. For Mo-Ni, Mo-Co and Mo-Fe ammoniacal-citrate baths within the pH range of 2 to 12, the maximum Mo content of the deposit and minimum FE were observed around pH = 8. An increase in current density within the range of 10–200 mA cm^{-2} yielded a decrease in Mo concentration in Mo-Ni and Mo-Co alloys, in contrast to the trend reported for W alloys deposited from ammoniacal baths. As in the electrodeposition of W alloys, the current density-potential curves of the deposition of Mo-Ni and Mo-Co alloys occurred at less negative potentials than the curve for the iron-group metal alone.[78]

Newer studies have demonstrated that the properties of Ni-Mo alloys can be improved by application of pulsed electrodeposition.[145,146] Compared to DC electrodeposition, a higher Mo content in the alloy was obtained, which was accompanied by reduced residual stresses, improved mechanical properties and improved corrosion resistance.

According to Brenner, most of the theories proposed to explain the mechanism of induced codeposition of W can be applied also to induced codeposition of Mo, and vice versa. However, a theory that was found satisfactory to explain the induced codeposition of Mo from pyrophosphate bath, but would not be applicable to W codeposition, is that of Myers.[141] According to this model, a layer of hydroxide of Mo and the iron-group metal forms on the cathode. The hydroxide of the iron-group metal supposedly alters the permeability of the film so that it can be penetrated by molybdate ions. Otherwise, only hydrogen is discharged. Ernst and Holt suggested another theory.[147] According to this theory, Mo was

first deposited as an oxide that, in the presence of the iron-group metal, could be reduced to metal by hydrogen. The number of unpaired electrons in the iron-group metal was considered as an index of its ability to form a bond with hydrogen and, thereby, reduce the Mo oxide.[78] However, the theoretical basis for this correlation could be questioned.

In recent years, several new papers have been published, attempting to explain the mechanism of induced codeposition of Mo with the iron-group metals. Podlaha and Landolt[95,96,148] studied the codeposition of Mo-Ni alloys from ammoniacal citrate solutions. They examined the influence of operating conditions on the composition of the alloy by means of rotating cylinder Hull (RCH) cell and RCE. The RCH cell is actually a cell with a rotating-cylinder working electrode, in which the anode and the cathode are concentric, and a third concentric cylinder, made of an electrically insulating material, is placed between them as shown in Fig. 11. This configuration forces a non-uniform current distribution on the cathode, thus allowing the evaluation of the properties of the elec-

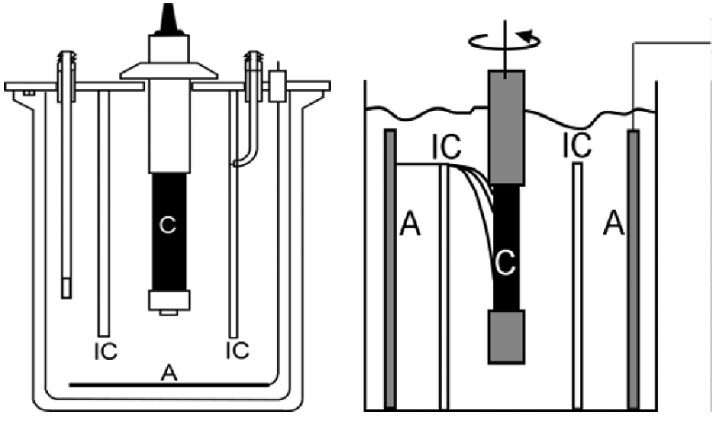

Figure 11. Illustration of two alternative designs for the rotating cylinder Hull (RCH) cell, which allows the study of non-uniform current distribution on the cathode, under controlled mass-transport conditions. A: anode, C: cathode, IC: insulating cylinder. Reproduced from Ref. 150 with kind permission of Springer Science and Business Media, and with permission from Ref. 95, Copyright (1996) The Electrochemical Society.

troplated film over a wide range of current densities in a single experiment. The RCH, developed by Landolt et al.[149-151] represents a significant improvement over the regular Hull cell, in that it allows measurements under controlled conditions of mass transport. In the cell used by these authors for the study of Mo deposition[95-97, 148] the radius of the rotating cylinder was 0.75 cm and the inner radius of the inert cylinder was 2.75 cm, thus leaving a space of 2 cm between them. The latter value is between two and three orders of magnitude larger than the thickness of the Nernst diffusion layer, ensuring a uniform rate of mass transport to the surface of the cylindrical cathode, while the current density on the cathode is non-uniform, of course. When the concentration of the Ni^{2+} ion in solution was much larger than that of MoO_4^{2-} (namely, 1.0 M $NiSO_4$, 0.005 M MoO_4^{2-}), the Mo-content in the alloy increased with rotation rate. This shows that a partial mass-transport limitation of the molybdate ion was involved, thereby lowering the Mo content in the deposit. From the measured alloy composition and film thickness, the partial current densities for Mo and Ni deposition were calculated. The results, shown in Fig. 12, demonstrate a rotation rate-dependent current plateau for Mo (Fig. 12a), and a largely activation-controlled reaction behavior for Ni (Fig. 12b). On the other hand, when the concentration of MoO_4^{2-} in the electrolyte was 0.4 M and that of Ni^{2+} was 0.005 M, the alloy composition was found to be independent of the rotation rate. The calculated partial current densities for Mo and Ni deposition are shown in Figs. 12c and 12d, respectively. Here, at current densities higher than about 50 mA cm^{-2}, Ni exhibits a mass-transport-limited plateau, the height of which increases with rotation rate. In this case, the partial current for deposition of Mo is also mass-transport controlled. As the rotation rate is increased, the two partial currents increase roughly in the same proportion, showing that the rate of deposition of Mo is controlled by the flux of the Ni^{2+} ion, which is the essence of induced codeposition.

In addition to the effects of convection discussed above, it was found[95] that increasing the concentration of the MoO_4^{2-} ion, the concentration of Cit^{3-} (up to a limit of 0.75 M) or the temperature resulted in an increase in the Mo-content in the deposit over a wide range of applied current densities. The concentration of ammonia was also found to have a significant effect—as it was increased

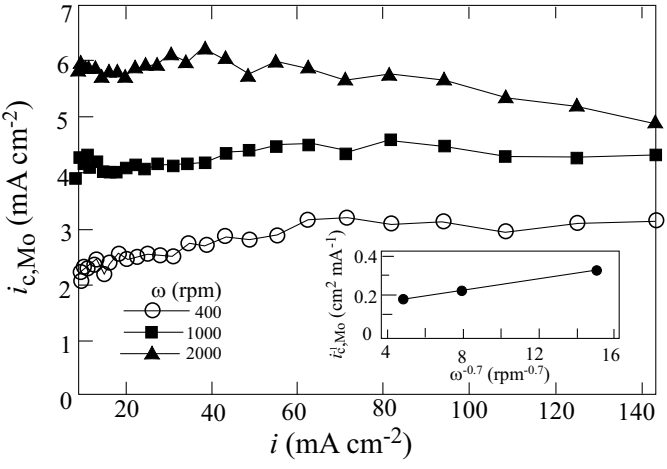

(a)

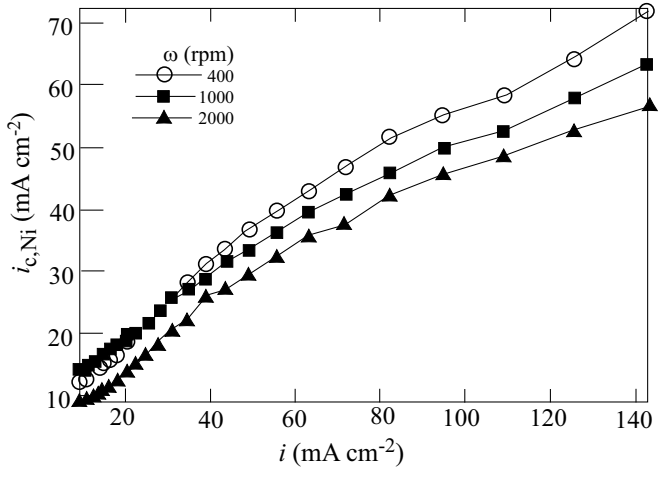

(b)

Figure 12. Partial current densities of Mo (a, c) and Ni (b, d) as a function of the approximate total current density for different rotation rates. The inset in (a) shows the inverse Mo partial current vs. $\omega^{-0.7}$. Electrolyte: 1.0 M Ni^{2+} and 0.005 M MoO_4^{2-} in (a) and (b); 0.005 M Ni^{2+} and 0.4 MoO_4^{2-} in (c) and (d). Reproduced with permission from Ref. 95, Copyright (1992), The Electrochemical Society.

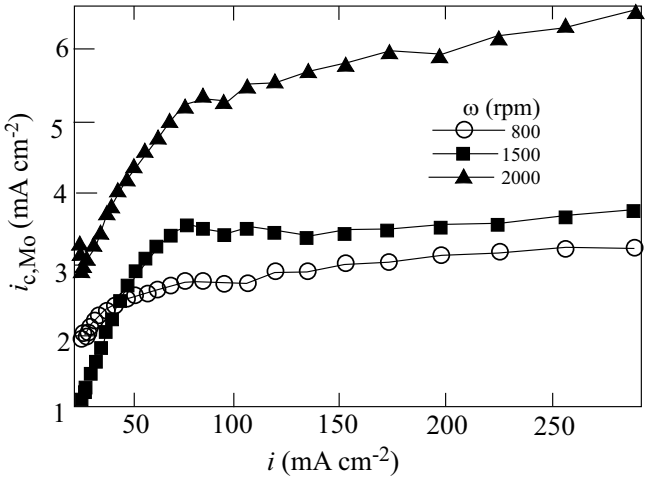

(c)

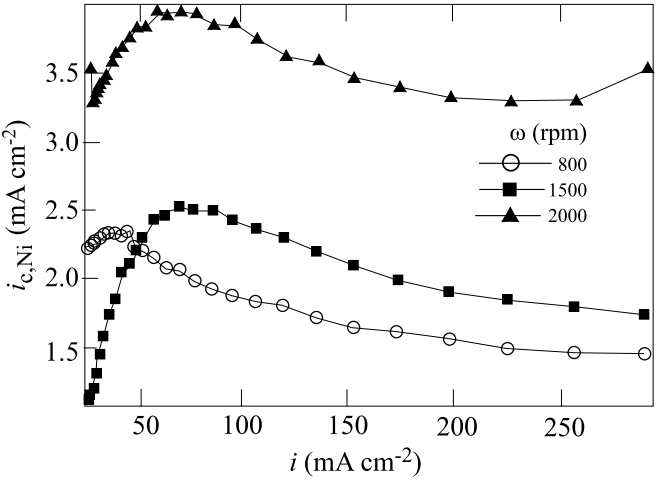

(d)

Figure 12. Continuation.

from 0 to 1 M, the FE increased, but the Mo-content in the deposits decreased.

On the basis of the observations described above, it was postulated that the precursor for the deposition of the Mo-Ni alloy was an adsorbed intermediate mixed-metal complex of the form $[NiCit(MoO_2)]^-_{ads}$. This intermediate can be reduced, thus allowing Mo deposition. The Ni^{2+} ion, complexed either with Cit^{3-} or with NH_3 (as discussed earlier for W codeposition), can be reduced in parallel with Mo, following the simple equations

$$[NiCit]^- + 2\,e^-_{crys} \rightarrow Ni + Cit^{3-} \tag{39}$$

$$[Ni(NH_3)_n]^{2+} + 2e^-_{crys} \rightarrow Ni + n\cdot NH_3 \tag{40}$$

The hydrogen evolution reaction is considered to be a side reaction, leading to a reduction of the FE to varying degrees, depending on the composition of the bath and the conditions of plating. In neutral or alkaline solutions this reaction can be written as

$$H_2O + e^-_{crys} \rightarrow \frac{1}{2}H_2 + OH^- \tag{41}$$

The reaction sequence leading to induced codeposition of Mo with Ni (as well as with Co and Fe) was assumed to be

$$[NiCit]^- + MoO_4^{2-} + 2\,H_2O + 2\,e^-_{crys} \rightarrow [(NiCit)(MoO_2)]^-_{ads} + 4\,OH^- \tag{42}$$

$$[(NiCit)(MoO_2)]^-_{ads} + 2\,H_2O + 4\,e^-_{crys} \rightarrow Mo + [NiCit]^- + 4\,OH^- \tag{43}$$

Thus, in solutions containing high $[MoO_4^{2-}]/[Ni^{2+}]$ ratio, the formation of the Ni-Mo intermediate is limited by transport of

$[NiCit]^-$ to the cathode surface. Because the deposition rate of the two metals is coupled, the alloy composition does not vary with rotation rate. In contrast, if the concentration of Ni^{2+} in solution is comparable to or higher than that of MoO_4^{2-}, the rate of formation of the Ni-Mo intermediate is limited by the transport of molybdate, while Ni can be deposited in parallel—its rate of deposition being independent of the rate of mass transport. Increasing either the rotation rate or the molybdate concentration—the partial current density of Mo deposition will also increase, while that of Ni deposition will not be affected.[95] Thus, it was proven beyond any doubt that the induced codeposition of Mo with Ni and other iron-group metals was dependent on the existence of the iron-group metal ions in solution.

However, the scheme proposed to explain the effect of Ni^{2+} ions on the codeposition of Mo (Eqs. 42 and 43) leaves some unanswered questions. Equation (39) shows the interaction between two soluble ions, leading to the two-electron reduction of one of them, and the formation of a mixed-metal complex adsorbed on the surface. All these processes cannot happen in a single step, but the authors did not specify what actually is assumed to happen: Is $[NiCit]^-$ first adsorbed on the surface and then acts as the catalyst for the reduction of MoO_4^{2-} to MoO_2? Or, perhaps, the two ions form a mixed-metal complex in solution, which is subsequently adsorbed and reduced?

Furthermore, $[NiCit]^-$ can readily be reduced to metallic nickel (c.f. Eq. 39) at the potential where the Ni-Mo alloy is formed. Yet, no such reduction is shown in Eqs. (42) and (43), in which Mo is first reduced from the hexavalent molybdate to the tetravalent molybdenum dioxide, and then further to metallic molybdenum. A solution, in which the concentrations of Ni^{2+} and Cit^{3-} were equal, was used and it was assumed that all citrate ions were bound to Ni in $[NiCit]^-$.[95] This assumption ignores the possible existence of complexes of the type $[(MoO_4)(Cit)(H)_m]^{-(5-m)}$ (written for short as $[1,1,m]^{-(5-m)}$, where *m* is the number of protons in the complex), in spite of the fact that such complexes are well known (cf., Fig. 13a). In addition, detailed calculation of the distribution of species in a Ni^{2+} and Cit^{3-} mixture shows that, when the ratio of the concentrations of the two ions is unity, there are still a few percents of free Ni^{2+} and Cit^{3-} ions not bound in the complex, as seen if Fig. 1b.

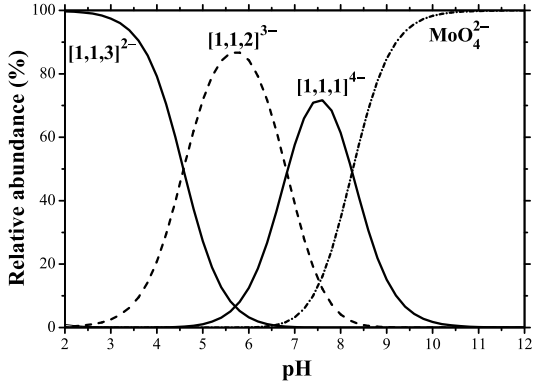

(a)

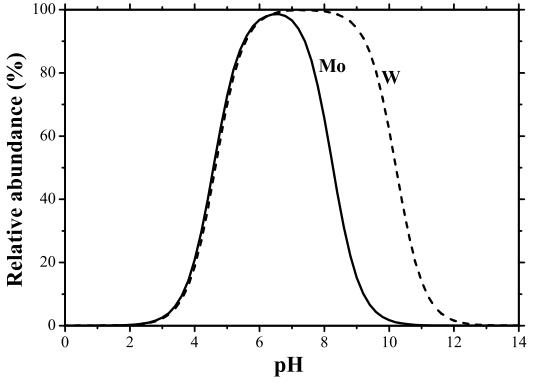

(b)

Figure 13. (a) The relative abundance of the protonated $[(MoO_4)(Cit)(H)_m]^{-(5-m)}$ complexes as a function of pH. The abbreviated forms $[1,1,1]^{4-}$, $[1,1,2]^{3-}$, and $[1,1,3]^{2-}$ refer to values of m = 1, 2 and 3, respectively, in the above complex. (b) Comparison between the sum of the concentrations of the complexes $[1,1,1]^{4-}$ and $[1,1,2]^{3-}$ of WO_4^{2-} and MoO_4^{2-} with Cit^{3-}, as a function of pH. The calculations are based on the data in Figs. 8 and 13.

In a following publication[96] a mathematical model was developed that was found to be in fairly good agreement with the experimental results. This, however, was based on a large number of adjustable parameters and several assumptions. Hence, this numerical agreement could at best be considered as consistent with the mechanism proposed, not proving the validity of the model. This model was extended by the same authors for the case of Mo alloys with Co and Fe.[97]

The shortcoming of the mathematical model in confirming the validity of the suggested physical model could best be demonstrated by the comparison of deposition of molybdenum ions with different iron-group metals.[97] In order to reduce the number of freely adjustable parameters, the authors plotted the partial current densities for Mo and Ni (or Co or Fe) as a function of potential, to obtain experimental values of respective Tafel slopes. The values obtained were very high, in the range of 0.36–0.59 V decade^{-1}, compared to typical values around 0.12 V decade^{-1} reported in the literature for deposition of the iron-group metals. No explanation was offered for this discrepancy and no mechanism was proposed that would explain such high Tafel slopes, which were subsequently used in the numerical simulation of the model.

The problem, in the view of the present authors, is that the partial current density for deposition of, say, nickel is determined from the total amount of nickel deposited per unit time. However, in a solution containing Ni^{2+}, MoO_4^{2-}, NH_3 and Cit^{3-}, there can be as many as nine different species from which nickel could be deposited (six complexes with 1–6 molecules of NH_3, two with citrate, and one adsorbed mixed-metal complex). The reversible potential for deposition of nickel is, in principle, different for each complex (depending on the stability constants). Hence, although all these parallel paths occur at the same *applied potential*, the *overpotential* is different for each of them. Moreover, there is no basis to assume that the exchange current densities or the Tafel slopes would be the same. If the observed Tafel plot would, nevertheless, be linear over at least two decades of current density, it could be argued that one of these parallel paths for deposition of nickel happens to be predominant. However, in the work quoted here, the apparent linearity of the Tafel plots extends only over a factor of about three in current density, namely over half a decade (cf., Fig. 4a in Ref. 97).

The difficulty in attempting to determine the mechanism of alloy deposition from the current-potential relationship observed in complex solutions, which sometimes contain more than one ligand, was alluded to in the introduction to this chapter (cf., Section 1.2.2). The comments made here are not meant to criticize the experimental work presented in these papers in the field of induced codeposition of Mo with iron-group metals. It is only given to show the limits of validity of mathematical models, particularly when the solution is complex and the number of freely adjustable parameters is large.

Figure 13a shows the calculated concentration distributions for molybdate-citrate complexes as a function of pH. This figure is analogous to Fig. 8 for tungstate-citrate complexes. The two figures are similar, but not identical. In particular, it is noted that the $[1,1,1]^{4-}$ species is predominant in the case of tungstate in the range of pH = 6.8–10.2. For molybdate, it reaches a maximum at pH = 7.6, but even there it only constitutes about 72% of all the species in solution. In Fig. 13b, the sum concentrations of $[1,1,1]^{4-}$ and $[1,1,2]^{3-}$ are compared. In studies of induced codeposition of Ni-W alloys it was found that the W-content of the alloy, measured as a function of pH, followed rather closely the variation of the relative abundance of the above sum of concentrations with pH, with the highest W concentration obtained at pH = 7 and a sharp decline above pH = 9.0. [93] If the same argument holds for induced codeposition of Mo, then the highest Mo concentration should be obtained at pH = 6.6, with a sharp decline at about pH = 8.3.

Gómez et al.[152] electrodeposited Co-Mo magnetic alloys from a sulfate-citrate bath on carbon electrodes. Although the focus of their paper was not on elucidating the mechanism of induced codeposition, it was suggested that hydrogen could not be responsible for the deposition of Mo in the Co-Mo system, because its concentration was fairly low and because another mechanism should explain the need for citrate or polycarboxylate anions in solution. The deposition process was found to be favored when molybdate was present in solution, even at very low concentrations. Hence, the authors adopted the model of Podlaha and Landolt, according to which a mixed-metal complex of cobalt(II), citrate and molybdenum dioxide is adsorbed on the surface and promotes Mo reduction.

Another mechanism for induced codeposition of Mo was suggested by Chassaing et al.[153] for electrodeposition of Mo-Ni alloys from citrate-ammonia electrolytes. Electrochemical impedance spectroscopy (EIS) measurements were carried out in order to better understand the different reactions occurring on the electrode surface during deposition. The proposed mechanism is based on a multi-step reduction of molybdate species. A MoO_2 layer is formed via reduction of molybdate ion as in Eq. (42). Then, if free Ni^{2+} is present in solution, this oxide can first combine at low polarization with Ni, following the reduction reaction:

$$MoO_2 + 4\,Ni^{2+} + 8\,e^-_{crys} \rightarrow MoO_2Ni_4 \tag{44}$$

A 25 nm-thick layer with a Ni/Mo atomic ratio of 4:1 was indeed detected by AES and EDS. The mixed Ni-Mo oxide is claimed to catalyze the HER. Next, when the polarization is increased, the mixed oxide is further reduced to a surface compound that inhibits the HER and is more catalytic for reduction of molybdate and nickel ions, forming an alloy according to the reaction:

$$MoO_4^{2-} + 3\,Ni^{2+} + 8\,e^-_{crys} + \;4 + n\cdot H_{ads} \rightarrow MoNi_3 + 4\,OH^- + n\cdot H_{abs} \tag{45}$$

The HER is claimed to take place in this case due to the alcohol functional group of the citrate ion, which is an unlikely reaction in solutions at pH 9.5. In the third stage, at still higher polarization, the Mo discharge is limited by diffusion, due to the low molybdate concentration of the electrolyte, thus decreasing the Mo content in the deposited alloy.

Several arguments against the last theory may be raised. First, the proposed mixed oxide contains nickel atoms that are fully reduced. If so, what makes this oxide stable? Secondly, no direct observation was provided for the reduction of this oxide into an alloy. Thirdly, the origin of the adsorbed hydrogen atoms included in Eq. (45) is not clear. Finally, it should be obvious that Eqs. (44) and (45) cannot be considered as elementary steps in the reaction sequence. Four Ni^{2+} ions could not be possibly reduced simultaneously. Neither could the eight-electron reduction of MoO_4^{2-} + $3Ni^{2+}$ occur in one step. Thus, there seem to be absolutely no basis

to claim that the above sequence represents the mechanism of formation of the Mo-Ni alloy.

The formation of an intermediate, which is then reduced to form Mo—with either Ni or Fe acting as a catalyst, was also claimed, based on in-situ Raman spectroscopy studies.[154,155] Although the exact composition of the intermediate was not identified in these studies, it was argued that at low cathodic polarization, the main species on the electrode surface were polymolybdates, that could be reduced to Mo(IV) at a higher cathodic polarization. The species of Mo(IV) could be further reduced to Mo atoms only when cations of the iron-group metal were present in the electrolyte.

Crousier et al.[156] examined the role of hydrogen evolution in the process of deposition of Mo-Ni alloys on different substrates (glassy carbon, Ni and Pd). It was found that on carbon and Ni substrates, bright and smooth deposits were formed, while on Pd no alloy was formed. This observation was related to easy absorption and diffusion of atomic hydrogen into Pd, which prevented its availability for the alloy codeposition process. Hence, it was concluded that hydrogen plays an important role in the codeposition of the alloy. This conclusion of the authors is, however, not convincing. Firstly, it is known that hydrogen atoms can also permeate into Ni to some extent. Secondly, unsuccessful attempt to deposit Mo-Ni alloys on Pd may also be attributed, for example, to kinetic limitations.

3. Rhenium and its Alloys

(*i*) *Properties of Rhenium and its Alloys*

Rhenium (Re) differs from the other refractory metals (Nb, Ta, Mo and W) in that it has an hcp structure, and does not form carbides. Because it does not have a ductile-to-brittle transition temperature, Re retains its ductility from subzero to high temperatures. In addition, it can be mechanically formed and shaped to some degree at room temperature. It also has a very high modulus of elasticity that, among metals, is second only to those of Ir and Os. Compared with other refractory metals, Re has superior tensile strength and creep-rupture strength over a wide temperature range.

Among all elements, except W and C, Re has the highest melting point. It also has high electrical resistivity over a wide temperature range, and less volatilization in vacuum compared to W. At elevated temperature, Re resists attack in hydrogen and inert atmospheres. It is resistant to hydrochloric acid and seawater corrosion, and to the mechanical effects of electrical erosion (i.e., extensive destruction of an electrode in some forms of electrical discharge). Rhenium is nowadays available mainly as perrhenic acid ($HReO_4$), ammonium perrhenate (NH_4ReO_4), and metal powder.

The major drawbacks of Re include high density (that is exceeded only by those of Os, Ir and Pt), limited availability (that delayed its discovery until 1925), high cost of the raw material, and the need for intricate processing methods (e.g., because of its very high strain-hardening rate), which results in high fabrication costs. Rhenium is oxidized catastrophically in moist air at temperatures above 600°C; oxidation occurs as a result of the formation of rhenium heptoxide (Re_2O_7). In order to protect rhenium from oxidation at high temperatures, iridium (Ir) is often used as an oxidation-resistant coating.[157-161]

(*ii*) *Applications of Rhenium and its Alloys*

The scarcity and high cost of Re have limited its use. Nevertheless, its unique properties can be useful in important, albeit special, applications. Rhenium alloys are used in nuclear reactors, semiconductors, electronic tube components, thermocouples, gyroscopes, miniature rockets, electrical contacts, thermionic converters (i.e., direct producers of electric power from heat by thermionic electron emission), etc. Platinum-rhenium reforming catalysts are probably still the major end-use products of Re. They are used for the hydrogenation of fine chemicals and for hydrocracking, reforming and disproportionating of olefins, including increasing the octane rating in the production of lead-free petroleum products.[157,158] Rhenium has several properties of potential interest to the electronics industry, particularly its very high melting point and low volatility. In the electrical contact industry, Re is used because of its wear resistance and its ability to withstand arc erosion,[158] and since the oxides formed on its surface are relatively good conductors.[162] Thermocouples made of Re-W alloys are used

for measuring temperatures up to 2,200°C, and Re igniter wires are used in photoflash bulbs for photography. Rhenium alloys are also used in grid heaters and cathode cups. The metal is used as a filament material for mass spectrographs and ion gages, because of its high electrical resistivity and low vapor pressures at high temperatures.[158] Tungsten-rhenium alloys are used to coat the surface of Mo targets in X-ray tube manufacture. Other applications of Re include heating elements, metallic coatings, alloying of W- and Mo-based alloys as well as of superalloys, fuel cell electrodes, and coordination compounds in radiopharmacy. [158,163,164]

Since the 1990s, much work has been focused on developing Re-based parts for aerospace applications. For example, Re has been considered for use in divert and attitude propulsion subsystems. Recession rates of Ir-lined Re thrust chambers have been estimated to be 0.42 μm h^{-1} at 2,200°C.[165] In addition, Re wets nicely carbon and does not form carbides, which makes it attractive as a coating material for carbon-carbon composites.[166] In the absence of a protective atmosphere, a protective coating (e.g., of Ir, Pt or Rh), to inhibit oxygen attack, can be applied on top of Re.[157,158] A combustion chamber material system composed of a Re substrate and an Ir coating has already been proven to operate for longer lifetimes at higher temperatures of up to 2,200°C (compared to the state-of-the-art material system for radiation-cooled rockets, which is a C103 niobium alloy coated with R512E fused silica). The added thermal margin afforded by Ir-coated Re allows the virtual elimination of film cooling, leading to higher performance and cleaner spacecraft environments.[167]

Most of the published reports to-date deal with fabrication of Re-based items by chemical vapor deposition (CVD), as compared to any other coating process. Reed et al.[167] claimed that CVD is the only established process, by the year 1998, for fabricating Ir/Re combustion chambers. However, delamination-related failures have been reported on Re-coated components made by CVD. Fortunately, electroplating at near-room temperature may become a successful alternative and allow for fairly uniform Re coatings on such complex shapes. Although Re may be deposited as pure metal, binary Re-Rh or Re-Ir coatings should possess higher oxidation resistance and thermal stability. The second metal can also aid in healing of micro-cracks that form in the Re coating during electrodeposition or service (as discussed in the next section).

(*iii*) *Electrodeposition of Rhenium and its Alloys*

Compared to tungsten and molybdenum, much less information is available on electrodeposition of rhenium, possibly due to the confidentiality of many related projects worldwide. Furthermore, most studies have focused on the technological aspects, properties and applications of Re electrodeposition, while overlooking its electrochemistry. Rhenium belongs to a group of metals that are difficult to obtain by electrolysis of their aqueous solutions. This behavior has been attributed mainly to its very low overpotential for hydrogen evolution. For example, in a 2 N sulfuric acid solution, at a cathodic current density of 5 mA cm^{-2}, the overpotential for hydrogen evolution on Re was estimated to be no more than 90 mV.[160] In addition, because no simple Re(VII) salt is soluble in water without hydrolysis, it was further suggested that Re^{Z+} ions are unlikely to exist in solution, or can exist only in very low concentrations.[162]

Figure 14 shows the Pourbaix equilibrium diagram for the Re-H_2O system at 25°C. In this figure, the lines for hydrogen and

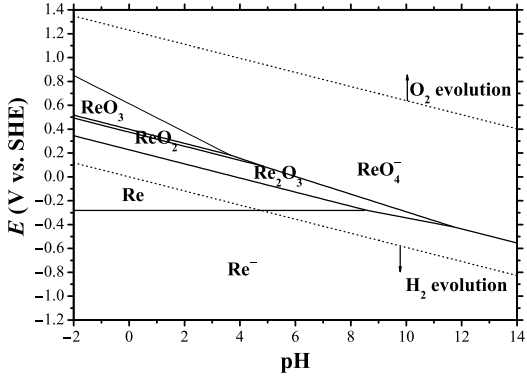

Figure 14. Potential-pH equilibrium diagram for the rhenium-water system at 25°C.

oxygen evolution are also shown. Between these two lines, water is stable. Figure 14 comprises an anodic corrosion domain (corresponding to the formation of ReO_4^-), a cathodic corrosion domain (formation of Re^-), an immunity domain (formation of Re), and a passivation domain (formation of more or less hydrated Re_2O_3). This figure is valid only in the absence of substances with which Re can form soluble complexes or insoluble salts. Metallic Re, shiny-white in the compact state and gray-black in the dispersed state, is a relatively base metal, having a very small zone of stability in common with that of water. Rhenium can be obtained, possibly mixed with some lower oxides, by the electrolysis of near-neutral or acidic solutions of perrhenates or perrhenic acid. It is obtained in a finely divided gray-black form when using current densities between 10 and 100 mA cm^{-2}. At higher current densities, lead-colored tree-like growths are formed at the cathode; these are thought to be compounds of metallic Re with brown hydrated lower oxides. Rhenium can also be produced by chemical reduction, but only with difficulty. More powerful reducing agents than zinc, such as stannous chloride ($SnCl_2$) and hydriodic acid (HI), reduce heptavalent rhenium only to the tetravalent state. Rhenium is easily oxidized in alkaline solutions, with the formation of various oxides (e.g., Re_2O_3, ReO_2, and ReO_3), as well as perrhenic acid and soluble perrhenates. In addition, it is easily reduced with the formation of soluble rhenide (Re^-). In the presence of moist air, Re is oxidized to perrhenic acid, even at room temperature. This oxidation is very rapid in the case of finely divided Re, which is occasionally pyrophoric. The oxidation of Re, even when compact, is rapid in the presence of solutions of hydrogen peroxide, alkaline or acid oxidizing solutions, solutions of nitrites/nitrates or alkali metal peroxides, and nitric acid solutions. Concentrated sulfuric acid also dissolves Re, but more slowly.[168] From Fig. 14 it may be concluded that a fine control of both potential and pH is required in order to form metallic rhenium without significant hydrogen evolution, which might result in hydrogen embrittlement and cracking.

Electrolysis has been applied primarily to extract metallic Re from solutions, and to produce Re coatings. In electrolytic extraction, the metal can be obtained in the form of a bright deposit or a black powder, depending on the conditions of electrolysis.[160] The

overall reaction in a potassium perrhenate ($KReO_4$) solution was represented as:[162]

$$4\,HReO_4 + 2\,H_2O \rightarrow 4\,Re + 4\,KOH + 7\,O_2 \qquad (46)$$

Different mechanisms have been proposed for the electrodeposition of Re, involving the stepwise reduction of the ReO_4^- ion, the role of adsorbed hydrogen atoms, following initial reduction to ReO_3, and even formation of the highly charged Re^{7+} ion as an intermediate.[160,162] No solid evidence was given for any of the reduction routes proposed; however, it is evident that the seven-electron reduction of ReO_4^- and the parallel removal of four oxygen atoms must involve many consecutive steps, even if the nature of the intermediates formed, some in solution and some perhaps adsorbed on the surface, is unknown. It should be noted, however, that a mechanism postulating the reduction of a heptavalent cation (Re^{7+}) can be rejected out of hand, since such ions are not known to exist in aqueous solutions. Moreover, the solvation energy of ions in aqueous solutions is roughly proportional to the square of the charge (namely, 5, 20 and 50 eV for Me^+, Me^{2+} and Me^{3+}, respectively). Extrapolating to Me^{7+} would lead to a solvation energy of 200–250 eV. Thus, if a Re^{7+} ion did exist in solution, it would be energetically impossible to remove its solvation shell and deposit metallic rhenium from it.

An early, relatively short, review on electrodeposition of Re alloys with iron-group metals was presented by Brenner.[78] In an acid perrhenate solution, the overall reaction can be written as

$$ReO_4^- + 8\,H^+ + 7\,e^-_{crys} \rightarrow Re + 4\,H_2O \qquad (47a)$$

with a standard potential of +0.34 V vs. SHE,[169] which is more noble than that of hydrogen. In alkaline solutions, on the other hand, the overall reaction can be written as

$$ReO_4^- + 4\,H_2O + 7\,e^-_{crys} \rightarrow Re + 8\,(OH)^- \qquad (47b)$$

and the corresponding standard potential is –0.604 V vs. SHE.[169] This value is approximately +0.21 V vs. RHE in a 1 M NaOH so-

lution (pH 13.8). On the basis of the standard potentials, it should be possible to reduce Re from either aqueous or alkaline solutions. Yet, in practice the plating process takes place with a very low FE, of the order of 10%. Hence, Brenner concluded that the deposition of Re is subjected to some restraints, similar (but to a lesser degree) to those observed in deposition of W and Mo.

Typical bath compositions and operating conditions for electrodeposition of Re are listed in Appendix C. An acid sulfate solution, based on potassium perrhenate, was suggested by Fink and Deren.[170] Netherton and Holt[171] worked with similar baths, to which they added either citric acid or ammoniacal citrate.* Sligh and Brenner used more concentrated solutions of perrhenate, but still could not increase the FE significantly. Their deposits exfoliated when produced thicker than 10 μm, and oxidized rapidly upon exposure to air. Therefore, it was hypothesized that the electrodeposited metal was not pure, but contained oxide inclusions.[78]

Several recommendations regarding the electrodeposition process were later drawn by other authors. According to Lebedev,[160] the most widely used baths contain potassium perrhenate and free sulfuric acid, whereas Pt is the commonest anode material. One limitation in the use of potassium perrhenate is its low solubility in water (0.037 M at 21.5°C, compared to 0.215 M and 3.45 M at 20°C for ammonium and sodium perrhenates, respectively). However, its solubility is increased in acidic solutions. The deposition potential of Re was found to depend on the material of the cathode. On a Re cathode, the deposition potential was the less negative, with the lowest overpotential for hydrogen evolution. Additions of ammonium sulfate $\{(NH_4)_2SO_4\}$ and gelatin to the bath resulted in an increase in the FE. In contrast to Lebedev's claim, a preliminary work of Treska et al.[166] recently demonstrated that the use of ammonium perrhenate, instead of potassium perrhenate, could result in fewer surface cracks, a higher metallic Re content in the coating, with no traces of undesired potassium contamination. Colton[159] claimed, on the basis of previous studies, that sulfuric acid solutions yield the best Re coatings. In addition, bet-

* It should be noted that at low pH citric acid exists in its fully protonated, uncharged form (cf., Fig. 1a). In this form, it is not a good complexing agent.

ter deposits were obtained if only a thin film of Re was deposited, followed by annealing at high temperature. Additional deposits of Re could then be added in a similar manner, forming a heavy deposit that had good chemical and mechanical stability. Meyer[162] suggested that the deposit properties could be improved by adding magnesium sulfamate $\{Mg[SO_3(NH_2)]_2\}$, which reduced the residual stresses, thus permitting the formation of thicker deposits at high current densities. It was also shown that addition of ammonium sulfate increased the conductivity and FE, particularly at low current densities. Lowering the pH to 1.0–1.5, by addition of sulfuric acid, resulted in higher FE and brighter deposits. The dependencies of FE on pH, current density and temperatures were also studied. While, at $i = 100$ mA cm^{-2} and $T = 60$°C, the deposits were bright and reasonably ductile in the range pH = 0.5–2.0, at higher pH the deposits were darker and with higher level of residual stresses. It was realized that Re has a very low hydrogen overpotential, which is comparable to that of electrodeposited Pt. It was also found that Re could be easily codeposited with several other metals, forming thicker, low-stressed alloy deposits at a much higher FE (as high as 80%, instead of 15% for the pure metal). This behavior was related to a decreased rate of hydrogen evolution. Such alloy coatings typically possess higher oxidation resistance and thermal stability, with a much lower crack density. Although Meyer himself claimed to be able to deposit Re of good quality, he criticized that previously-electrodeposited Re had been highly stressed, brittle, and of poor appearance – particularly when the thickness of the deposit exceeded 1 μm.[162]

Root and Beach[172] also found that the as-deposited Re was not stable in air and moisture, because of the inclusion of rhenium hydride impurities. The quantity of hydride depends on the pH of the bath and the cathode potential.[172, 173] Rhenium hydride is unstable in aqueous solutions and in moist air, and gradually transforms into rhenium oxides. After a time, the hydride-containing surface layer could contain some fine, powdery rhenium oxides, along with the metal. This could hinder the ability of the coating to act as a suitable oxidation barrier. In addition, residual stresses and cracks might form due to the presence of the brittle hydride phase per se. If small oxide impurities exist in the coating, they can readily be transformed into a tarnish-resistant metallic Re by annealing in pure hydrogen at 900–1,000°C for at

least 15 min,[172] but preferably for 1–1.5 h.[173] Temperatures lower than 800°C and other annealing environments were found ineffective. This treatment above the hydride decomposition temperature, however, might introduce some cracks due to shrinkage of the coating during conversion of residual hydride to metallic Re. These cracks can allow oxidizing gases to gain access to the substrate. One way to heal these cracks is to fill them with additional metal, e.g., Ir or Rh. The best way to eliminate (or, at least, control) this problem is to establish optimum bath composition and operating conditions, so that the as-deposited coating would be hydride-free (or near hydride-free).[173] Figure 15 shows the transformation from an amorphous hydride phase into crystalline Re, following hydrogen firing.[166] In order to produce Re deposits thicker than 0.5 mil (12.7 μm), Root and Beach[172] had to employ alternate plating and hydrogen firing. This inability to deposit thick Re coating in one step was related to a lower overpotential of hydrogen on rhenium hydride, as compared to that on other metal surfaces. Hydrogen-fired Re deposits were found to be disconti-

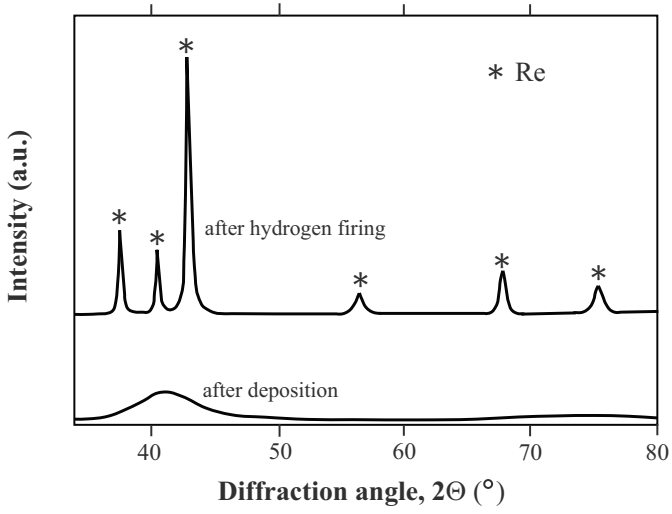

Figure 15. Phase transformation from amorphous rhenium hydride to crystalline Re following hydrogen annealing (T = 900-950°C, t = 1–1.5 h). Reprinted from Ref. 166, Copyright (1997) with permission from the Institute of Materials, Minerals and Mining.

nuous. This characteristic was related to shrinkage of the electrodeposited rhenium hydride, forming rhenium and hydrogen. Since the plating was postulated to involve the deposition of rhenium hydride, it was suggested that conditions, which minimize hydrogen absorption in the cathode, would reduce the FE. The FE was found to decrease due to periodic reverse current plating and to increase as a result of either addition of ammonium nitrate to the bath or increase of bath temperature.

One of the authors of this chapter (Eliaz) was involved for a short period of time in a related project that focused on electrodeposition of pure Re on parts made from graphite or carbon-carbon composites for aerospace applications. It was shown that, in the absence of fine pH and potential control, hydride formation led to significant cracking—mainly around carbon fibers (see Fig. 16). Preliminary runs of potentiodynamic polarization experiments were made to demonstrate that fine control of the potential, to within the immunity domain in the Pourbaix diagram, may aid in reducing the absorption of hydrogen and related cracking. However, neither optimization of the bath chemistry and operating conditions nor attempts to form Re-Rh alloy codeposition were made in that part of the research. Yet, it was found that better qual-

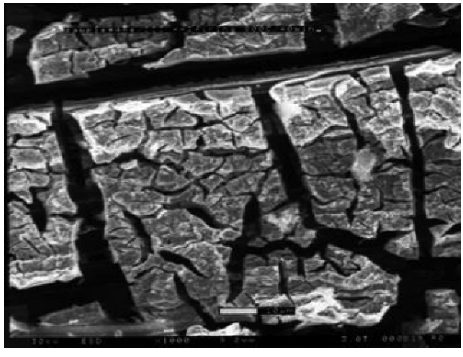

Figure 16. Cracking in a rhenium electrodeposit around carbon fibers in a carbon-carbon composite, as observed by SEM. The bath composition and operating conditions were not optimized; therefore, high contents of hydrogen resulted in cracking.[173]

ity coatings could be formed at high current densities. Pulse shapes that typically yielded reasonable results included 6-8 pulses forward (negative, plating, 140 mA each, 1.2 ms on, 4 ms off) and 1 reverse pulse (positive, metal-bridge dissolution, 10-mA peak, 9 ms on). Complex shapes (including wedge, throat and sphere) were coated, yielding nice visual appearance. The infiltrated and coated outer surfaces of these shapes were subsequently stabilized by an elevated temperature hydrogen anneal.[173]

Pemsler et al.[174,175] earlier introduced the concept of carbon fiber reinforced internal barrier, where diffusion barrier metals are infiltrated electrochemically into matrix-free carbon fibers in a specially oxidized surface ply of C-C. Infiltration was carried out successfully with Re, Rh and Ir. The rhodium coatings were found non-cracked, adherent, and survived thermal cycles to as high as 1,600ºC.

Paris[176] described a method for Re electroplating of the hot plate used for contact ionization of barium in a Q-plasma source. In this case, the reason for coating the tungsten hot plate with rhenium was to increase the probability of ionizing barium (W and Re have work functions of 4.52 and 4.8–5.1 eV, respectively, whereas the ionization potential of Ba is 5.21 eV). Paris discussed some of the technical issues involved in the electrodeposition process, including the effectiveness of a slow rotation of the plate during deposition and a gentle removal of the bubbles from the solution by means of stirrers in producing more uniform coatings, short current reversal to remove roughness of non-uniform plating, and post-treatment in distilled water—followed by drying in an oven at 50–60°C for at least one hour—to prevent peeling of the Re deposit due to exposure to humid air.

Since the early 1990s, Bakos, Horányi, Szabó et al. have had a major contribution on the way to understanding the electrochemistry of Re.[177-185] The electrodeposition of metallic Re from aqueous perrhenate solutions on Au was found to take place at potentials within the hydrogen evolution region.[178] Next, potential oscillations during galvanostatic electrodeposition of Re from ReO_4^- species dissolved in perchloric acid ($HClO_4$) supporting electrolyte were reported.[179] No similar behavior was observed when sulfuric acid was used as the supporting electrolyte. Therefore, the oscillatory phenomenon was related to the reduction of ClO_4^- ions. In a following paper,[180] the electrodeposition of Re

from ReO_4^- species dissolved in $HClO_4$ and H_2SO_4 supporting electrolytes was studied by coupling electrochemical and radiochemical (namely, backscattering of β^- radiation) methods. The rate of Re deposition at a given potential was very low in sulfuric acid compared to that in perchloric acid. It was suggested that deposition of metallic Re took place by at least two fundamental steps:

Step 1: formation of an oxide (or oxidized) layer, possibly ReO_2; and
Step 2: reduction of this layer to metallic Re.

The ratio between the rates of the two steps was expected to be potential and time dependent; the more negative the potential, the lower the ratio of the rate of Step 2 to that of Step 1.

The next paper dealt with Re deposition on Pt by reduction of perhhenic acid with methanol.[181] It had been suggested earlier[182] that methanol could act as the reducing agent, instead of preadsorbed hydrogen, in Re deposition on Pt surface, in the absence of electric polarization. In Ref. 177, pure Re was said to have been deposited via ReO_4^- reduction reaction with adsorbed hydrogen, which was one of the products of decomposition of methanol. It was concluded that this method of Re deposition resulted in the same adsorbed rhenium species as in reduction of ReO_4^- ions either with adsorbed hydrogen or with electric polarization. Almost the same amount of Re could be deposited via ionization of preadsorbed hydrogen as by reduction with methanol. It was later suggested[183] that during deposition of Re on Pt, ReO_2 adsorption took place prior to adsorption of atomic hydrogen, and consequently the hydrogen overpotential was decreased. After a monolayer had been formed, bulk phases of ReO_2 and ReO_3 could also be observed.

In a subsequent paper,[184] electrodeposition of rhenium species from sulfuric acid solutions of perhhenic acid onto polycrystalline Pt and Au surfaces was carried out both in underpotential and overpotential regimes. Metallic Re could be obtained by applying relatively high cathodic current densities, whereas Re(IV) compounds were more likely to form in reduction of ReO_4^- at low current densities. Lastly, the deposition of rhenium species on Au from $Re_2O_7^-$ containing sulfuric acid solutions was studied.[185] It was shown that the chemical nature of electrodeposited rhenium

species depends on the concentration of H_2SO_4 in the supporting electrolyte, from which deposition took place. From H_2SO_4 solutions at pH ≈ 0.9, metallic rhenium was deposited and later oxidized at 0.67–0.7 V vs. RHE, which is far above the standard potential of +0.34 V vs. SHE for Eq. (47a).[169]

Zerbino et al.[186] used in-situ ellipsometry to study the initial stages of deposition of Re, comparing the effect of the substrate (Au and Pt). It was concluded that, on Au, a monolayer of Re was formed in parallel with hydrogen evolution. On Pt, a monolayer could be deposited in the region of formation of adsorbed atomic hydrogen (at +0.1 V vs. RHE). When the potential was shifted to –0.1 V vs. RHE, layers of metallic Re as thick as 5–30 nm were deposited.

Schrebler et al.[187] studied the nucleation and growth mechanisms for Re deposition on polycrystalline Au electrodes, from a bath containing 0.75 mM perrhenic acid and 0.1 M sodium sulfate at pH = 2. The potentiostatic step technique was simultaneously employed with measurements of mass changes in an electrochemical quartz-crystal microbalance. The mass vs. time transients were fitted with equations deduced from the current versus time relationships of the conventional nucleation and growth models. It was concluded that electrodeposition of Re started with progressive nucleation and two-dimensional growth, followed by two other contributions:

1. progressive nucleation, and three-dimensional growth under diffusion control,
2. progressive nucleation and three-dimensional growth under charge-transfer control, which was observed at longer times.

From these three contributions, the progressive nucleation and two-dimensional growth corresponded to the charge of a monolayer, and were attributed to two-dimensional nuclei of Re produced by the reduction of adsorbed perrhenate. The three-dimensional growth under diffusion control was the most important contribution, and represented 70–80% of the mass increase. The FE for the electrodeposition process was in the range of 12–18%. The nature of the adsorbed layer, however, was not identified in this study.

The last paragraphs of this chapter shall deal with electrodeposition of Re-based alloys. Based on the relatively positive

reversible potential of Re, one might expect it to codeposit readily with other metals, in particular in alkaline solutions, where its deposition potential could be shifted in the negative direction. However, Brenner noted the unexpectedly low FE as an indicator to the difficulty of codeposition.[78] Fink and Deren[170] stated that Re could be codeposited with Co and Ni. Later, Netherton and Holt reported the successful codeposition of Re with Ni,[188] Co and Fe.[189] The iron-group metals were introduced into the bath in the form of simple salts, such as chloride or sulfate. Brenner[78] postulated that the citrate ion, that was contained in most of the baths, complexed the iron-group metal, thereby shifting its deposition potential cathodically and, consequently, favoring the deposition of Re. The presence of the citrate ion in the bath considerably increased the Re-content in the deposit and lowered the FE. The considerably more positive reversible potential of Re in acid solutions, compared to those of the iron-group metals, allowed for production of alloys with Re content that was significantly higher than its ionic content in the bath. Variation of the pH in the range 3 to 8 did not affect much the Re content in alloys with iron-group metals. The FE, on the other hand, increased considerably from pH 3 to 4, reached a maximum around pH = 5.5, and then decreased mildly. In any case, the FE for alloy deposition was much higher than for pure Re deposition. The Re-content in the deposit decreased with increasing current density, as commonly observed for the more noble metal in alloy deposition. This effect was most pronounced in baths containing a low concentration of ReO_4^-. An increase in bath temperature resulted in a considerable increase of the FE and in the concentration of Re in the Re-Ni alloy, but had little effect on the composition of the Re-Co alloy.

Meyer[162] claimed that both Ni and Co seem to stabilize the presence of ReO_4^- anions near the cathode. He proposed that there was a catalytic effect of Ni on the decomposition of ReO_4^-. Sadana and Wang[190] studied the effects of bath composition, pH, temperature, stirring, current density and pulsed current on the characteristics of Au-Re deposits, which contained 0.25–63.4 wt.% Re. The solution consisted of citric acid and potassium perrhenate. The Re-content of the deposit was found to increase markedly as a result of stirring, increase in current density, decrease in bath pH and temperature, and the use of pulsed current. In addition, the as-deposited alloys exhibited XRD patterns of supersaturated solid

solution of Re in Au for Re contents lower than 21.7 wt.%, and XRD patterns of a mixture of Au fcc phase and an amorphous Re-Au phase for Re contents between 23.4 and 63.4 wt.% (ca. 24.4–64.7 at.%).

Kvokova and Lainer[191] electrodeposited pure Re and Re-Cr alloy on Mo substrate. For the deposition of Re itself, two baths were used: one containing perhhenic acid, and the other containing potassium perrhenate. In the first bath, the discharge of hydrogen ions was enhanced. The authors attributed the low overpotential of hydrogen on Re to its lattice parameter (a = 2.758 Å). However, a justification to this theory has not been proposed. For both deposition of Re and Re-Cr alloy, the concentration polarization was found to be insignificant compared to the activation polarization.

In the sections dealing with electrodeposition of W- and Mo-based alloys, the role of citrate as a complexing agent was described in detail (see, for example, Figs. 8 and 13). In an attempt to better understand the similarities and differences between electrodeposition of Re and that of W or Mo, a literature survey was conducted on electroreduction of perrhenate in the presence of citrate. Only one relevant, well-written, paper was found. Vajo et al.[192] applied polarography and controlled-potential coulometry to study the electroreduction of perrhenate in acidic solutions (pH = 1.6-5.4) of perhhenic acid with citrate (or oxalate). The presence of citrate was found to markedly enhance the reduction of perrhenate through reversible formation of a 1:1 complex, $[(ReO_4)(H_2Cit)]^{2-}$. This complex was sufficiently stable, that it yielded a diffusion-limited current. The very low value of the limiting current allowed for concluding that the equilibrium concentration of ReO_4^- was nearly equal to its analytical concentration. For a constant concentration of ReO_4^- (2.03 mM) and a varying excess concentration of citrate (from 0.05 to 0.4 M), the limiting current increased linearly with increased concentration of citrate, indicating that the equilibrium concentration of ReO_4^- indeed remained essentially equal to its analytical concentration independent of the citrate concentration, and that the electroactive complex contained one citrate moiety. Similarly, the linear increase of the limiting current density with increased concentration of ReO_4^- indicated that the electroactive species contained one Re-atom. When assuming that the citrate species reacting with ReO_4^- was H_2Cit^-, and taking into account pK_a = –1.25 for perrhenic acid, an excellent agreement

was observed between the theoretical and experimental values of limiting current density versus pH. Hence, the stoichiometry of the formation of the perrhenate-citrate complex was claimed to be as follows; below pH = 3:

$$ReO_4^- + H_3Cit \rightarrow \left[\left(ReO_4\right)\left(H_2Cit\right)\right]^{2-} + H^+ \quad (48a)$$

and above pH = 3:

$$ReO_4^- + H_2Cit^- \rightarrow \left[\left(ReO_4\right)\left(H_2Cit\right)\right]^{2-} \quad (48b)$$

These two reactions are in accordance with the stepwise deprotonation of citric acid (c.f. Fig. 1a). The oxidation state of Re generated by electroreduction of the perrhenate-citrate complex was found to be Re(V), which could easily be reduced further, forming Re(IV). The enhanced reduction of the perrhenate-citrate complex was ascribed to expansion of the Re coordination sphere from 4 to 6, through formation of chelated structures by a concerted process, in which the incoming ligand transferred protons to coordinated oxo-groups.

In conclusion, it would seem that the chemistry of Re is very different from that of W and Mo. First, Re has a 7-valent form, while the other two do not exceed the 6-valent state. In addition, while the perrhenate is stable in strong acids, the tungstate and molybdate tend to hydrolyze and/or polymerize. Hence, it would be interesting to study further the mechanisms of electrodeposition of Re.

III. CONCLUDING REMARKS

It is pointed out above that metal deposition is different from outer-sphere charge-transfer reactions in that charge is carried across the metal/solution interface by the ions, not by electrons. Although this has been acknowledged by several noted electrochemists, a theory of charge transfer by ions, comparable in detail and depth to the theories of electron transfer, has yet to be developed. So far,

metal deposition has been treated by the formalism developed successfully for electron transfer.

One of the unique features of metal deposition is that the surface is constantly being renewed. This is a mixed blessing: on the one hand it allows some reduction in the required purity level. On the other hand, the surface morphology and its roughness could change in the course of metal deposition, leading to a change of the real current density, although the applied current density i_{dep} is maintained constant.

The analysis of the kinetics of alloy deposition is complicated by the fact that at least two reactions occur in parallel. Consequently, the current-potential relation observed represents a combination of the contributions of two processes, each having its own overpotential, rate constant and potential dependence of the current density. Thus, any information obtained from the current-potential relation observed is of questionable value in evaluating the mechanism of the formation of the alloy.

The reduction of a large oxy-ion such as WO_4^- is a very complex process. It involves the transfer of six electrons and eight protons, and must proceed in several elementary steps. It is thus unrealistic to expect that one could determine this mechanism in detail, determine the nature of each step, the types of intermediates formed, the surface coverage by each of these intermediates, and so on. Nevertheless, there are certain aspects of this mechanism that can be studied in some detail, helping us to understand the fundamental factors that are critical for the operation of the plating bath. Such understanding is important in the general context of alloy plating, and could also help in systematic design of better plating parameters for industrial applications.

The unique feature of plating of tungsten (and, similarly, of molybdenum) from aqueous solutions is that they cannot be plated in the pure form. On the other hand, alloys of these metals can readily be deposited. The most common alloying elements are the iron-group transition metals (Ni, Co and Fe), but there are indications in the literature that other metals (e.g., Zn and Cd) could form similar alloys. The third metal discussed in this chapter is rhenium. Unlike W and Mo, Re can be deposited from aqueous solutions, albeit with great difficulty, but adding a nickel salt to the solution improves the process significantly, forming the Re-Ni

alloy at a much higher FE, and producing much superior, smooth and crack-free deposits.

The above observation, called induced codeposition, which was first made about 70 years ago, presents a very interesting question: What is the mechanism by which the presence of ions of one of the iron-group metals in the plating bath enhances the deposition of W, Mo and Re, or indeed makes it possible? The purpose of this chapter is to answer this question, to the best of presently available knowledge. The section regarding alloys of tungsten relies heavily on work performed in our own laboratory, although a critical review of other work is also given, of course. The discussion of electrodeposition of molybdenum alloys is based heavily on the work of Landolt and his research group. The electrochemistry of rhenium deposition is much less understood, and the review represents what is known at present.

It should not be surprising that an ion such as WO_4^- cannot be reduced readily all the way to metallic tungsten. Indeed, it is surprising that there are certain conditions under which it can be reduced. Moreover, alloy deposition is often a complex, and quite unpredictable, process. In what is called *anomalous deposition* we classify processes that behave unexpectedly – the composition of the alloy cannot be predicted from the current-potential relation of the alloying elements studied each by itself. When forming a Ni-Fe alloy it seems that Fe^{2+} ions in solution inhibit the rate of deposition of nickel, while Ni^{2+} ions accelerate the rate of deposition of iron. In the deposition of a Ni-Zn alloy the situation is somewhat different. Here, one finds a complete synergistic effect: adding either ion to the solution enhances the rate of deposition of the other metal.

Anomalous alloy deposition is common in electroplating. Actually, it is so common that it is the rule rather than the exception. What could be the cause of this phenomenon? In general, it is postulated that one of the alloying elements forms a hydroxide on the surface, which inhibits the deposition of the other. This could explain the inhibiting effect, but it is much more difficult to explain the enhancement. Another explanation is that the two ions form a mixed-metal complex that, for some reason, is more readily reduced at the surface than each of the metal ions separately. Naturally, such complexes can only be expected to exist in solution

containing a negatively charged complexing agent, which would hold the two positive metal ions together, for example:

$$Fe^{2+} + Cit^{3-} \rightarrow [FeCit]^{-} \tag{49}$$

$$Ni^{2+} + Cit^{3-} \rightarrow [NiCit]^{-} \tag{50}$$

followed by

$$[FeCit]^{-} + [NiCit]^{-} \rightarrow [FeNiCit]^{+} + Cit^{3-} \tag{51}$$

If the mixed-metal complex is the precursor for deposition of the alloy, then it can be seen that adding either of the two ions would increase the rate of deposition of the other. This simplistic interpretation could lead only to alloys having equal concentrations of the two elements. However, if the concentration of the two elements in solution is not equal, one could have a parallel reaction, in which one of the metals would also be deposited in parallel from its complex with citrate, giving rise to a whole range of alloy compositions.

This brings us to one of the main point made in this chapter, which is relevant both for anomalous alloy deposition and for induced codeposition: in order to understand the process, one should understand the chemistry of the solution, and particularly the distribution of species in plating baths that contain complexes. This type of analysis is shown in Figs. 1, 2, 8, 13 and 14, and has been used in our own work to explain the induced codeposition of tungsten.

Many publications were devoted over the years to explain the mechanism by which induced codeposition proceeds. None have been proven beyond doubt, and one has to look for the explanation that is consistent with the widest range of experimental observations.

For induced codeposition of Ni-W alloys, we concluded that the precursor for deposition of the alloy is a mixed-metal complex of the type $[(Ni)(HWO_4)(Cit)]^{2-}$. This complex is formed from a nickel citrate complex (cf., Eq. 50) and a tungstate citrate complex $[(WO_4)(Cit)(H)]^{4-}$. It may be somewhat surprising that the nega-

tive citrate ion forms a complex with a negative tungstate ion, but this is a well-established fact, and the stability constant of this complex is available in the literature. This should lead to a mutual synergistic effect of Ni on the rate of deposition of W and vice versa, which was confirmed experimentally. The partial current density for deposition of tungsten was found to be mass-transport dependent, although it was only a few percent of the limiting current density, calculated for the concentration of either Na_2WO_4 or $NiSO_4$ in solution. This indicates that the concentration of the above precursor is much smaller, and its rate of formation is low. The latter is not surprising, in view of the fact that it is formed by an interaction between two negatively charged ions, one of which having a high charge of –4. Alloys having a wide range of compositions were obtained, depending mostly on the composition of the bath. In most cases, the concentration of Ni in the alloy was higher than that of W, since there is a parallel path for deposition of Ni from its complex with citrate (or with NH_3, when present in solution). Nevertheless, conditions were found, under which an alloy with a 1:1 Ni:W ratio could be deposited. Different crystal structures were identified by X-ray diffraction. The structure was found to depend on the atomic composition of the alloy, not on the way it was prepared. The dependence of the alloy composition on pH was found to be consistent with the distribution of the relevant species in solution, as shown in Fig. 8. Finally, linear relationships were observed between the product of concentrations of the two complexes that form the mixed-metal complex and the partial current densities for deposition of tungsten.

Plating of alloys of Mo was studied intensively in recent years by Landolt and his co-workers. It was shown that in formation of Ni-Mo alloys, the rate of deposition of Mo (i.e., the partial current density for deposition of this metal) is controlled by the concentration of Ni in solution. This is consistent, of course, with the idea that the precursor for deposition of the alloy is a mixed-metal complex, as proposed for Ni-W alloys by Gileadi et al. It is also expected in view of the similarity of the chemistry of W and Mo ions in aqueous solutions. However, the mixed metal complex for Ni-Mo alloy deposition was assumed to be $[NiCit(MoO_2)]_{ads}^{-}$. The most important difference between the assumed mixed-metal complexes are that in the case of W the complex is in solution, while in the case of Mo it is assumed to be adsorbed on the surface. More-

over, in the precursor for deposition of Ni-W alloys, the mixed-metal complex contains the protonated tungstate anion HWO_4^-, while in the case of Ni-Mo alloys it is the neutral dioxide MoO_2, which has been formed from reduction of the MoO_4^{2-} ion in a previous step. In both cases, the authors have been able to deposit alloys with a range of concentrations of the refractory metals. However, in the case of W it was concluded that the mixed-metal complex was the source of deposition of an alloy of equal concentrations of Ni and W, while Ni was deposited in parallel from its complex with citrate. In the case of Mo it was assumed that the reaction proceeded by a four-electron reduction of the mixed-metal complex, while Ni was deposited independently from its complex with citrate.

The electrochemistry of rhenium is quite different from that of W and Mo, and has not been investigated in similar detail. To begin with, the most stable ion in solution is the perrhenate, ReO_4^-, from which metallic rhenium can be deposited directly, not only as an alloy. The hexavalent ReO_4^{2-} (similar to MoO_4^{2-}) does not exist in aqueous solutions. On the other hand, there are definite indications (which admittedly should be confirmed by further detailed studies) that forming alloys with Pt, and possibly with the iron-group transition metals, leads to higher-quality coatings with lower residual stresses, less cracking and lower hydride content.

In conclusion, it can be stated that alloys of the three refractory metals discussed in this chapter may be of significant importance for practical application, in view of their high corrosion resistance, stability at high temperatures and wear resistance. Some of these advantages are already being implemented, mainly for alloys of tungsten and of molybdenum, but only marginally for rhenium. Deeper understanding of the phenomenon of induced codeposition could lead to increasing the range of applications of such alloys in specialized applications.

ACKNOWLEDGEMENT

The authors wish to thank Prof. E. Kirowa-Eisner for her assistance in calculating the distribution of species shown in the relevant figures.

LIST OF ABBREVIATIONS AND SYMBOLS

ACD	Anomalous Codeposition
EIS	Electrochemical Impedance Spectroscopy
EMF	Electromotive Force
FE	Faradaic Efficiency
HAC	Hydrogen-Assisted Cracking
HE	Hydrogen Embrittlement
HER	Hydrogen Evolution Reaction
HIC	Hydrogen-Induced Cracking
HRC	Hardness Rockwell C
MEMS	Micro-Electro-Mechanical Systems
OCP	Open-Circuit Potential
OHP	Outer Helmholtz Plane
RHE	Reversible Hydrogen Electrode
SHE	Standard Hydrogen Electrode
ULSI	Ultra-Large-Scale Integration
UPD	Underpotential Deposition
VHN	Vickers Hardness Number

b	Tafel slope (V decade^{-1})
c	The subsurface solubility of a dissolved atom in a solid metal, expressed as solute-to-metal atom ratio
c_{bulk}	Bulk concentration of the electro-active species (mol cm^{-3})
$c_{Me^{z+}}$	Concentration of the metal cation (mol cm^{-3})
c_{surf}	Concentration of the electro-active species at the surface (mol cm^{-3})
D	Diffusion coefficient (cm^2 s^{-1})
E	Young's modulus of elasticity (GPa)
E^0	Standard (equilibrium) potentials (V)
$E^{0\prime}$	Standard potential in the presence of a complexing agent (V)
E_{corr}	Corrosion potential (V)
E_{dep}	Deposition potential (V)
E_{rev}	Reversible potential (V)
F	Faraday's constant (96,485 C equiv^{-1})
f	Fugacity (Pa)
I	Total current passed (A)

i	Current density (A cm^{-2})
i_{ac}	Activation-controlled current density (A cm^{-2})
$i_{c,i}$	Partial cathodic current density of the i^{th} element in alloy deposition (A cm^{-2})
i_L	Limiting current density (A cm^{-2})
i_0	Exchange current density (A cm^{-2})
i_{pass}	Passivation current density (A cm^{-2})
K	Stability constant of a complex
K_S	Solubility (Sieverts') constant for dissociative adsorption of a diatomic gas, followed by absorption ($Pa^{-0.5}$)
K_{Ic}	Fracture toughness (MPa $\sqrt{m}$)
L	Ligand
l	Characteristic length
Me_i	Metal i
M_i	Atomic mass of the i^{th} element (g mol^{-1})
n_i	The number of electrons transferred in the reduction of one atom of the i^{th} element (equiv mol^{-1})
P	Partial pressure (Pa)
R	The ideal gas constant (1.987 cal $K^{-1}mol^{-1}$, or 8.314 J $K^{-1}mol^{-1}$)
R_{conc}	Mass transport resistance (Ω cm^{-2})
R_{ct}, R_F, R_{ac}	Charge transfer (Faradaic) resistance (Ω cm^{-2})
R_{soln}	Ohmic solution resistance (Ω cm^{-2})
r	Radius of the rotating cylinder electrode (cm)
r_{metal}	Atomic radius (Å)
T	Absolute temperature (K or°C)
T_m	Melting temperature (K or°C)
t_d	Deposition time (s)
W_a	Wagner number
w	The measured weight of a deposit (g)
x_i	The weight (or mole) fraction of an element in an alloy deposit
α	Linear thermal expansion coefficient ($^oC^{-1}$)
α	Transfer coefficient for the overall electrode reaction
β	Symmetry factor for an elementary charge-transfer step in the reaction sequence
β_n	Equilibrium constant for formation of complexes in the reactions Me + n·L $\rightarrow$ [MeL_n], usually given in its log form

δ	The thickness of the Nernst diffusion layer (cm)
Δ_{UPD}	UPD potential shift (V)
ε_f	Strain at fracture (%)
η	Observed overpotential (V)
η_{ct}	Charge-transfer (activation) overpotential (V)
η_{conc}	Concentration overpotential (V)
η_{iR}	Resistance overpotential (V)
κ	Specific conductance of solution (S cm^{-1})
κ	Thermal conductivity (W $m^{-1}K^{-1}$)
ν	Kinematic viscosity (cm^2 s^{-1})
ν	Poisson's ratio ($\equiv -\varepsilon_{zz}/\varepsilon_{xx} = -\varepsilon_{yy}/\varepsilon_{xx}$, where ε_{xx} is the principal strain in the x direction of the applied force, and ε_{yy} and ε_{zz} are the resulting principal strains in the orthogonal directions y and z, respectively)
ω	Angular velocity, or rotation rate (rad s^{-1}, or rpm)
ρ	Density (g cm^{-3})
ρ	Specific resistivity (Ohm·cm)
σ_u	Tensile strength (Pa)
σ_y	Yield strength (Pa)
θ	Partial surface coverage

APPENDICES

Appendix A

Typical bath compositions and operating conditions for electrodeposition of W-based alloys, cf., Table 3.

Appendix B

Typical bath compositions and operating conditions for electrodeposition of Mo-based alloys, cf., Table 4.

Appendix C

Typical bath compositions and operating conditions for electrodeposition of Re-based alloys, cf., Table 5.

Table 3
Typical Bath Compositions and Operating Conditions for Electrodeposition of W-Based Alloys

Bath composition				pH	T (°C)	i (mA cm^{-2})	FE (%)	wt.% W in deposit	Ref.
[WO_4^{2-}] (M)	Iron-group metal in bath (M)	Organic acid/salt (M)	Others (M)						
0.03	Co: 0.60	Sodium citrate: 0.60	Ammonium chloride: 0.94	9.0	95	20	87	23	119
1.00	Co: 0.07	Tartaric acid: 0.13	Boric acid: 0.32	7.0	100	20	30	50	120
0.22	Co: 0.10	Citric acid: 0.65	Ammonium chloride: 0.94	8.2	50–55	150–200 (pulse plating)	20	65	121
0.27-0.54	Ni: 0.42	Rochelle salt: 1.4 or sodium citrate: 0.6 or hydroxyacetic acid: 2.6	Ammonium chloride: 0.94	9.0	95	20	85–93	10–20	119
0.15	Ni: 0.07	Citric acid: 0.34	—	8.0	70	70–150	45	35	122
0.40	Ni: 0.01–0.10	Tri-sodium citrate: 0.25–0.60	None or nickel sulfamate: 0.062–0.124 or saccharin: 0.0146 or sodium chloride: 0.002–0.005 or sodium sulfate: 0.176	8.0	RT–70	5–15	8–21	25–90	104 108

Table 3. Continuation

Bath composition				pH	T (°C)	i (mA cm^{-2})	FE (%)	wt.% W in deposit	Ref.
$[WO_4^{2-}]$ (M)	Iron-group metal in bath (M)	Organic acid/salt (M)	Others (M)						
0.01-0.50	Ni: 0.01–0.20	Tri-sodium citrate: 0.10–1.0	Ammonia: 0–1.7	6.0–12.0	10–62	15	0.5–98	5–74	91–93 105
0.003–0.006	Ni: 0.38	Ammonium chloride: 0.93	With or without diammonium citrate: 0.013–0.044	Not stated	30–70	5–30	43–90	12–20 (at.% or wt.% not stated)	113
0.14	Ni: 0.06	Tri-sodium citrate: 0.3-0.5	Ammonium chloride: 0.5, sodium bromide: 0.15	8.5	60–90	0.5–2	Not stated	40–51	123
0.09	Ni: 0.051	Sodium citrate: 0.31	Sulfamate: 0.102	4.0–8.0	30–70	5–100	4–85	19–81 (at.% or wt.% not stated)	112
0.09–0.14	Fe: 0.27–0.43	Ammonium citrate: 0.40 or sodium citrate: 0.30 or ammonium malate: 1.5	Ammonium sulfate: 0.76	9.0	95	50	45–75	30–45	119

Table 4
Typical Bath Compositions and Operating Conditions for Electrodeposition of Mo-Based Alloys

Bath composition									
$[MoO_4^{2-}]$ (M)	Iron-group metal in bath (M)	Organic acid/salt (M)	Others (M)	pH	T (°C)	i (mA cm^{-2})	FE (%)	wt.% Mo in deposit	Ref.
0.02	Ni: 0.22	Citric acid: 0.31	—	4	25	50	32	17	138
0.52	Co: 0.17	Hydroxyacetic acid: 1.3	—	1.5–2.5	25	30–100	35	20–30	78
0.052	Ni: 0.22	Rochelle salt: 0.27	Sodium chloride: 0.12, ammonia	11	27	100	67	18	139
0.2	Ni: 0.30	Sodium citrate: 0.3	Ammonia	10.5	25	100	70	18	140
0.1	Fe: 0.30	Sodium citrate: 0.3	Ammonia	10.5	25	200	12	57	140
0.14	Co: 0.034	—	Sodium bicarbonate: 1.0, sodium pyrophosphate: 0.13	8.0	22	40	20	50	141

Table 4. Continuation

Bath composition				pH	T (°C)	i (mA cm^{-2})	FE (%)	wt.% Mo in deposit	Ref.
[MoO_4^{2-}] (M)	Iron-group metal in bath (M)	Organic acid/salt (M)	Others (M)						
0.17	Fe: 0.033	—	Sodium pyrophosphate: 0.1, sodium bicarbonate: 0.9	8.0	50	150	44	61	142
0.52	Co: 0.17	—	Potassium carbonate: 4.7	11.0	100	10	75	25	143
0.067	Ni: 0.20	—	Sodium chloride: 0.05, ammonium hydroxide (25%): 5.71	10.7	30–40	100	41	17.5	144
0.005–0.05	Ni: 0.20	Sodium citrate: 0.25–0.95	Ammonia: 0-1.0	7.5–11.4	25–80	10-200	8–79 (partial range)	1–71	95
0.005	Ni: 0.7 or Co: 0.7 or Fe: 0.7	Sodium citrate: 0.70	Ammonia	7.4	25	35 (Mo-Co) 50 (Mo-Fe)	22–36 (Mo-Co), 7–21 (Mo-Fe), 61–95 (Mo-Ni)	31–43 (Mo-Co), 11–14 (Mo-Fe), 7–23 (Mo-Ni)	97
1.0–15.0	Co: 0.10	Sodium citrate: 0.20	—	6.6	25	—	—	max. 60	152
0–0.03	Ni: 0.2	Sodium citrate: 0.25	Ammoia	9.5	37	—	—	—	153

Table 5
Typical Bath Compositions and Operating Conditions for Electrodeposition of Re-Based Alloys

Bath composition			pH	T (°C)	i (mA cm^{-2})	FE (%)	wt.% Re in deposit	Ref.
[ReO_4^-] (M)	Organic acid/salt (M)	Others (M)						
0.052	—	Ammonium sulfate: 0.030, sulfuric acid: 0.122, gelatin (4 g L^{-1})	0.9–1.0	85–90	100–150	—	—	160
0.035	—	Sulfuric acid: 0.1, ammonium sulfate: 0.89, magnesium sulfamate: 0.22	1.0–1.5	25–80	20–150	1.3–12	—	162
0.038	—	Sulfuric acid	1.0	RT–90	100–140	—	—	170
0.16	—	Sulfuric acid: 0.89, ammonium hydroxide: 0.71	0.9–1.1	21–88	108–2,800	—	—	172
0.048–0.052	—	Sulfuric acid: 0.122	1.0	50–70	5–150 (DC & pulse plating)	—	—	166 173
0.14	Sulfamic acid: 1.11	Magnesium sulfate: 0.22, ammonium sulfate: 0.76	1.0–1.5	—	—	—	—	176
0.0035	Boric acid: 0.49	Ni: 1.0	4.6	70	30	98	6	188
0.0035	Boric acid: 0.49, citric acid: 0.37	Ni: 1.0	2.3	70	30	35	45	188
0.035	Citric acid: 0.34	Co: 0.21, ammonium hydroxide	7-8	70	50	80	80	189
0.035	Citric acid: 0.34	Fe: 0.22, ammonium hydroxide	7-8	70	50	65	58	189

REFERENCES

[1]E. Raub and K. Müller, *Fundamentals of metal deposition*, Elsevier Publishing Company, Amsterdam, 1967.
[2]J. W. Dini, *Electrodeposition: the materials science of coatings and substrates*, Noyes Publications, New Jersey, 1993.
[3]E. Budevski, G. Staikov, and W.J. Lorenz, *Electrochemical phase formation and growth*, VCH, Weinheim, 1996.
[4]M. Paunovic and M. Schlesinger, *Fundamentals of electrochemical deposition*, John Wiley & Sons, New York, 1998.
[5]M. Schlesinger, M. Paunovic, (eds) *Modern electroplating*, 4th edn, Wiley- Interscience, New York, 2000.
[6]N. Kanani, *Electroplating: basic principles, processes and practice*, Elsevier, Oxford, 2004.
[7]D. Landolt, *J. Electrochem. Soc.* **149** (2002) S9.
[8]ASTM B 374 – 96: *Standard Terminology Relating to Electroplating*, American Society for Testing and Materials, Pennsylvania.
[9]H.H. Wan and H.Y. Cheh, *J. Electrochem. Soc.* **135** (1988) 643.
[10]O. Dossenbach, in *Theory and practice of pulse-plating*, Ed. by J.C. Puippe, F. Leaman, AESF, Florida, p. 73, 1986.
[11]D. Landolt, *Plat. Surf. Finish* **88** (2001) 70.
[12]P. J. Moran and E. Gileadi, *J. Chem. Education* **66** (1989) 91.
[13]H. L. F. von Helmholtz, *Ann. Physik*, **89** (1853) 211.
[14]H. L. F. von Helmholtz, *Ann. Physik* **7** (1879) 337.
[15]G. Gouy, *J. Phys. Radium* **9** (1910) 457.
[16]G. Gouy, *Compt. Rend. Acad. Sci.* **149** (1910) 654.
[17]D.L. Chapman, *Phil. Mag.*, **25** (1913) 475.
[18]O. Stern, *Zeit. Elektrochem.* **30** (1924) 508.
[19]E. Gileadi, in *Fifth international symposium on proton-exchange-membrane fuel cells*, Ed. by T. Fuller, C. Bock, C. Lamy, *Electrochem Soc. Trans.* 1:3, 2006.
[20]R. A. Marcus, *J. Chem. Phys.* **24** (1956) 4966.
[21]R. A. Marcus, *J. Chem. Phys.* **43**(1965) 679.
[22]R. A. Marcus, *Electrochim. Acta* **13** (1968) 955.
[23]R. R. Dogonadze, *Dokl. Akad. Nauk. SSSR* **133** (1960) 1368.
[24]R. R. Dogonadze and Y.A. Chizmadzhev, *Dokl. Akad. Nauk. SSSR* **144** (1962) 1077.
[25]R. R. Dogonadze, A. Kuznetzov, and Y. A. Chizmadzhev, *Zh. Fiz. Khim.* **38** (1964) 1195.
[26]V.G. Levich, in *Advances in electrochemistry and electrochemical engineering*, Interscience, Vol. 4, Ed. by P. Delahay, New York, 1966, p. 249.
[27]C. Grahame, *Ann. Rev. Phys. Chem.*, **6** (1955) 337.
[28]K. Vetter, *Electrochemical kinetics*, Academic Press, New York, p. 134, 1967.
[29]V. V. Losev, in *Modern Aspects of Electrochemistry*, Ed. by B. E. Conway, J. O'M. Bockris, Plenum Press, New York, 1972, Vol. 7, p 314.
[30]N. Sato, *Electrochemistry of metal and semiconductor electrodes*, Elsevier, Amsterdam, p. 289, 2002.

[31]E. Gileadi, *Interface*, **12** (2003) 10.
[32]E. Gileadi, *Chem. Phys. Lett.* **393** (2004) 421.
[33]E. Gileadi, in *Electrochemical Processing in ULSI and MEMS,* Ed. by H. Deligianni, T.P. Moffat, S.T. Mayer, and G.R. Stafford, *Proc. Electrochem. Soc. ECS*, Vol. 17, New Jersey, 2004, p. 3.
[34]E. Gileadi, E. Kirowa-Eisner, *Corros. Sci.* **47** (2005) 3068.
[35]E. Gileadi, *J. Electroanal. Chem.* **532** (2002) 181.
[36]E. Gileadi, *Electrode kinetics for chemists, chemical engineers and material scientists*, VCH, New York, 1993, pp. 159, 540.
[37]A. Vaskevich, M. Rosenblum, and E. Gileadi, *J. Electroanal. Chem.* **167** (1995) 383.
[38]D.M. Kolb, in *Advances in electrochemistry and electrochemical engineering*, Vol. 11, Ed. by H. Gerischerand, and C. W. Tobias, Wiley, New York, 1978.
[39]X. Zong and S. Bruckenstein, *J. Electrochem. Soc.* **146** (1999) 2555.
[40]B.E. Conway and J. S. Chacha, *J. Electroanal. Chem.* **287** (1990) 13.
[41]E. Herrero, L. J. Buller and H. D. Abruna, *Chem. Rev.*, **101**(2001) 1897.
[42]R. Adzic, in *Advances in electrochemistry and electrochemical engineering*, Vol. 13, Ed. by H. Gerischerand and C. W. Tobias, Wiley, New York, 1984.
[43]R. Adzic, E. Yeager, and B. D. Cahan, *J. Electrochem. Soc.* **121**(1974) 474.
[44]K. Engelsmann, W. J. Lorenz, and E. Schmidt, *J. Electroanal. Chem.* **114** (1980) 1.
[45]A. Hamelin, and J. Lipkowski, *J. Electroanal. Chem.* **171** (1984)317.
[46]J. Clavilier, J. M. Orts, J. M. Feliu, and A. Aldaz, *J. Electroanal. Chem.* **293** (1995) 197.
[47]H. Bort, K. Juttner, and W. J. Lorenz, *J. Electroanal. Chem.*, **90** (1978) 413.
[48]C. L. Faust, in *Modern electroplating*, 2nd edn. Ed. by F.A. Lowenheim, John Wiley & Sons, New York, 1963, p. 453.
[49]N. Eliaz, E. Moshe, S. Eliezer, and D. Eliezer, *Metall. Mater. Trans. A* **31** (2000)1085.
[50]N. Eliaz, D. Eliezer, E. Abramov, D. Zander, and U. Köster, *J. Alloys Compd.* **305** (2000) 272.
[51]N. Eliaz and D. Eliezer, *Metall. Mater. Trans. A,* **31** (2000)2517.
[52]A. S. Tetelman and W. D. Robertson, *Trans. Met. Soc. AIME* **224** (1962) 775.
[53]N. Eliaz, L. Banks-Sills, D. Ashkenazi, and R. Eliasi, *Acta Mater.* **52** (2004) 93.
[54]H. G. Nelson, in *Embrittlement of engineering alloys,* Ed. by C. L. Briant, S. K. Banerji, Academic Press, New York, 1983, p. 275.
[55]N. Eliaz, *J. Adv. Mater.* **34** (2001) 27.
[56]N. Eliaz, A. Shachar, B. Tal, and D. Eliezer, *Eng. Fail.Anal.*, **9** (2002) 167.
[57]W. J. Barnett, A. R. Troiano **209** (1957)486.
[58]R. A. Oriani, *Ann. Rev. Mater. Sci.* **8** (1978) 327.
[59]N. J. Petch, and P. Stables, *Nature* **169** (1952) 842.
[60]D. G. Westlake, *Trans. ASM* **62** (1969) 1000.
[61]H. K. Birnbaum, in *Hydrogen embrittlement and stress corrosion cracking*, ASM, Ed. by R. Gibala, and R. F. Hehemann, Metals Park, Ohio, 1984, p 153.
[62]H. K. Birnbaum, in *Hydrogen effects on material behavior, TMS*, Ed. by N. R. Moody, A. W. Thompson, Warrendale, Pennsylvania, 1990, p. 639.
[63]J. P. Hirth, *Metall. Trans.* **11A** (1980) 861.
[64]C. D. Beachem, *Metall. Trans.* **3** (1972) 437.
[65]S. P. Lynch, *Met. Forum* **2** (1979)189.
[66]J. J. Gilman, *Phil. Mag.* **26** (1972) 801.

[67]P. Bastien and P. Azou, in *Proceedings of the first world metallurgical congress,* ASM, Ed. by W. M. Baldwin, Metals Park, Ohio, 1951, p 535.
[68]A. N. Stroh, Adv. Phys. **6** (1957) 418.
[69]D. S. Shih, I. M. Robertson, and H. K. Birnbaum, *Acta Metall.* **36** (1988) 111.
[70]J. K. Tien, A. W. Thompson, I. M. Bernstein, and R. J. Richards, *Metall Trans.* **7A** (1976) 821.
[71]QQ-C-320 (1987) Federal Specification.
[72]ASTM F 519 (1993) Standard Test Method, West Conshohocken.
[73]F. C. Frank and J. H. van der Merwe, *Proc. Roy. Soc. London A* **198** (1949) 205.
[74]M. Volmer and A. Weber, *Z. Physik. Chem.*, **119** (1926) 277.
[75]I. N. Stranski and L. Krastanov,*Sitzungsber Akad Wiss Wien Math*, **146** (1938) 797.
[76]H. Liebscher, *Galvanotechnik* **88** (1993) 754.
[77]N. Kanani, U. Landau, and R. Kammel, *Erzmetall* **54** (2001) 369.
[78]A. Brenner, *Electrodeposition of alloys*, Vol. I & II. Academic Press, New York, 1963.
[79]H. Dahms and I. M. Croll, *J. Electrochem. Soc.* **112** (1965) 771.
[80]S. Hessami, C. W. Tobias, *J. Electrochem. Soc.* **136** (1989) 3611.
[81]I. M. Croll, L. T. Romankiw, in *Electrodeposition technology, theory and practice*, ECS, Ed. by L. T. Romankiw, New Jersey, 1987, p 285.
[82]M. Matlosz, *J. Electrochem. Soc.* **140** (1993) 2272.
[83]K. Y. Sasaki and J. B. Talbot, *J. Electrochem. Soc.* **142** (1995) 775.
[84]K. Y. Sasaki and J. B. Talbot, *J. Electrochem. Soc.* **145** (1998) 981.
[85]T. Erdey-Grúz, *Kinetics of electrode processes.* Wiley-Interscience, New York, 1972, p 25.
[86]L. J. Gao, P. Ma, K. M. Novogradecz, and P. R. Norton, *J. Appl. Phys.* **81** (1997) 7595.
[87]S. H. Liao, *IEEE Trans. Magn.* **26** (1990) 328.
[88] E. E. Castellani, J. V. Powers, and L. T. Romankiw, US Patent 4 102 756, 1978.
[89]N. Zech, E. J. Podlaha, and D. Landolt, *J. Electrochem. Soc.* **146** (1999)2886.
[90]N. Zech, E. J. Podlaha, and D. Landolt, *J. Electrochem. Soc.* **146** (1999) 2892.
[91]O.Younes, L. Zhu, Y. Rosenberg, Y. Shacham-Diamand, and E. Gileadi, *Langmuir* **17** (2001) 8270.
[92]O. Younes, E. Gileadi, *J. Electrochem. Soc.* **149** (2002) C100.
[93]O.Younes-Metzler, L. Zhu, and E. Gileadi, *Electrochim. Acta*, 48 (2003)2551.
[94]A. Brenner, D. E. Couch, and E. K. Williams, *J. Res. Natl. Bur. Stand.* **44** (1950) 109.
[95]E. J. Podlaha and D. Landolt, *J. Electrochem. Soc.* **143** (1996) 885.
[96]E. J. Podlaha and D. Landolt, *J. Electrochem. Soc.* **143** (1996) 893.
[97]E. J. Podlaha and D. Landolt, *J. Electrochem. Soc.* **144** (1997) 1672.
[98]Y. Shacham-Diamand, Y. Sverdlov, and N. Petrov, *J. Electrochem. Soc.* **148** (2001) C162.
[99]A. Kohn, M. Eizenberg, and Y. Shacham-Diamand, *J. Appl. Phys.* **92** (2002) 5508.
[100]Y. Shacham-Diamand and S. Lopatin, *Microelectron Eng.* **37/38** (1997) 77.
[101]A. Kohn, M. Eizenberg, Y. Shacham-Diamand, B. Israel, and Y. Sverdlov, *Microelectron Eng.* **55** (2001) 297.
[102]A. Kohn, M. Eizenberg, Y. Shacham-Diamand, and Y. Sverdlov, *Mater. Sci. Eng.*, **A302** (2001) 18.

[103]Cambridge Engineering Selector (CES), ver 3.1, Granta Design Limited, Cambridge, United Kingdom, 2000.
[104]N. Eliaz, T. M. Sridhar, and E. Gileadi, *Electrochim. Acta* **50** (2005) 2893.
[105]O.Younes and E. Gileadi, *Electrochem. Solid-State Lett.* **3** (2000) 543.
[106]O. Younes, *PhD thesis*, Tel-Aviv University, 2001.
[107]L. Zhu, O.Younes, N. Ashkenasy, Y. Shacham-Diamand, and E. Gileadi, *Appl. Surf. Sci.* **200** (2002) 1.
[108]T. M. Sridhar, N. Eliaz, and E. Gileadi, *Electrochem. Solid-State Lett.* **8** (2005) C58.
[109]S. Yao, S. Zhao, H.Guo, and M. Kowaka, *Corrosion*, **52** (1996) 183.
[110]PWA 36975: Electroplated NiW – Thin Deposit (Enloy Ni-500); http://www.enthone.com.
[111]P. Schloßmacher and T. Yamasaki, *Mikrochim. Acta* **132** (2000) 309.
[112]N. Atanassov, K. Gencheva, and M. Bratoeva, *Plat. Surf. Finish.* **84** (1997) 67.
[113]R. M. Krishnan, C. Joseph Kennedy, S. Jayakrishnan, S. Sriveeraraghavan, S. R. Natarajan, and P. G. Venkatakrishnan, *Metal Finish* **93** (1995) 33.
[114]L. Namburi, MSc thesis, Louisiana State University, 2001.
[115]N. Suliţanu, *J. Magnetism and Magnetic Mater.* **231** (2001) 85.
[116]N. D. Suliţanu, *Mater. Sci. Eng.* **B95** (2002) 230.
[117]C. G. Fink and F. L. Jones, *Trans. Electrochem. Soc.* **59** (1931) 461.
[118]L. N. Gol'tz and V. N. Kharlamov, *Zhur. Priklad. Khim.* **9** (1936) 640.
[119]A. Brenner, P. S. Burkhead, and E. Seegmiller, *J. Res. Natl. Bur. Standards* **39** (1947) 351.
[120]H. Offermanns and Mv. Stackelberg, *Metalloberfläche* **1** (1947) 142.
[121]T. P. Hoar and I. A. Bucklow, *Trans. Inst. Metal. Finishing* **32** (1955) 186.
[122]L. E.Vaaler and M. L. Holt, *Trans. Electrochem. Soc.* **90** (1946) 43.
[123]T. Yamasaki, R. Tomohira, Y. Ogino, P. Schloßmacher, and K. Ehrlich, *Plat. Surf. Finish* **87** (2000) 148.
[124]H. Cesiulis, A. Baltutiene, M. Donten, M. L. Donten, and Z. Stojek, *J. Solid State Electrochem.* **6** (2002) 237.
[125]M. Donten, Z. Stojek, and H. Cesiulis, *J. Electrochem. Soc.* **150** (2003) C95.
[126]W. H. Safranek, *The properties of electrodeposited metals and alloys*, 2nd edn. American Electroplaters and Surface Finishers Society, Florida, 1986, p 348.
[127]C. H. Huang, *Plat. Surf. Finish* **84** (1997) 62.
[128]T. F. Frantsevich-Zabludovskaya, and A. I. Zayats, *Zh. Prikl. Khim.* **30** (1957) 764.
[129]C. H. Huang, W. Y. She, and H. M. Wu, *Plat. Surf. Finish* **86** (1999) 79.
[130]M. Donten, and Z. Stojek, *J. Appl. Electrochem.* **26 (**1996) 665.
[131]K. Wikiel, and J. Osteryoung, *J. Appl. Electrochem.* **22** (1992) 506.
[132]C. L. Aravinda, V. S. Muralidharan, and S. M. Mayanna, *J. Appl. Electrochem.* **30** (2000) 601.
[133]K. S. Jackson, A. S. Russell, and J. L. Merrill, *J. Chem. Soc.* (1929) 2394.
[134]A. G. Glazunov and V. Jolkin, *Chem. Listy.* **31** (1937) 309,322.
[135]G. L. Davis and C. H. R. Gentry, *Metallurgia* **53** (1956) 3.
[136]Z. A. Solovyerva and A. T. Vagramyan, *Izvest. Akad. Nauk. Otdel. Khim. Nauk.* **2** (1954) 230.
[137]J. J. Cruywagen, L. Krüger and E. A. Rohwer, *J. Chem. Soc. Dalton Trans.* (1991) 1727.
[138]H. J. Seim and M. L. Holt, *J. Electrochem. Soc.* **96** (1949) 205.

[139]T. F. Frantsevich-Zabludovskaya, A. I. Zayats, and K. D. Modylevskaya, *Zhur. Priklad. Khim.* **29** (1956) 1811.
[140]D. W. Ernst, R. F. Amlie and M. L. Holt, *J. Electrochem. Soc.* **102** (1955) 461.
[141]H. S. Myers, PhD thesis, Columbia University, 1941.
[142]L. O. Case and A. Krohn, *J. Electrochem. Soc.* **105** (1958)512.
[143]A. Brenner and P. Burkhead, US Patent 2 653 127, 1953.
[144]T. F. Frantsevich-Zabludovskaya, and A. I. Zayats, *Zhur. Priklad. Khim.* **31** (1958) 224.
[145]C. C.Nee, W. Kim, and R. Weil, *J. Electrochem. Soc.* **135** (1988) 1100.
[146]E. Chassaing, M. P. Roumegas, and M. F. Trichet, *J. Appl. Electrochem.* **25** (1995) 667.
[147]D. W. Ernst, and M. L. Holt, *J. Electrochem. Soc.* **105** (1958) 686.
[148]E. J. Podlaha and D. Landolt, *J. Electrochem. Soc.* **140** (1993) L149.
[149]C. Madore, C. West, M. Matlosz and D. Landolt, *Electrochim. Acta*,**7** (1992) 69.
[150]C. Madore, M. Matlosz and D. Landolt, *J. Appl. Electrochem.* **22** (1992) 1155.
[151]C. Madore and D. Landolt, *Plat. Surf. Finish* **80** (1993) 73.
[152]E. Gómez, E. Pellicer, and E. Vallés, *J. Electroanal. Chem.* **517** (2001) 109.
[153]E. Chassaing, K. V. Quang, and R. Wiart, *J. Appl. Electrochem.* **19** (1989) 839.
[154]Z. J. Niu, S. B. Yao, and S. M. Zhou, *J. Electroanal. Chem.* **455** (1998) 205.
[155]Y. Zeng, Z. Li, M. Ma, and S. Zhou, *Electrochem. Commun.* **2** (2000) 36.
[156]J.Crousier, M. Eyraud, J. P. Crousier, and J. M. Roman, *J. Appl. Electrochem.* **22** (1992) 749.
[157]J. B. Lambert, in *ASM handbook*, 10th ed., Vol. 2, ASM International, Ohio, 1990, p. 557.
[158]T. Grobstein, R. Titran and J. R. Stephens, in ibid, 1990, p 581.
[159]R. Colton, *The chemistry of rhenium and technetium*, John Wiley & Sons, London, 1965.
[160]K. B. Lebedev, *The chemistry of rhenium*, Butterworths, London, 1962.
[161]D. Mittendorf and G. A. West, *Mater. Manuf. Processes* **13** (1998) 749.
[162]A. R. Meyer, *Trans. Inst. Metal Finishing* **46** (1968) 209.
[163]G. Erickson, K. Harris, and R. Schwer, *Development of CMSX-5: a third-generation high strength single crystal superalloy.* Cannon-Muskegon Corp., Michigan, 1985.
[164]N. Czech, F. Schmitz, and W. Stamm, *Surf. Coatings Technol.* **68/69** (1994) 17.
[165]S. J. Schneider, *High temperature thruster technology for spacecraft propulsion*, NASA technical memorandum 105348, IAF-91-254, 1991.
[166]M. Treska, L. W. Hobbs, and J. P. Pemsler, in *Microscopy of oxidation 3*, Ed. by S. B. Newcomb, J. A. Little, Institute of Materials, London, 1997, p 720.
[167]B. D. Reed, J. A. Biaglow, and S. J. Schneider, *Mater. Manuf. Processes* **13** (1998) 757.
[168]M. Pourbaix, *Atlas of electrochemical equilibria in aqueous solutions*, NACE, Texas, 1974, p 300.
[169]A. J. Bard, R. Parsons, and J. Jordan, *Standard potentials in aqueous solutions*, Dekker, New York, 1985, p 444.
[170]C. G. Fink and P. Deren, *Trans. Electrochem. Soc.* **66** (1934) 471.
[171]L. E. Netherton and M. L. Holt, *Trans. Electrochem. Soc.* **95** (1949) 324.
[172]G. S. Root, J. G. Beach, in *Rhenium – Electrochemical Society Symposium*, Ed. by B. W. Gonser, Elsevier, New York, 1962, p. 181.
[173]N. Eliaz, M. Treska, L. W. Hobbs, Pemsler JP (2000) unpublished data.

[174]S. A. Sastri, J. P. Pemsler, R. A. Cooke, J. K. Litchfield, and M. B. Smith U.S. Patent 5, 495, 979, 1996.
[175]P. Pemsler, *Electrochemical coating of complex carbon-carbon parts for low mass divert propulsion systems*, SBIR Phase I Contract N00167-99-C-0058, Castle Technology Corp., Massachusetts, 2000.
[176]P. J. Paris, *Rev. Sci. Instrum.* **60** (1989) 2802.
[177]G. Horányi, I. Bakos, S. Szabó, and E. M. Rizmayer, *J. Electroanal. Chem.* **337** (1992) 365.
[178]I. Bakos, G. Horányi, S. Szabó, and E. M. Rizmayer, *J. Electroanal. Chem.* **359** (1993) 241.
[179]I. Bakos and G. Horányi, *J. Electroanal. Chem.* **375** (1994) 387.
[180]G. Horányi and I. Bakos, *J. Electroanal. Chem.* **378** (1994) 143.
[181]S. Szabó and I. Bakos, *React. Kinet. Catal. Lett.* **62** (1997) 267.
[182]S. Szabó, *Int. Rev. Phys. Chem.* **10** (1991) 207.
[183]S. Szabó and I. Bakos, *Stud. Surf. Sci. Catal.* **118** (1998) 269.
[184]S. Szabó and I. Bakos, *J. Electroanal. Chem.* **492** (2000) 103.
[185]S. Szabó and I. Bakos, *J. Sol. State Electrochem.* **8** (2004) 190.
[186]J. O. Zerbino, A. M. Castro Luna, C. F. Zinola, E. Méndez, and M. E. Martins, *J. Braz. Chem. Soc.* **13** (2002) 510.
[187] R. Schrebler, P. Cury, M. Orellana, H. Gómez, R. Córdova, and E. Dalchiele *Electrochim. Acta* **46** (2001) 4309.
[188]L. E. Netherton and M. L. Holt, *J. Electrochem. Soc.* **98** (1951)106.
[189]L. E. Netherton and M. L. Holt, *J. Electrochem. Soc.* **99** (1952) 44.
[190]Y. N. Sadana and Z. Z. Wang, *Surf. Coatings Technol.* **37** (1989) 419.
[191]I. M. Kvokova and V. I. Lainer, *Zashchita Metallov* **1** (1965) 515.
[192]J. J. Vajo, D. A. Aikens, L. Ashley, D. E. Poeltl, R. A. Bailey, H. M. Clark, and S. C. Bunce, *Inorg. Chem.*, 20 (1981) 3328.
[193]L. R. Sillén and A.E. Martell, *Stability constants of metal-ion complexes, supplement 1,* The Chemical Society, London, 1971.
[194]L. R. Sillén and A.E. Martell, *Stability constants of metal-ion complexes, supplement 17*. The Chemical Society, London, 1964.
[195]G. R. Hedwig, J. R. Liddle and R. D. Reeves, *Aust. J. Chem.* **33** (1980) 1685.
[196] J. J. Cruywagen and R. F. van de Water, *Polyhedron* **5** (1986) 521.